TRANSPORTATION RESEARCH RECORD 640

Multiple Aspects of Soil Mechanics

TRANSPORTATION RESEARCH BOARD

COMMISSION ON SOCIOTECHNICAL SYSTEMS
NATIONAL RESEARCH COUNCIL

NATIONAL ACADEMY OF SCIENCES
WASHINGTON, D.C. 1977

Transportation Research Record 640
Price $4.00
Edited for TRB by Susan Lang

subject area
63 mechanics (earth mass)

Transportation Research Board publications are available by ordering directly from the board. They may also be obtained on a regular basis through organizational or individual supporting membership in the board; members or library subscribers are eligible for substantial discounts. For further information, write to the Transportation Research Board, National Academy of Sciences, 2101 Constitution Avenue, N.W., Washington, D.C. 20418.

Notice

The project that is the subject of this report was approved by the Governing Board of the National Research Council, whose members are drawn from the councils of the National Academy of Sciences, the National Academy of Engineering, and the Institute of Medicine. The members of the committee responsible for the report were chosen for their special competence and with regard for appropriate balance.

This report has been reviewed by a group other than the authors according to procedures approved by a Report Review Committee consisting of members of the National Academy of Sciences, the National Academy of Engineering, and the Institute of Medicine.

The views expressed in this report are those of the authors and do not necessarily reflect the view of the committee, the Transportation Research Board, the National Academy of Sciences, or the sponsors of the project.

Library of Congress Cataloging in Publication Data
National Research Council. Transportation Research Board.
Multiple aspects of soil mechanics.

(Transportation research record; 640)
Includes bibliographical references.

1. Soils–Testing–Addresses, essays, lectures. 2. Soil mechanics–Addresses, essays, lectures. 3. Pavement–Testing–Addresses, essays, lectures. I. Title. II. Series.
TE7.H5 no. 640 [TE208] 380.5'08s [624'.1513]
ISBN 0-309-02669-5 78-19076

Sponsorship of the Papers in This Transportation Research Record

GROUP 2–DESIGN AND CONSTRUCTION OF TRANSPORTATION FACILITIES
Eldon J. Yoder, Purdue University, chairman

Soil Mechanics Section
Lyndon H. Moore, New York State Department of Transportation, chairman

Committee on Strength and Deformation Characteristics of Pavement Sections
Richard D. Barksdale, Georgia Institute of Technology, chairman
Stephen F. Brown, Jim W. Hall, Jr., Amir N. Hanna, R. G. Hicks, Frank L. Holman, Jr., Ignat V. Kalcheff, Bernard F. Kallas, William J. Kenis, Thomas W. Kennedy, Kamran Majidzadeh, Fred Moavenzadeh, Quentin Robnett, Jatinder Sharma, Eugene L. Skok, Jr., Ronald L. Terrel, Peter J. Van de Loo

Committee on Embankments and Earth Slopes
Raymond A. Forsyth, California Department of Transportation, chairman
Thomas A. Bellatty, A. Alexander Fungaroli, David S. Gedney, Wilbur M. Haas, William P. Hofmann, Robert D. Holtz, Henry W. Janes, Charles C. Ladd, Richard E. Landau, Harry E. Marshall, Glen L. Martin, R. M. Mattox, Lyndon H. Moore, Melvin W. Morgan, Lyle K. Moulton, Gerald P. Raymond, Dwight A. Sangrey, Walter C. Waidelich, William G. Weber, Jr.

Committee on Foundations of Bridges and Other Structures
Clyde N. Laughter, Wisconsin Department of Transportation, chairman
Arnold Aronowitz, William Bootz, Michael Bozozuk, Bernard E. Butler, Ronald G. Chassie, Harry M. Coyle, M. T. Davisson, Frank M. Fuller, David S. Gedney, Stanley Gordon, Bernard A. Grand, Robert J. Hallawell, T. J. Hirsch, W. Kenneth Humphries, Hal W. Hunt, Henry W. Janes, Philip Keene, G. A. Leonards, R. M. Mattox, Alex Rutka, John L. Walkinshaw, James Doyle Webb

Committee on Subsurface Drainage
George W. Ring III, Federal Highway Administration, chairman
Charles C. Calhoun, Jr., Harry R. Cedergren, Barry J. Dempsey, Ernest L. Dodson, Edward N. Eiland, David S. Gedney, Alfred W. Maner, Glen L. Martin, K. H. McGhee, Lyndon H. Moore, Lyle K. Moulton, Travis W. Smith, W. T. Spencer, William D. Trolinger, Walter C. Waidelich, Clayton E. Warner, Thomas F. Zimmie

John W. Guinnee, Transportation Research Board staff

Sponsorship is indicated by a footnote at the end of each report. The organizational units and officers and members are as of December 31, 1976.

Contents

Pull Resistance and Interaction of Earthwork Reinforcement and Soil

Jerry C. Chang, Joseph B. Hannon, and Raymond A. Forsyth, Division of Structures and Engineering Services, California Department of Transportation, Sacramento

Results are presented of tests on different kinds of earthwork reinforcement to study pull resistance and soil-reinforcement interaction in reinforced earth. Three kinds of pull tests were conducted. Results indicate that the soil will not be significantly strained until a proportional limit is reached on a load-deformation curve. For the same surface area, bar-mesh reinforcement has nearly six times the pull resistance as that of flat steel-strip reinforcement. Bar-mesh reinforcement embedded in a dense cohesive soil exhibited greater pull resistance than that embedded in a less dense cohesionless soil. An increase in size of mesh opening will substantially reduce the pull resistance of the bar mesh. The minimum length of steel-strip reinforcement required for a low-height, reinforced earth wall was found to be at least 3.1 m (10 ft).

The use of steel strips as earthwork reinforcement has been reported by Vidal (8, 9), Lee and others (6, 7), and Chang and others (1, 2, 3, 4). More than a dozen reinforced earth walls have been constructed in the United States in recent years under a patented design (5). The California Department of Transportation built the first of these walls with steel-facing and steel-strip reinforcements in 1972 on Cal-39 in the San Gabriel Mountains of Los Angeles County. A second reinforced earth wall with concrete-facing and steel-strip reinforcements was constructed on I-5 near Dunsmuir, California, in 1974.

Two other experimental projects designated as mechanically stabilized embankment with concrete-beam facing and bar-mesh reinforcements were also constructed on I-5 in September 1975 and May 1976 respectively (Figures 1 and 2). These experimental projects were designed and constructed by the California Department of Transportation under an agreement with the Reinforced Earth Company of Washington, D.C. Future construction that uses this kind of system will be under the license of that company.

For the purpose of studying the pull resistance and the interaction of different kinds of reinforcement and soil for these construction projects, field and laboratory pull tests were conducted on both large and small scales. These tests and the results are discussed.

FIELD PULL TESTS ON STEEL STRIPS

The pull resistance of soil reinforcements in the field was studied by installing additional dummy steel strips in the reinforced earth wall located on Cal-39 in the San Gabriel Mountains, California, at different elevations during construction. Three steel strips, 1.5, 3.1, and 4.6 m (5, 10, and 15 ft) long, were embedded at each of three levels under overburden heights of 2.3, 3.8, and 5.6 m (7.5, 12.4, and 18.2 ft) respectively. Three 7 and 14-m (23 and 46-ft) steel strips were also embedded at depths of 5.5 and 11.60 m (18 and 38 ft) respectively. Both the 7 and 14-m (23 and 46-ft) strips were instrumented with strain gauges on both top and bottom at 1.5-m (5-ft) intervals. All of the steel strips are 3 mm (0.118 in) thick and 60 mm (2.362 in) wide. The fill material is primarily decomposed granite. The physical properties of soil samples obtained from a nearby borrow site are given in Table 1.

Figure 3 shows six typical load-deformation curves obtained from field pull tests for 1.5, 3.1, 4.6, 7, and 14-m (5, 10, 15, 23, and 46-ft) steel strips. Three pull loads selected for analysis are indicated on these curves:

1. Yield load, which represents the proportional limit of the load-deformation relation,
2. Peak load, which represents the maximum pull load observed, and
3. Residual load, which represents the pull load when deformation increased appreciably without changing pull load.

Tensile strength tests on a small-sized sample of the reinforcing strip resulted in yield and ultimate capacities of 45.8 and 61.8 kN (10.3 and 13.9 kips) respectively. At the site, one of the 7-m (23-ft) strips broke at a pull load slightly over 62.3 kN (14 kips). Three of the 14-m (46-ft) strips broke at pull loads of 59.9, 63.2, and 64.3 kN (13.46, 14.20, and 14.45 kips). The rest of the steel strips failed by slipping.

The straight line portion of the load-deformation curve represents the elastic properties of the steel. When the steel strip has sufficient length and overburden, i.e., when the frictional grip is great enough, the proportional limit will reflect the yield capacity of the steel. If the frictional grip is not sufficient at the loaded end of the strip, the soil will start to strain at a proportional limit lower than that for reaching the yield strength of the steel. Therefore, it appears that the yield load represents either the yield capacity of the steel or the initial point of soil-steel interaction as a composite material. The values of the yield load depend on the length of the reinforcement and the overburden load. The peak load represents the maximum mobilized pull resistance of the composite material of reinforcement and soil. Once the peak load is reached, the strips begin to slip and the pull load drops to the residual or ultimate level. Figure 4a shows the relations between the peak pull load and the overburden load and the height of overburden and the length of the strips. At the same height of overburden, the peak pull load is proportional to the overburden load, shown by the solid straight lines. The slopes of these lines decrease as the overburden height increases. For the same strip length, the relation between the peak pull load and overburden load is approximately linear, indicated by the dashed lines. The solid lines suggest that the longer strips have higher peak pullout resistance for the same height of overburden. For a given strip length, the pull resistance increases as overburden heights increase. The rate of increase in peak pull load caused by an increase in overburden is much smaller than that caused by an increase in strip length. Figure 4b shows similar characteristics for the yield load.

Since the peak load represents the maximum mobilized friction force, the factor of safety can be evaluated by using the peak load as failure load and the factor of safety against slippage can be evaluated by using the following equation proposed by Chang (1, 2, 3, 4).

Factor of safety against slippage = peak failure pull load
$$\div K_a \gamma H d \Delta H \quad (1)$$

where

K_a = coefficient of active earth pressure,
γ = unit mass of soil,
H = height of fill above the reinforcement,
d = horizontal spacing of reinforcement, and
ΔH = vertical spacing of reinforcement.

The relations between overburden height (H), strip length (L), and the factor of safety (FS) are shown in Figure 4c, which can be used as a guide for selecting the minimum length of strip reinforcement required for a given height of fill.

The relation between the peak pull load and the skin friction force is shown in Figure 4d and calculated by using the following equation.

$$2F = 2\gamma HbL \tan \delta \quad (2)$$

where

F = friction force on one face of the reinforcement,
b = width of reinforcing strip,

Figure 1. Concrete-beam facing of mechanically stabilized embankment on I-5 at Dunsmuir, California.

Figure 2. Bar-mesh reinforcement in mechanically stabilized embankment on I-5 at Dunsmuir, California.

Table 1. Physical properties of soil samples.

Location and Soil Classification	Sample	Effective Friction Angle (degrees)	Cohesion (kPa)	Max. Dry Density (kg/m^3)	Sand Equivalent Value
Highway 39					
Sand gravel	72-RE8	40	29	2227	28
I-5					
Gravel sand	73-1803	35	55	1233	27
Highway 101					
Silty clay and gravel	74-1231	34	97	2034	15

Notes: 1 kPa = 0.145 lbf/in^2 and 1 kg/m^3 = 0.624 lb/ft^3.

Figure 3. Load-deformation curves from field pull tests on Cal-39.

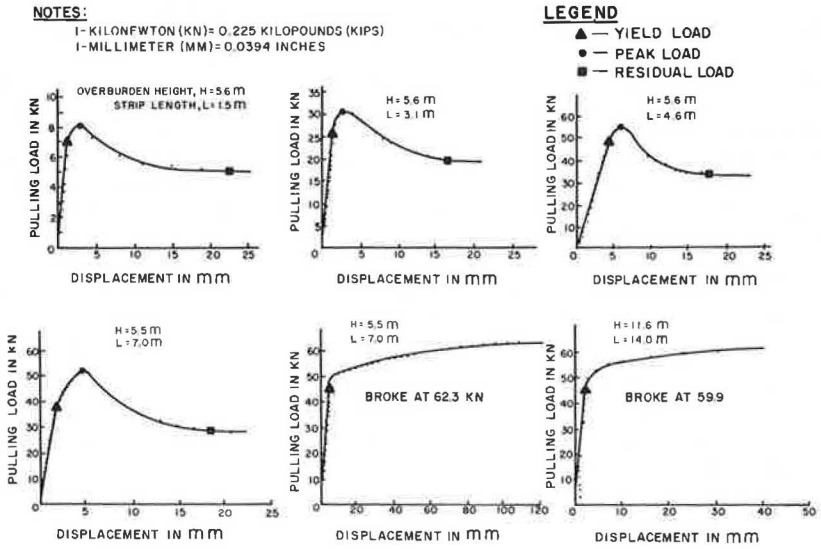

Figure 4. Summary results of field pull test.

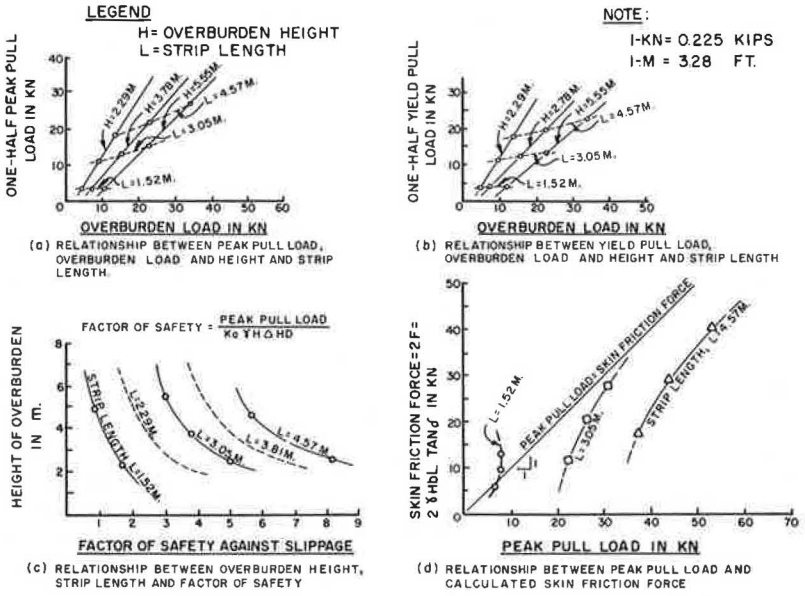

Figure 5. Axial force in 7 and 14-m dummy steel strips.

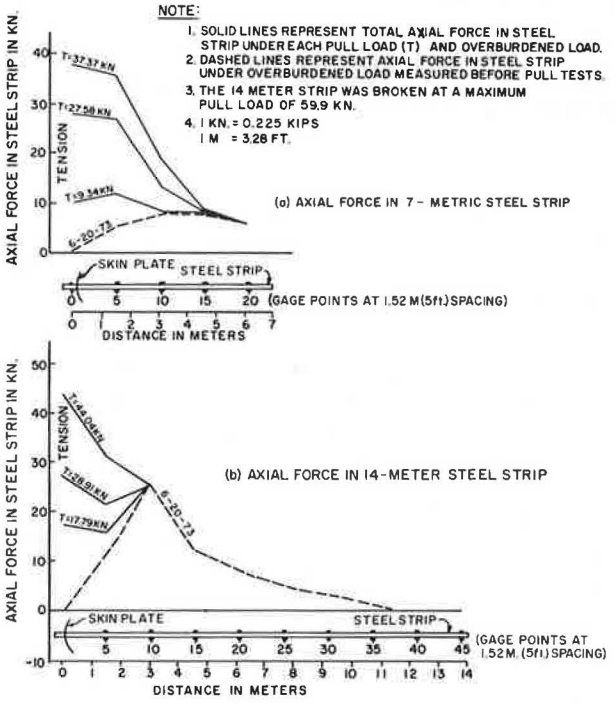

Figure 6. Laboratory facility for pull test.

L = length of reinforcing strip, and
δ = skin friction angle between soil and steel reinforcement.

It can also be seen that the peak pull loads exceed the calculated skin-friction force when the strip length exceeds 3.1 m (10 ft). Thus, it may be concluded that the minimum strip length should be 3.1 m (10 ft).

Figure 5 shows the distribution of tensile and compressive forces measured by strain gauges spaced at 1.5-m (5-ft) intervals along the length of the 7 and 14-m (23 and 46-ft) strips respectively. The dashed lines indicate the tensile or compressive forces in the steel strip measured at each strain gauge location under the embankment load. Each solid line represents the distribution of the total tensile forces along the length of strip that includes the forces induced by each applied pull load and the existing forces induced by the measured embankment load. Figure 5a shows that each external-applied pull load induced additional tensile forces for almost the entire length of the 7-m (23-ft) strip. However, the external-applied pull load only stressed the 14-m (46-ft) strip to gauge point that is a 3.1-m (10-ft) distance into the fill. There were no additional forces measured beyond gauge point 10 other than the existing forces induced by the embankment load before testing. The 14-m strip broke at the external-extended portion under the maximum pull load of 59.9 kN (13.46 kips). Because the 14-m strip was longer and under a heavier embankment load, the strip appeared to develop a fixed point at gauge point 10; therefore, no additional tensile forces developed beyond 3.1 m (10 ft) of the strip length within the fill.

LARGE-SCALE LABORATORY PULL TESTS

Large-scale laboratory pull tests were conducted so that the interaction between the soil and reinforcements could be understood. The test facility consists of a rigid steel box, 45.70, 91.40, and 137.20 cm (18, 36, and 54 in) high, wide, and long respectively, with pro-

Figure 7. Test runs with each kind of reinforcement.

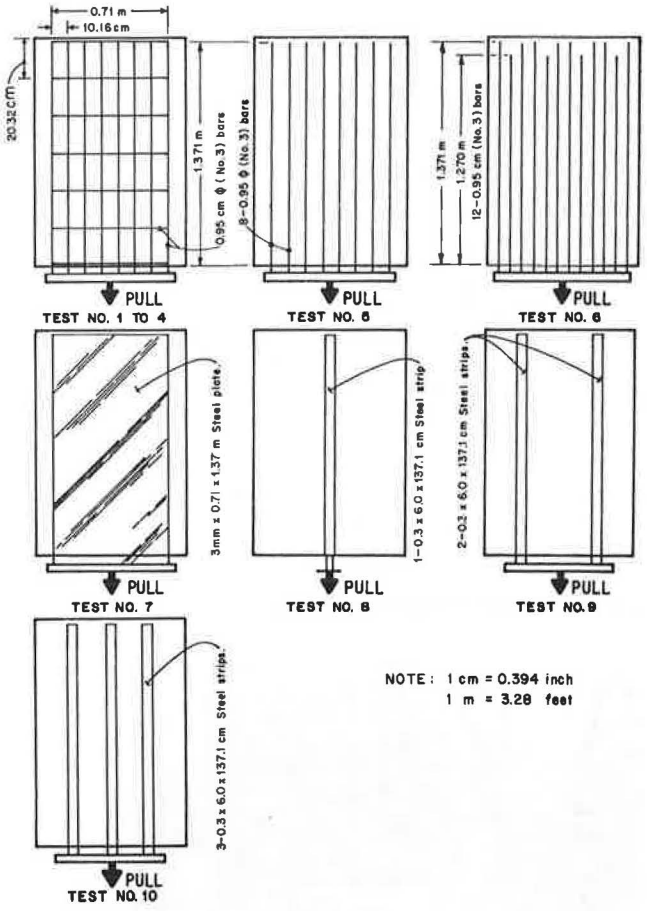

Figure 8. Typical time and load-deformation curves for bar mesh with 10.16 by 20.32-cm openings embedded in gravel-sand soil.

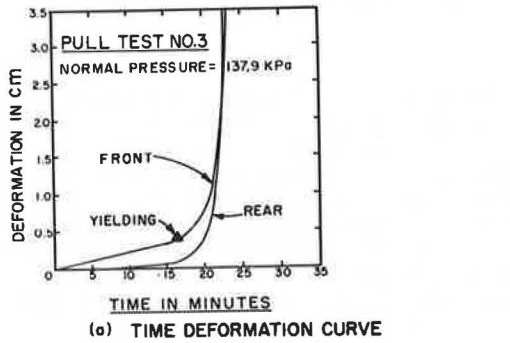

(a) TIME DEFORMATION CURVE

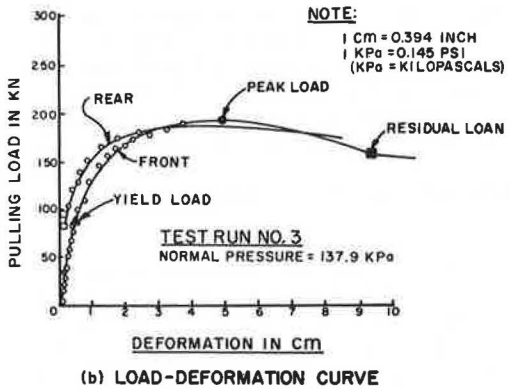

(b) LOAD-DEFORMATION CURVE

visions for applying vertical pressure to simulate the overburden load up to 15.2 m (50 ft) of earth fill (Figure 6). The test specimen is compacted in the box with reinforcement placed horizontally in the middle height of the specimen. A vertical normal load is applied to consolidate the specimen. Reinforcement can then be pulled out at a controlled rate of 0.05 mm/1min (0.002 in/1 min). During pull testing, the front face of the box is removed so that a free unrestrained face of the soil specimen is provided.

Figure 7 shows the 10 tests that were conducted with four different kinds of reinforcements. A description of the reinforcements follows:

1. Bar mesh made by crossing and welding smooth longitudinal bars with 0.95-cm (3/8-in) diameters to provide 10.20 by 20.30-cm (4 by 8-in) openings for tests 1 through 4;
2. Longitudinal smooth bars with 0.95-cm (3/8-in) diameters and 1.37-m (54-in) lengths were spaced differently for tests 5 and 6;
3. Solid steel plate that was 3 mm (1/8 in) thick, 71.1 cm (28 in) wide, and 1.37 m (54 in) long was used for test 7; and
4. Steel strips that were 3 mm (1/8 in) thick, 6 cm (2.3 in) wide, and 1.37 m (54 in) long were used for tests 8 through 10.

Figure 9. Typical load-deformation curves for bar mesh embedded in silty clay with gravel soil.

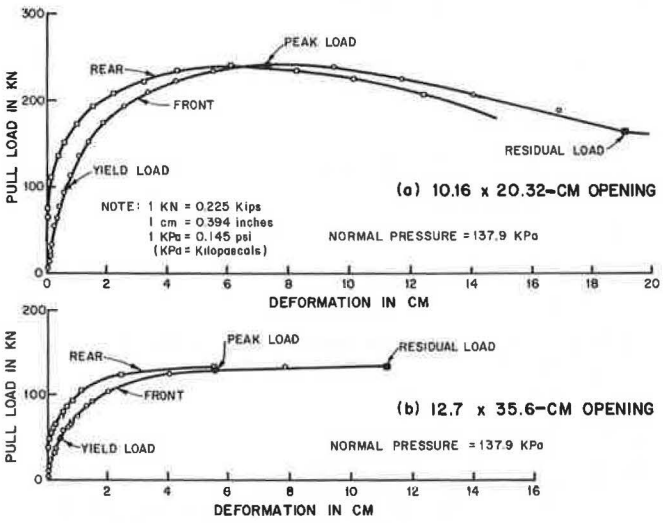

Figure 10. Cone-shaped failure in specimen with bar-mesh reinforcement.

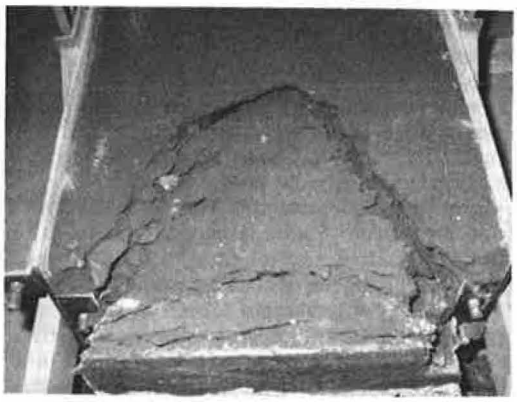

Tests 1 to 4 were performed under normal pressures of 34.47, 68.95, 137.90, and 172.34 kPa (5, 10, 20, and 25 lbf/in^2) respectively. Tests 5 through 10 were conducted under a normal pressure of 68.95 kPa (10 lbf/in^2).

The soil samples used in the tests were obtained from the job site on I-5. This material is primarily poorly graded gravelly sand. The physical properties of the soil samples are given in Table 1.

Figure 11. Failure in specimen with eight longitudinal-bar reinforcement for test 5.

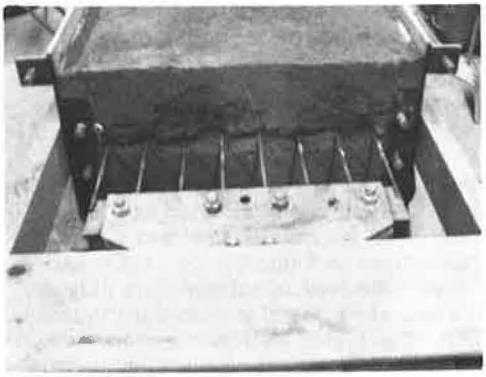

Figure 12. Failure in specimen with three steel-strip reinforcement for test 10.

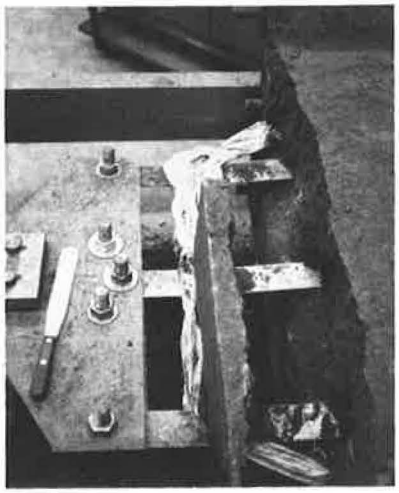

Figure 13. Cone-shaped failure in specimen with solid steel-plate reinforcement for test 7.

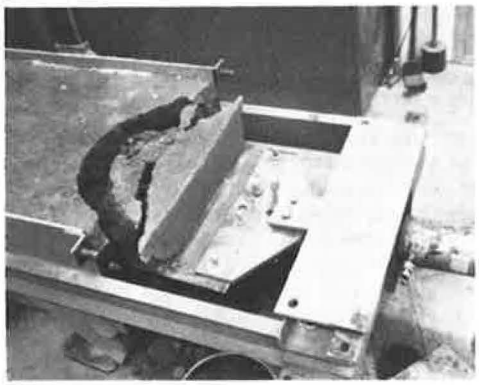

Time- and Load-Deformation Curves

During the pull tests, the deformations of the reinforcements were measured by two extensometers: one located at the front and at the rear of each specimen. The normal and pull loads were measured by load cells. A typical time-deformation curve for test 3 on bar mesh under a normal pressure of 137.90 kPa (20 lbf/in^2) is shown in Figure 8a. A typical load-deformation curve for the same test is also shown in Figure 8b. The load-deformation characteristics were found to be quite different for each kind of reinforcement.

The following observations were noted.

1. The strain response at the rear of the specimen is always behind that at the front or loaded end of the specimen (Figure 8); and
2. When the pull load is sufficient to cause an abrupt change in deformation at the rear of the specimen (time-deformation curve), the proportional limit or yielding point (load-deformation curve) is attained, i.e., the yield point occurred at the same strain level measured at the front end.

It can be hypothesized that the applied pull load only strains the reinforcement without causing any significant strain in the soil until the yielding load is reached when the whole length of the reinforcement exhibits an abrupt change in deformation.

Figure 9 shows the typical load-deformation curves obtained from pull tests that used bar-mesh reinforcement with mesh openings of 10.20 by 20.30 cm (4 by 8 in) and 12.7 by 35.6 cm (5 by 14 in) respectively that were embedded in silty clay soil under a normal pressure of 137.90 kPa (20 lbf/in^2). This material was obtained

Figure 14. Relation between normal and pull loads for bar mesh with 10.16 by 20.32-cm opening embedded in gravel-sand soil.

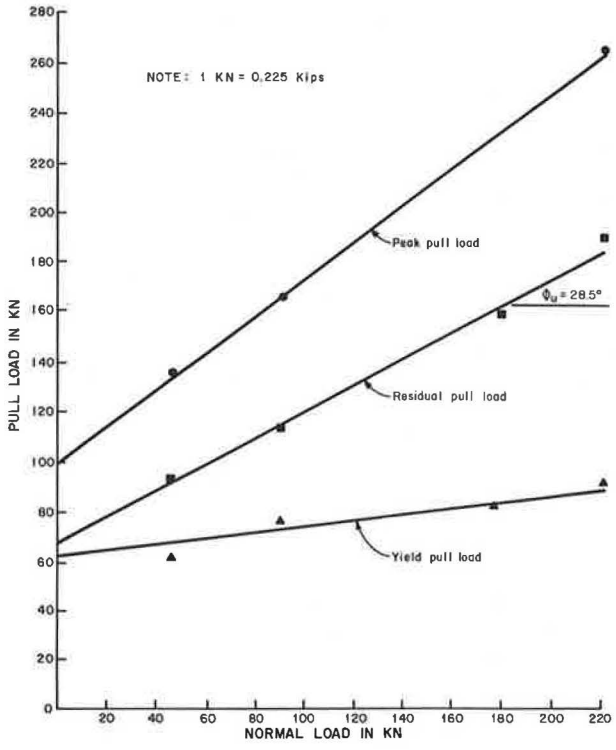

Table 2. Pull resistance for different reinforcements and soils.

Test	Reinforcement	Total Surface Area (Percent of Bar Mesh With 10 by 20-cm Openings)	Peak Resistance (kN) Under Normal Pressure (70 kPa)	
			Gravel Sand	Silty Clay and Gravel
2	Bar mesh (10 by 20-cm openings)	100	167	176
5	8 longitudinal bars	69	15	–
6	12 longitudinal bars	100	30	23.1
7	1 solid steel plate	409	79	–
8	1 galvanized steel strip	34	12	–
9	2 galvanized steel strips	68	24	22.2
10	3 galvanized steel strips	102	30	25.8
–	Bar mesh (13 by 36-cm openings)	97	–	129

Notes: 1 kN = 0.225 kips, 1 kPa = 0.145 lbf/in^2, and 1 cm = 0.394 in.

Figure 15. Shear-box, test for skin friction.

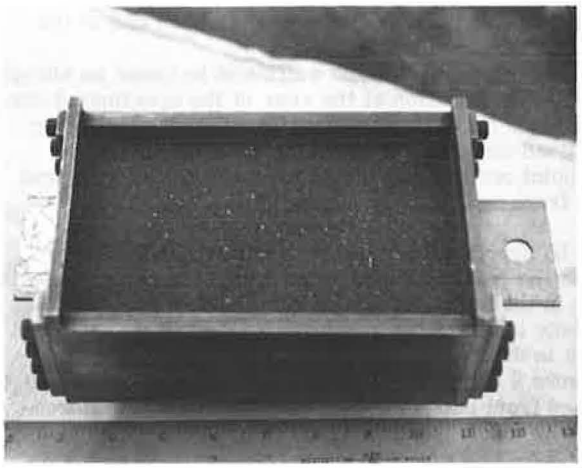

from a project site on US-101 at Cuesta Grade near San Luis Obispo, California.

For the same bar-mesh reinforcement, the peak pull loads were higher in a dense silty clay soil (Figure 9a) than those in a less dense gravelly sand soil (Figure 9). However, in the same soil, the peak pull load decreased substantially when mesh openings increased to 12.7 by 35.6 cm (5 by 14 in), as shown in Figure 9b.

Failure Mode

The failure mode resulting from laboratory tests indicated that all the specimens with bar-mesh reinforcement failed because a cone-shaped soil wedge developed (Figure 10) while the specimens with longitudinal-bar and steel-strip reinforcements failed because of slippage, with only a local slump of the soil at the front face of the specimens (Figures 11 and 12). The specimen with a solid steel-plate reinforcement also failed because small cone-shaped soil wedges developed (Figure 13) that are similar to the specimen with bar-mesh reinforcement (Figure 10). This mode of failure is believed to represent full mobilization of soil resistance, i.e., the development of a passive pressure wedge. The cone-shaped failure mode indicates that the soil and bar-mesh reinforcement failed as a unit.

Comparison of Test Results

The pull test results for the smooth bar-mesh reinforcement with 10.20 by 20.30-cm (4 by 8-in) openings embedded in gravelly sand soil under three different normal loads are shown in Figure 14. The yield, peak, and residual loads are all proportional to the normal loads.

The comparison of the pull resistance for different kinds of reinforcement embedded in gravelly sand soil are given in Table 2. The smooth bar-mesh reinforcement has a much higher pull resistance than the other kinds. For the same surface area, the bar-mesh reinforcement has a peak pull resistance about six times that of the longitudinal-bar and steel-strip reinforcement.

A comparison of the pull resistance for bar-mesh reinforcement embedded in gravelly sand and silty clay respectively is also given in Table 2. The same bar-mesh reinforcement embedded in a dense silty clay soil has greater pull resistance than that embedded in the gravelly sand soil. The higher pullout resistance could reflect the higher density or effect of cohesion present in the silty clay sample. For the same soil material, the bar-mesh reinforcement with larger mesh openings produced lower pull resistance.

SMALL-SCALE LABORATORY PULL TESTS

Small-scale laboratory pull tests were also conducted in a specially designed shear box (Figure 15) to determine the skin friction between the galvanized reinforcing steel strip and two types of soil, namely, decomposed granite from Cal-39 and gravelly sand material from I-5. These test results (Table 1) suggest that the skin friction angle is slightly smaller than the internal friction angle of the soil for granular material.

FIELD AND LABORATORY TEST CONCLUSIONS

Field Test

1. The soil will not be strained significantly until the proportional limit (or yield point) is reached. At this point, the load-deformation curve becomes nonlinear for the composite steel strip and soil material.
2. The maximum tensile stress in the reinforcement is developed near the front face of the wall for any external-applied pull force.
3. The required minimum length of steel strip is about 3.1 m (10 ft) for a reinforced earth fill lower than 3.1 m (10 ft) in height.

Laboratory Test

1. The proportional limit on the front-end, load-deformation curve can be determined from the displacement on the front-end, time-deformation curve at the point where an abrupt increase in deformation occurs on the time-deformation curve for the rear of the specimen. Thus, the soil will not be significantly strained until reaching a proportional limit that defines the initial point of soil-steel interaction as the composite material.
2. For the same surface area, plain bar-mesh reinforcement has nearly six times the pullout resistance

as steel-strip or plain longitudinal-bar reinforcements in gravelly sand soil.

3. Bar-mesh reinforcement embedded in dense silty class soil exhibited greater pull resistance than bar-mesh reinforcement embedded in less dense gravelly sand soil.
4. An increase in mesh opening will substantially reduce the pullout resistance of the bar-mesh reinforcement.
5. The skin friction angle between a galvanized steel strip and soil for granular material is only slightly smaller (6 to 13 percent) than the internal friction angle of the soil. For practical design purposes, the skin friction angle between the galvanized steel strip and soil material can be assumed to be 10 percent smaller than the internal friction angle of the soil.
6. Cohesive soil of low plasticity can be used in reinforced earth providing that bar-mesh reinforcement is used.

REFERENCES

1. J. C. Chang, R. A. Forsyth, and T. Smith. Reinforced Earth Highway Embankment: Road 39. Federal Highway Administration, U.S. Department of Transportation. Highway Focus, Vol. 4, No. 1, Jan. 1972.
2. J. C. Chang, J. L. Beaton, and R. A. Forsyth. Design and Field Behavior of the Reinforced Earth Embankment: California Highway 39. Paper presented at National Water Resources Engineering Meeting, ASCE, Los Angeles, 1974.
3. J. C. Chang, R. A. Forsyth, and J. L. Beaton. Performance of a Reinforced Earth Fill. TRB, Transportation Research Record 510, 1974, pp. 56-68.
4. J. C. Chang. Earthwork Reinforcement Techniques. Transportation Laboratory, California Department of Transportation, Res. Rept. CA-HY-TL-2115-9-74-1, Sept. 1974.
5. D. S. Gedney and D. P. McKittrick. Reinforced Earth: A New Alternative for Earth-Retention Structures. Civil Engineering, Oct. 1975, pp. 58-61.
6. K. L. Lee, B. D. Adams, and J. J. Vagneron. Reinforced Earth Retaining Walls. Journal of Soil Mechanics and Foundations Division, ASCE, Vol. 99, No. SM10, Oct. 1973, pp. 745-764.
7. K. L. Lee and G. N. Richardson. Seismic Design of Reinforced Earth Walls. Journal of Geotechnical Engineering Division, ASCE, Vol. 101, No. GT2, Feb. 1975.
8. H. Vidal. The Principle of Reinforced Earth. HRB, Highway Research Record 282, 1969, pp. 1-16.
9. H. Vidal. Reinforced Earth—Recent Application. Translation of Annales de l'Institute Technique du Batiment et des Travaux Publics, Series Material, Vol. 38, July-Aug. 1969, pp. 259-260.

Publication of this paper sponsored by Committee on Embankments and Earth Slopes.

Some Uncertainties of Slope Stability Analyses

Robert C. Deen, Tommy C. Hopkins, and David L. Allen,
Division of Research, Kentucky Department of Transportation,
Frankfort

Some practical limitations of total stress and effective stress analyses are discussed. For clays having a liquidity index of 0.36 or greater, ϕ-equal-zero analyses based on laboratory undrained shear strengths give factors of safety close to the actual factor of safety. However, ϕ-equal-zero analyses based on field vane sheer strengths may yield factors of safety that may be too high. The difference between field vane and calculated shear strengths increases as the plasticity index increases. For clays having a liquidity index less than 0.36, ϕ-equal-zero analyses that use laboratory undrained shear strengths give factors of safety that are too high; however, the strength parameters can be corrected by the empirical relation presented here. An empirical relation for correcting field vane shear strength is also presented. A method is proposed for predicting the probable success of ϕ-equal-zero analysis. Data suggest that overconsolidated clays and clay shales or clays having a liquidity index less than 0.36 pose a slope design dilemma for engineers. An effective stress analysis based on peak triaxial shear strength parameters generally yields factors of safety that are too high; residual shear strength parameters frequently yield factors of safety that are too low. The theoretical strength of an overconsolidated clay that has undergone a softening process is approximated by using the effective stress parameters that might be obtained from triaxial tests performed on remolded, normally consolidated clay. It is suggested the soil be remolded to a moisture content equal to the plastic limit plus the product of 0.36 and the plasticity index.

Two limiting conditions (2) must be considered when designing a cutting in a clay or an embankment on a clay foundation to ensure against a first-time failure (no preexisting shear plane). The first condition is the short-term or end-of-construction case in which the water content of the clay does not change. In this case, excess pore pressures are controlled by the magnitude of the stresses acting in the clay or tending toward instability; therefore, significant dissipation of pore pressure does not occur. However, it is difficult to predict the excess pore pressures. Consequently, the short-term design is made by using the ϕ-equal-zero analysis and the undrained shear strength obtained from unconsolidated-undrained (UU) triaxial tests, unconfined compression (U) tests, field vane shear (FV) tests, or a combination of these tests.

The second condition is the long-term, steady seepage case. In this case, pore pressure do not depend on the magnitude of total stresses but are controlled by the flow pattern of underground water or the groundwater level. Excess dissipation of pore pressure occurs and the clay exists in a drained state. Long-term design is performed in terms of effective stress and the drained shear strength parameters (ϕ' and c') that are conventionally obtained from consolidated isotropically, drained (CID) triaxial tests; consolidated isotropically, undrained (CIU) triaxial tests with pore pressure measurements; consolidated-drained, direct shear (CDS) slow tests; or a combination of these tests.

For a cutting in a clay, the long-term stability is considered critical because pore pressures are initially

low or negative and gradually increase toward steady seepage pore pressures. The increase of pore pressures causes a decrease in the shear strength of the clay because there is a reduction in effective stresses. For an embankment on a clay foundation, the short-term stability is considered critical because pressures steadily increase to maximum values during construction and gradually decrease thereafter toward the initial pore pressures thus increasing shear strengths with time.

LIMITATIONS OF TOTAL STRESS ANALYSES

If the stress history and moisture state of the clays in the foundation or slope are not regarded, then application of the ϕ-equal-zero analysis for designing embankments founded on clay foundations or a slope cut in a clay may lead to erroneous conclusions concerning the safety factor (11). These conclusions may be erroneous because the undrained shear strengths obtained from laboratory or field tests may be higher than the actual (back-computed) shear strengths existing at failure.

Long-Term Stability of Cut and Natural Slopes

Bishop and Bjerrum (2) summarized the results of a number of failures in natural slopes and cuts and showed that application of the ϕ-equal-zero analysis for slopes where pore pressure and water content equilibrium have been attained is unreliable. In these cases, the ϕ-equal-zero analysis gave safety factors ranging from 0.6 for sensitive soils to 20 for heavily overconsolidated soils. Two reasons for the differences between the in situ shear strength and the shear strength obtained from the undrained test are differences between field and laboratory pore pressures and migration of water to the failure zone of a slide in overconsolidated clays (9, 18). Lo and others (13) have also shown that for stiff-fissured clays the effect of sample size is an important factor in stability analyses. The shear strength of large samples is less than that of small samples.

Examination of case records for long-term failures in cuts and natural slopes revealed that high safety factors are associated with low to negative values of the liquidity index while low safety factors are associated with high values of the liquidity index. In data cited by Bishop and Bjerrum (2) there were four cases in which the safety factor was near one; the liquidity indexes ranged from 0.20 to 1.09. In the other cases, the liquidity indexes ranged from about 0.19 to -0.36 while the safety factors ranged from 1.9 to 20.

Short-Term Stability of Loads on Soft Foundations

A number of case records was assembled by Bjerrum (3, 5) to show that the procedures normally used to determine the short-term stability of embankments, footings, and load tests on soft clay foundations are unsatisfactory. In those cases, use of ϕ-equal-zero analysis and undrained shear strengths from field vane shear tests overestimated the safety factor for soils having liquid limits and plasticity indexes in excess of approximately 80 and 30 percent respectively. Also, the difference between field vane $[(S_u)_{vane}]$ and corrected shear strengths $[(S_u)_{corrected}]$ increases as the plasticity index (PI) and the liquid limit of the clay increase. By assuming that there is a linear relation between safety factor and plasticity index, the corrected shear strength may be expressed as follows:

$$(S_u)_{corrected} = (S_u)_{vane}/[(0.84 + 0.0082\ PI) \pm 0.12] \quad (1)$$

Figure 1 shows a comparison of data representing end-of-construction failures of footings, fills, and excavations on saturated clay foundations assembled by both Bishop and Bjerrum (2) and Bjerrum (3, 5). Liquidity indexes by the former ranged from about 0.25 to 1.44. The undrained strengths of the soils in these analyses were obtained primarily from unconsolidated-undrained tests. Bjerrum's data showed that the difference between vane and back-computed shear strengths increases as the plasticity index of the clay increases whereas Bishop and Bjerrum's data, in marked contrast, showed that the back-computed shear strength and laboratory shear strength were almost equal.

Short-Term Stability of Embankments on Overconsolidated Clays and Clay Shales

A number of short-term failures of embankments on overconsolidated soils occurred even though the ϕ-equal-zero analysis indicated the embankment slopes should have been stable. Some examples include case histories by Beene (1), Wright (20), Peterson and others (16), and Hopkins and Allen (10). Safety factors from ϕ-equal-zero analyses ranged from 1.23 to 4.0 for these cases; all had liquidity indexes less than 0.36.

Short-Term Stability of a Cut or Excavated Slope in Overconsolidated Clays and Clay Shales

Because the short-term safety factory is usually at maximum during or near the end of construction, the ϕ-equal-zero analysis is often used to determine the short-term stability of a cut or excavated slope. However, stability of cuts in overconsolidated clays and clay shales may not always conform to this concept. For instance, Skempton and Hutchinson (19) described two slides in a stiff overconsolidated London clay. Based on a ϕ-equal-zero analysis and undrained shear strengths, the short-term safety factors were about 1.8.

Proposed Method of Predicting Success in a ϕ-Equal-Zero Analysis

Peck and Lowe (15) presented a portion of Bishop and Bjerrum's data (long-term failures in cuts and natural slopes) that showed that the computed safety factor of failed slopes, obtained from a ϕ-equal-zero analysis and undrained strengths, was apparently a function of the liquidity index. Peck and Lowe suggested the possibility of using that empirical relation to determine correction factors for laboratory undrained strength parameters.

By plotting additional portions of Bishop and Bjerrum's data (2) and Bjerrum's data (5) (safety factor as a function of liquidity index), a distinctive division can be observed. All data in Figure 2 represent failures obtained by using the ϕ-equal-zero analysis and undrained shear strengths from UU, U, or FV tests. For failures in soils with a liquidity index equal to or greater than approximately 0.36, the safety factors estimated by using ϕ-equal-zero analysis and UU or U strengths should have an accuracy with ±15 percent (Figure 2), and design safety factors as low as 1.3 may be justified in many routine designs. For obtaining undrained strength from in situ vane shear tests, the vane strength should be corrected.

For failures in soils with a liquidity index less than about 0.36, use of ϕ-equal-zero analysis and UU or U strengths gives safety factors that are too high; in situ

shear strengths are overestimated by laboratory tests. For soils having liquidity indexes less than 0.36, the safety factor appears to be a function of the liquidity index (LI) as follows:

$$F = (3.98)(0.0192)^{LI} \quad (2)$$

The safety factor can be expressed as

$$F = S_u/S_s, \quad (3)$$

where S_u is the laboratory undrained shear strength; therefore, the corrected laboratory or softened shear strength may be expressed in terms of the standard error as follows:

$$S_s \approx (0.252)S_u(0.0192)^{-LI}(10^{\pm 0.24}) \quad (4)$$

The error in the corrected shear strength may be as large as 70 percent.

LIMITATIONS OF EFFECTIVE STRESS ANALYSES

Uncertainties in the application of the effective stress approach to the design of earth slopes arise in the selection of shear strength parameters (ϕ' and c') and the evaluation of pore pressures. Although the effective stress method has been successfully applied to normally consolidated and lightly overconsolidated clays and silty clays having an intact structure (free of fissures or joints), the method is not successfully applied to the design of slopes composed of overconsolidated clays and clay shales. Although much research (4, 17, 18) has been directed toward understanding the characteristics of those soils, overconsolidated soils still pose a slope design dilemma for engineers.

Shear Strength

Typical stress-strain curves for normally consolidated

Figure 1. Factor of safety as a function of plasticity index.

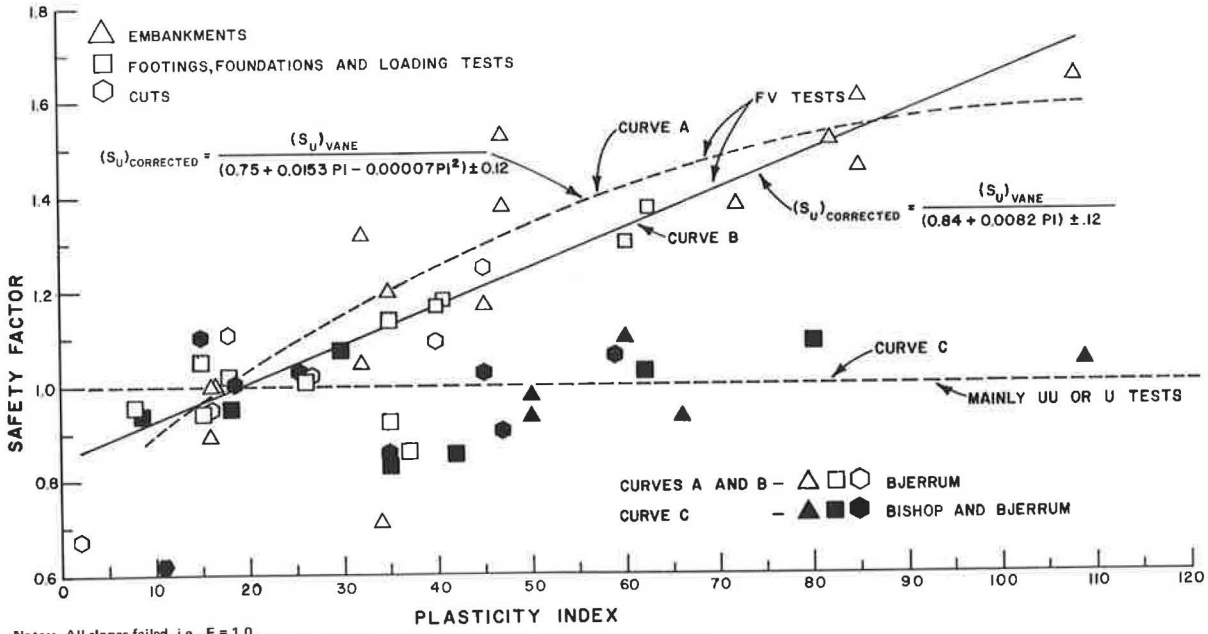

Notes: All slopes failed, i.e., F = 1.0.
Data are from Tables 1, 4, 5, and 7 in Bjerrum (3, 5) and from Table 2 in Bishop and Bjerrum (2).
All curves are by Hopkins and others (11).

Figure 2. Factor of safety as a function of liquidity index.

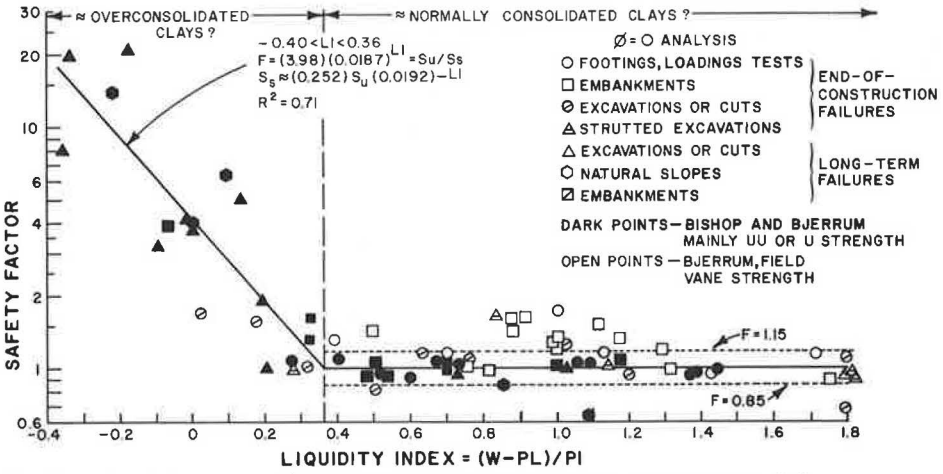

Note: Data are from Tables 2, 3, and 5 in Bishop and Bjerrum (2); Peterson and others (16); and Hopkins and others (11).

and overconsolidated clays, similarly tested under drained conditions, show that both clays reach a peak strength. When the overconsolidated soil is strained beyond peak strength, shear resistance decreases until higher strains are attained in which case the strength value decreases to a (nearly) constant value. This lower limit of resistance is the residual or ultimate strength (17, 18, 19). After the peak strength has been attained, the shear resistance of the normally consolidated clay may decrease only slightly. After higher strains are attained, the shear resistance of the overconsolidated and normally consolidated clays coincide. In heavily overconsolidated plastic clays, there is a large difference in the peak and residual strengths. In silty clays and soils of low plasticity, this difference is very small. With an increase in clay content, this difference increases even in normally consolidated clays, although not as much as in overconsolidated clays.

The softened shear strength of an overconsolidated clay (as obtained from Equation 4) may be defined as the intersection of a horizontal line projected from the peak strength of the normally consolidated clay with the stress-strain curve of the overconsolidated clay (17). The softened strength is intermediate to the peak and residual strengths and probably occurs at much lower strains (representing a condition in which a number of small, independent shear planes exist) than the residual strength (representing a condition in which the shear planes have joined to form a well-defined failure plane).

The critical state of a normally consolidated clay can be defined (17) as the state (in a drained condition) in which any further increment in shear distortion will not result in any change in water content. The water content at the critical state is equal to that ultimately attained in an overconsolidated clay that has expanded during shear.

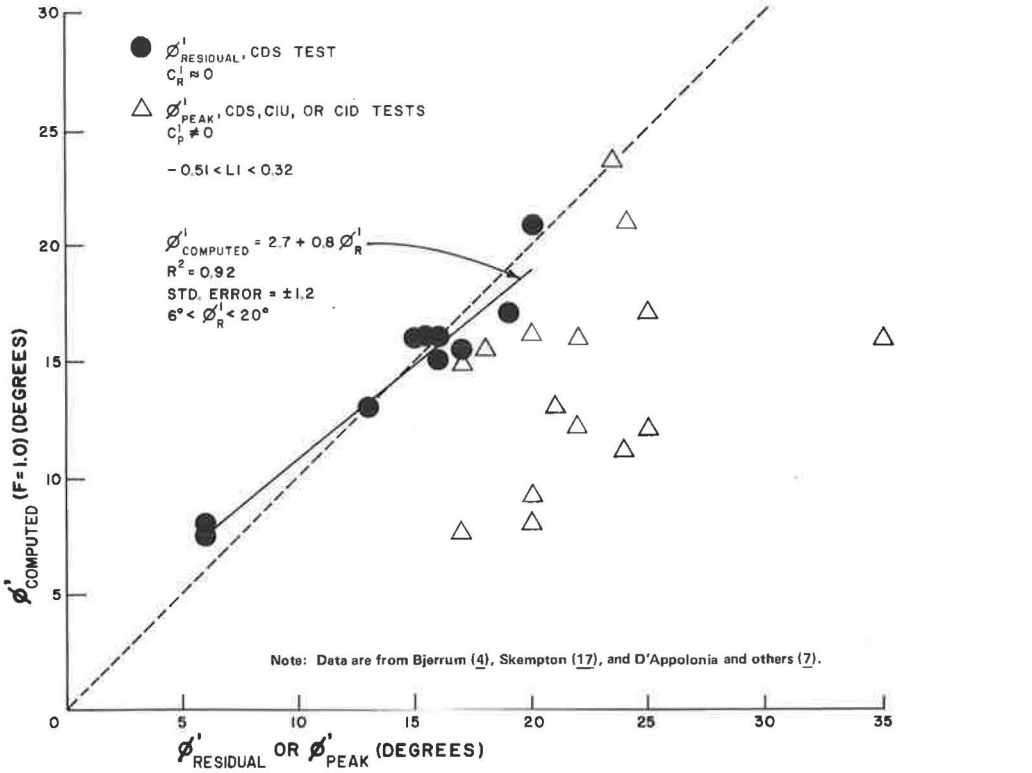

Figure 3. Back-computed shear strength parameter as a function of peak shear strength parameter from triaxial tests and residual shear strength parameter from consolidated-drained, direct shear tests.

Table 1. Case histories based on effective stress analysis.

Location	Type of Slope	Stress Analysis Factor					Factor of Safety			Reference
		w	PL	LL	PI	LI	Peak	c = 0	Residual	
Bluegrass Pky, MP 21	Fill[a]	20	24	34	10	-0.40	1.46	—	—	11
West Ky Pky, MP 96	Fill[a]	15	19	31	12	-0.33	1.94	1.12	—	11
Bluegrass Pky, MP 43	Fill	17	34	16	18	-0.08	≥1.00	1.10	—	11
Selset	NS	12	13	26	13	-0.08	1.03	<1.00	0.69	2
I-64, MP 118	Fill[a]	23	25	53	28	-0.07	1.28	0.97	0.77	10
Weirton, W. Va.	Cut	26	25	51	26	0.04	1.51	—	≈1.00	7
Northolt	Cut	30	28	79	51	0.04	1.63	0.77	0.54	19
Jackfield	NS	21	22	44	22	0.05	2.06	>1.00	1.11	18
Kensel Green	RW	33	30	83	53	0.06	1.60	—	0.60	18
Sudburry Hill	Cut	31	28	82	54	0.06	2.27	1.05	0.74	19
I-64, MP 44	Fill[a]	21	18	40	22	0.14	1.01	0.72	—	11
Amuay	NS	30	24	64	41	0.15	2.27	<1.00	0.50	12
US 119	Fill[a]	21	19	24	7	0.25	1.13	1.13	—	11
Seven Sisters, S-6	Fill	45	26	85	59	0.32	1.65	—	—	16
Lodalen	NS	31	18	36	18	0.72	1.07	—	0.73	19
Drammen	NS	35	18	25	17	1.00	1.01	—	—	19

Note: NS = natural slope and RW = retaining wall.

[a] Fills located on sloping foundations.

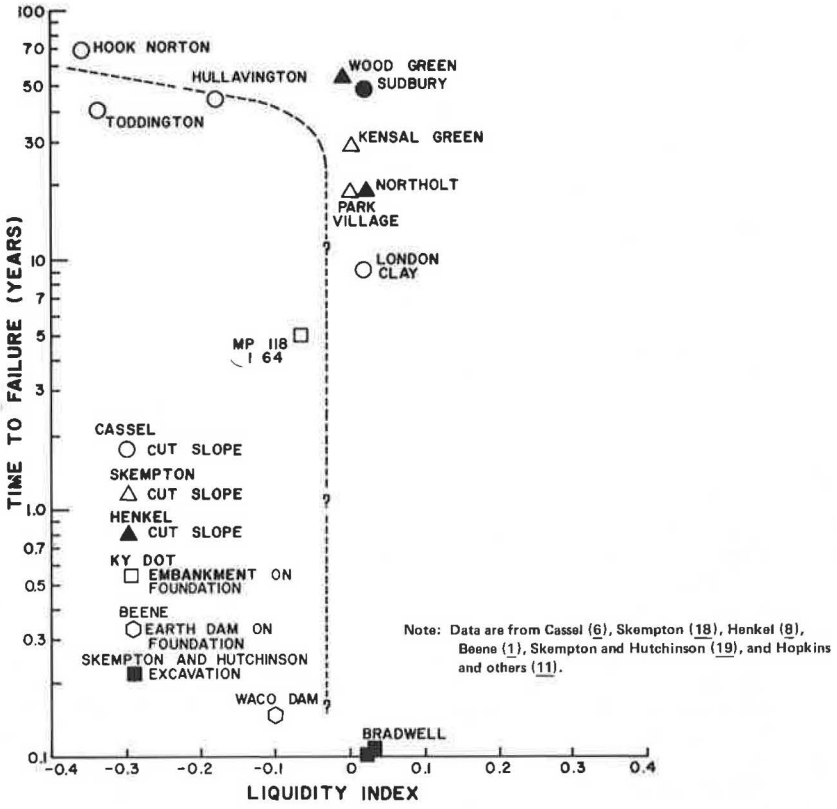

Figure 4. Time to failure of overconsolidated clays and shales as a function of liquidity index.

Peak and Residual Shear Strengths

Bjerrum (4) assembled shear strength data on a number of first-time failures of natural and cut slopes in overconsolidated clays and clay shales that showed that the average shear stress along the failure surface was much lower than the shear strength measured from laboratory triaxial tests. In each case, the peak shear strength parameters (ϕ_p' and c_p') were higher than the back-computed parameters (ϕ_c' and c_c'), which are assumed equal to zero, and, therefore, the safety factors were too high. The liquidity indexes of these clays ranged from -0.51 to 0.25. Discrepancies between the field (back-computed) and laboratory strengths are shown in Figure 3. The back-computed effective stress angle of shearing resistance is plotted as a function of the peak effective stress parameter obtained from triaxial tests. Even though cohesion was not considered, the data plot below the line of equality. If residual shear strengths are used, there is better agreement between thre computed shear strengths and those determined by direct shear tests.

Use of the residual shear strength parameters (ϕ_r' and c_r') in effective stress analyses does not necessarily yield safety factors that are in agreement with the actual safety factor at failure, although the error in the safety factor based on residual strength is generally smaller than the error in the safety factor based on peak strength. Table 1 gives a number of well-documented embankment, cut slope, and natural slope failures based on the effective stress analysis summarized and arranged according to increasing values on the liquidity indexes. Except for the case by D'Appolonia and others (7), all cases are first-time failures. Those case records clearly show that the effective stress analysis based on residual strength generally gives safety factors that are less than one. All of those cases, except for the last two failures given in the table, involve soils that have liquidity indexes less than 0.36. Also, the effective stress analysis based on peak strength yields safety factors that are too high and may be as much as 100 percent in error. Additionally, the use of c_p' equal to zero and ϕ_p' does not always yield the correct safety factor.

Evaluation of Pore Pressures

If the excess and initial pore pressures are known when designing a cutting in a clay or an embankment on a clay foundation, the stability of these earth structures may be determined during or at any time after construction piezometers are installed to obtain the necessary pore pressure data, the effective stress analysis is limited pore pressures are difficult, and the results obtained from such methods are highly questionable [Moh and others (14]. Additionally, determination of stability of the cut or embankment at any time requires that dissipation of excess pore pressures must be estimated, and these estimations are generally based on the results of consolidation tests that may be inaccurate. Unless percent in error. Additionally, the use of c_p' equal to zero and ϕ_p' does not always yield the correct safety factor. to analyzing the long-term stability of cuts and embankments. For this condition, the excess pore pressures are assumed equal to zero. In the case of a cutting in clay, the pore pressures are obtained from a prediction of the steady seepage pore pressures. In the case of an embankment, the pore pressures are usually obtained from groundwater level observations in boreholes. If large fluctuations in groundwater levels may exist, then pore pressure data may be inaccurate. If the embankment is located on a sloping foundation and damming of the groundwater may occur, then prediction of the steady seepage pore pressures is difficult, especially where large fluctuations of the groundwater level may occur.

If a valid comparison between field and laboratory shear strengths in terms of effective stress is to be made, then accurate values of pore pressures existing at the time of failure must be known. The back-computed

shear strength parameters (ϕ'_c and c'_c) are particularly sensitive to the magnitude of the pore pressures used in the computation. Inaccurate pore pressures may produce an error of several degrees in the computed parameter (ϕ'_c). An accurate determination of the pore pressures in a landslide at failure poses certain difficulties. Even when piezometers are installed, measurements obtained may not correspond to the pore pressures existing at the time of failure, particularly when the failure is preceded by a heavy rainfall and field personnel may not be present at the time of failure. For delayed failures in which several years may be required for the pore pressures to reach the steady-state values, use of measured pore pressures obtained before pore pressure equalization has occurred will lead to computed parameters (ϕ'_c and c'_c) that cannot validly be compared to laboratory shear strength parameters.

Slope Design Dilemma

Observations (4) suggest the rate of development of a continuous sliding surface in a clay slope before failure varies from one type of clay to another. In the stiffer clays, the rate may be very slow; delay of the failure may be in years. The data shown in Figure 4 suggest that, for clay soils having liquidity indexes less than approximately -0.1 to -0.2 (very stiff clays), the failure delay may be several years. In slopes where the liquidity indexes are higher, the delay in failure may be very short.

Because the critical-state shear strength of overconsolidated clays cannot readily be determined, a practical approximation to the critical state might be obtained from triaxial tests performed on normally consolidated samples remolded at a water content (w_c) as follows:

$$w_c = (0.36)PI + PL \qquad (5)$$

where PL is the plastic limit and the constant 0.36 is the liquidity index at the break point shown in Figure 2.

SUMMARY AND CONCLUSIONS

1. If the stress history and moisture state of the clay are not regarded, then application of the ϕ-equal-zero analysis for designing an embankment on a clay foundation or a slope cut in a clay may lead to erroneous conclusions concerning the stability of the slope. For clays having a liquidity index equal to or greater than approximately 0.36, ϕ-equal-zero analysis based on laboratory undrained strengths will yield fairly reliable safety factors, provided the liquid limit and plasticity index of the clay are equal to or below values of about 80 and 30 percent respectively. For clays having a liquidity index below a value of about 0.36, ϕ-equal-zero analysis will probably yield safety factors that are too high. The reliability of the high safety factors may depend on the liquidity index of the clay. For clays having a liquidity index less than about -0.1, the time to failure may vary from a few days or months to several years. If high safety factors are obtained from a ϕ-equal-zero analysis, then Figure 2 should be reviewed to evaluate the probable success of the slope design. The stability of the slope might be checked by using the corrected undrained shear strength given by the empirical relation in Equation 4.

2. The use of uncorrected vane shear strength to determine the stability of an embankment on a soft foundation, cut slopes, footings, and loading tests may yield unreliable results. The vane shear strength should be corrected by the empirical relation in Equation 1.

3. The liquidity index appears to be a general indicator of the stress history of a clay. Clays having a liquidity index less than about 0.36 might be considered to be overconsolidated while clays having a liquidity index greater than 0.36 might be considered normally consolidated.

4. The use of residual shear strength may be too conservative and expensive in many slope design problems involving overconsolidated clay, especially in cases in which temporary cuts are made. However, the use of peak shear strength in such soils may be unreliable and unsafe. The intermediate shear strength obtained from triaxial tests performed on normally consolidated clays remolded to a water content given by Equation 5 might provide a practical value for use in designing slopes against first-time failures.

REFERENCES

1. R. B. Beene. Waco Dam Slide. Journal of the Soil Mechanics and Foundations Division, Proc., ASCE, Vol. 93, No. SM4, July 1967.
2. A. W. Bishop and L. Bjerrum. The Relevance of the Triaxial Test to the Solution of Stability Problems. Proc., ASCE, Research Conference on Shear Strength of Cohesive Soils, Boulder, Colo., June 1960.
3. L. Bjerrum. Embankments on Soft Ground. Proc., ASCE, Specialty Conference on Performance of Earth and Earth-Supported Structures, Purdue Univ., Lafayette, Ind., June 11-14, 1972.
4. L. Bjerrum. Progressive Failure in Slopes in Overconsolidated Plastic Clay and Clay Shales. Journal of the Soil Mechanics and Foundations Division, Proc., ASCE, Vol. 93, No. SM5, Sept. 1967.
5. L. Bjerrum. Problems of Soil Mechanics on Soft Clays and Structurally Unstable Soils. Proc., 8th International Conference on Soil Mechanics, Moscow, 1973.
6. F. L. Cassel. Slips in Fissured Clay. Proc., 2nd International Conference on Soil Mechanics and Foundation Engineering, Rotterdam, Vol. 2, 1948.
7. E. D'Appolonia, R. Alperstein, and D. J. D'Appolonia. Behavior of a Colluvial Slope. Journal of the Soil Mechanics and Foundation Division, Proc., ASCE, Vol. 93, No. SM4, July 1967.
8. D. J. Henkel. Investigation of Two Long-Term Failures in London Clay Slopes at Wood Green and Northolt. Proc., 4th International Conference on Soil Mechanics and Foundation Engineering, London, Vol. 2, 1957.
9. D. J. Henkel and A. W. Skempton. A Landslide at Jackfield, Shropshire, in a Heavily Over-Consolidated Clay. Geotechnique, Vol. 5, 1955.
10. T. C. Hopkins and D. L. Allen. Investigation of a Side-Hill Embankment Slope Failure on I-64, Bath County, Milepost 118. Division of Research, Kentucky Department of Highways, 1971.
11. T. C. Hopkins, R. C. Deen, and D. L. Allen. Effects of Water on Slope Stability. Division of Research, Kentucky Department of Highways, 1975.
12. T. W. Lambe. Soil Parameters for Predicting Deformations and Stability. Proc., 8th International Conference on Soil Mechanics, Moscow, 1973.
13. K. Y. Lo, J. I. Adams, and J. L. Seychuk. The Shear Behavior of a Stiff Fissured Clay. Geotechnique, 1970.
14. Z. Moh, E. W. Brand, and J. D. Nelson. Pore Pressures Under a Bund on Soft Fissured Clay. Proc., ASCE, Conference on Performance of Earth and Earth-Supported Structures, Purdue Univ., Lafayette, Ind., June 11-14, 1972.

15. R. B. Peck and J. Lowe. Shear Strength of Undisturbed Cohesive Soils. Proc., ASCE, Research Conference on Shear Strength of Cohesive Soils, Boulder, Colo., June 1960.
16. R. Peterson, J. L. Jaspar, P. J. Rivard, and N. L. Iverson. Limitations of Laboratory Shear Strength in Evaluating Stability of Highly Plastic Clays. Proc., ASCE, Research Conference on Shear Strength of Cohesive Soils, Boulder, Colo., June 1960.
17. A. W. Skempton. First Time Slides in Over-Consolidated Clays. Geotechnique, Vol. 20, 1972.
18. A. W. Skempton. Long-Term Stability of Clay Slopes. Geotechnique, Vol. 14, 1964.
19. A. W. Skempton and J. Hutchinson. Stability of Natural Slopes and Embankment Foundations—State-of-the-Art Report. Proc., 7th International Conference on Soil Mechanics and Foundation Engineering, Mexico, 1969.
20. S. G. Wright. A Study of Slope Stability and the Undrained Shear Strength of Clay Shales. Univ. of California, Berkeley, PhD thesis, 1969.

Publication of this paper sponsored by Committee on Embankments and Earth Slopes.

State-of-the-Art Report on Field Instrumentation for Pavement Experiments

S. F. Brown, University of Nottingham, England

The various instruments available for taking in situ measurements of stress, strain, deflection, temperature, pore pressure, soil suction, and axle load in pavement experiments are described. Discussions of the desirable objectives of pavement experiments and comments about instrumentation concerning the unavailability of general purpose equipment and the need to design instruments for specific applications are presented. Earth pressure cells are discussed and information is given on the theory of their in situ performance, design considerations, and installation procedures. The need for correct calibration is emphasized. Pressure cells that have been used in various projects are described as illustrative of the kinds of instruments that can be used. A detailed design procedure for the simplest type of cell and a discussion concerning the use of charts to assist with the calculations are provided. Strain measuring devices for use in soils, granular materials, and asphalt materials are described and comments are made on the relative merits of each. Even though there is a lack of available information about other instrumentation, the current state of the art is described for each case presented.

Developments in analytically based design procedures for flexible pavements have reached the stage in which information about theoretical analysis and material properties is available. Furthermore, design methods that use the information dealing with the traffic-associated failure mechanisms of cracking and rutting have been reported in some detail in the literature. However, in practice the situation is that design agencies still use empirical methods based on the findings from limited, full-scale test sections and often incorporate an overall California bearing ratio (CBR) thickness requirement.

The gap between current practice and current research knowledge available can best be bridged by more agencies carrying out well-instrumented, full-scale experiments that are properly planned to monitor for correct parameters. In short, recent research developments must be verified in practice on a scale larger than that previously used so that the economic worth of these developments can be assessed by highway engineers.

The success of full-scale or pilot-scale experiments in assisting with the development of improved design procedures depends to a large extent on the accuracy of the measurements made on the structure. This success can only be achieved by use of adequate instrumentation that is installed correctly. This report explains the principles of the various instruments that can be used in pavement experiments and describes many of those that are successful in practice. The emphasis is on stress-measuring devices because these have been researched in the past. Instrumentation for evaluating in situ stress, strain, deflection, temperature, pore pressure, soil suction, and axle load is discussed. Because the amount and kind of instrumentation depends on the objectives of the experiment and the money available, this report can be used to assist engineers in planning future experiments.

Instrumented pavement experiments, particularly on public highways, should not be undertaken lightly. These experiments can be expensive both in terms of instrumentation and labor as well as in interruptions to the normal processes of construction. It is better to use fewer instruments that are well understood and reliable to provide good but limited data, than to use a vast array of ironmongery whose behavior is something of a mystery. Currently, field instrumentation is definitely not a matter of buying commercial equipment that can be easily installed in the road and expected to produce quick and reliable answers. While there is some equipment commercially available for measuring some parameters, this equipment should only be used with a full understanding of its operating principles because it is rare that field instruments have universal applicability. These instruments generally need to be designed for a purpose.

Many of the difficulties and costs of full-scale experiments on public highways can be avoided by using pilot-scale experiments or full-scale trials on special test roads. Many more projects involving these more carefully controlled experiments seem desirable because, if new design concepts do not work under such

conditions, they are unlikely to be successful in practice.

Instruments that have to be installed in the pavement structure clearly need to be designed to resist the rigors of the construction process, both environmental and mechanical. These factors can account for several instrument failures in a particular experiment and point to the need for duplication of instruments. Instrumentation research has clearly shown that one of the major sources of error, even for well-designed instruments, arises from installation effects. Even experienced technicians using well-tried methods cannot guarantee freedom from this problem because it is related to the overall problem of interference. Interference results from the presence of the instrument in the pavement, which causes errors in reading. Because of these uncertainties, the more instruments that can be installed to provide duplicate measurements the better the results will be. However, this problem should not be allowed to create a situation in which instruments are placed too close to each other because a pavement full of instruments is unlikely to perform representatively.

A comprehensively instrumented test section is likely to produce a considerable amount of data and in such circumstances, particularly if the experiment is long term, thought should be given to the provision of adequate data-acquisition and data-processing procedures. It is important that full-scale performance data should be used and not left in the cupboard in the form of uninterpreted recorder traces. In this context, the relative costs of a labor-intensive simple system and of an automated procedure should be carefully weighed.

EARTH PRESSURE CELLS

Instruments for measuring both long-term changes in stress and transient effects under free-field and boundary conditions have been extensively studied. The performance of these earth pressure cells, or soil stress gauges as they are variously described, has received more attention in the literature than the performance of most other field instrumentation that is of interest to the highway engineer. Good reviews have been published by Selig (1) and Triandafilidis (2). The determination of in situ stress, however, remains a difficult problem because it cannot be measured directly and must rely on a measurement of strain or deformation within the instrument by using an appropriate transducer. Because of the many difficulties involved, accuracies better than about 20 percent cannot be expected.

All earth pressure cells incorporate a diaphragm that is in contact with the soil. The pressure exerted on the diaphragm by the soil is then evaluated in a variety of ways that depend principally on the particular practical application. A typical, simple type of cell is shown in Figure 1. This cell has a diaphragm that is built into an outer ring and is free to deflect under the action of soil pressure. The strain on the inside of the diaphragm, or its deflection, is then measured by using a suitable transducer. Other pressure cells have diaphragms that are restrained by mercury or oil contained within the cell and that transmit the pressure to a second internal diaphragm, which carries the strain gauges. Detailed descriptions of particular instruments of both kinds follow.

The introduction of a measuring instrument into a soil mass disturbs the stress distribution, as shown in Figure 2 (1). The overall aim in designing pressure cells is to obtain a measure of the free-field stress, that is, the value that would have occurred at the location if the instrument had not been present. This measurement can best be achieved by designing an instrument that has a minimum disturbing effect, though, as in most design problems, this involves certain compromises because of conflicting considerations. The redistribution of stress over the diaphragm, as shown in Figure 2, means that the instrument will usually overregister the free-field stress, though underregistration is also possible.

Theory

An understanding of the interaction between pressure cells and the surrounding soil has been developed by the use of both theory and experiment. The main requirement is that the degree of overregistration or underregistration should be predictable and that it should be relatively constant for a particular cell.

Cell registration (C) has been defined as follows:

$$C = \text{stress indicated by cell/free-field stress} \quad (1)$$

The stress indicated by the cell is based on relating the electrical output from the instrument to stress by way of a mechanical bench calibration test in which a known stress is applied directly to the diaphragm. Such a test can be carried out by placing the cell in a pressure chamber of by using the arrangement shown in Figure 3.

Early work on the theoretical evaluation of cell registration by Taylor (3) and Monfore (4) was extended by Tory and Sparrow (5). The latter considered the pressure cell to be located in a uniaxial stress field and summarization of their results are shown in Figure 4. The following equations indicate the importance of two parameters:

$$\text{Aspect ratio} = B/D \quad (2)$$

and

$$\text{Flexibility factor} = E_s d^3/E_c t^3 \quad (3)$$

where

- B = cell thickness,
- D = cell diameter,
- E_s = Young's modulus of the soil material,
- E_c = Young's modulus of the cell material,
- d = diameter of the cell diaphragm, and
- t = thickness of the cell diaphragm.

In effect, the flexibility factor (F) is the ratio of soil stiffness to diaphragm stiffness.

Figure 4 shows that the stiffness of the cell diaphragm should be relative to the soil in which it is installed so that the cell registration can be approximately constant. Ideally, a flexibility factor less than unity should be used. Also shown is how registration increases as aspect ratio increases.

In practice, pressure cells are generally used in three-dimensional stress fields and hence the influence of stresses acting parallel to the diaphragm needs to be quantified. Fossberg (6) carried out finite-element analyses of axisymmetric situations around a particular free-diaphragm, pressure cell that has dimensions similar to the Nottingham instrument shown in Figure 1. Figure 5 shows the results of Fossberg's analyses that indicate that increases in the cross stress (σ_T) cause decreases in cell registration, but that the influence of flexibility factor is similar to the uniaxial stress case. For a stress ratio of zero, which is the uniaxial case, Fossberg's results compare favorably with those of Tory and Sparrow (5).

Most of Fossberg's calculations were carried out under conditions of zero strain in the soil parallel to the cell diaphragm, i.e., K_o conditions. He also considered the case of no lateral restraint using the zero stress ratio. However, an induced lateral tensile stress, which could clearly not be transmitted to the cell, was indicated; therefore, an appropriate correction was made to eliminate the stress. Hence, the basic assumptions became similar to those of Tory and Sparrow (5).

A more extensive theoretical investigation has been reported by Collins and others (7). They evaluated cell registrations relative to stresses both normal and parallel to the diaphragm. These were defined as follows:

C_N = stress acting normal to diaphragm/free-field stress (4)

and

C_T = stress acting normal to diaphragm/free-field cross-stress (5)

Hence, for a pressure cell subjected to free-field stresses (σ_N) that are perpendicular to the diaphragm with σ_T in the two perpendicular directions the following equation is used.

$$C = (C_N \sigma_N + 2C_T \sigma_T)/\sigma_N = C_N + 2C_T (\sigma_N/\sigma_T) \quad (6)$$

As shown, both C_N and C_T depend on the aspect ratio and the elastic properties of the soil and the cell.

The major difference in basic assumptions between the work of Collins and others (7) and Fossberg (6) is that the former made no assumptions concerning lateral strain conditions and their cell was a homogeneous inclusion having the shape of a spheroid. Both Fossberg and Tory and Sparrow took account of the diaphragm deflection in modeling an actual pressure-cell situation. Hence, the theory by Collins and others is relevant to

Figure 1. Nottingham pressure cell.

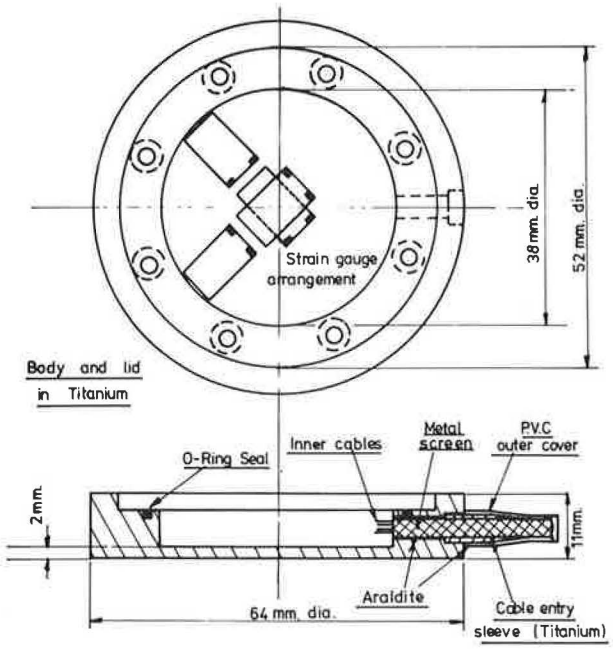

Figure 2. Redistribution of stress because of presence of a pressure cell.

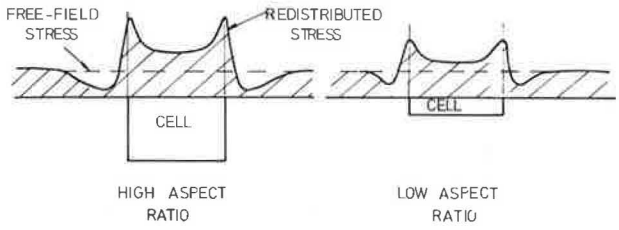

Figure 3. Arrangement for bench calibration of Nottingham pressure cell.

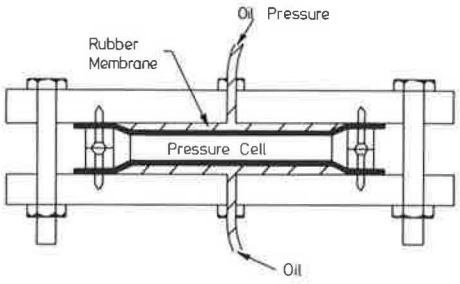

Figure 4. Theoretical pressure cell registrations.

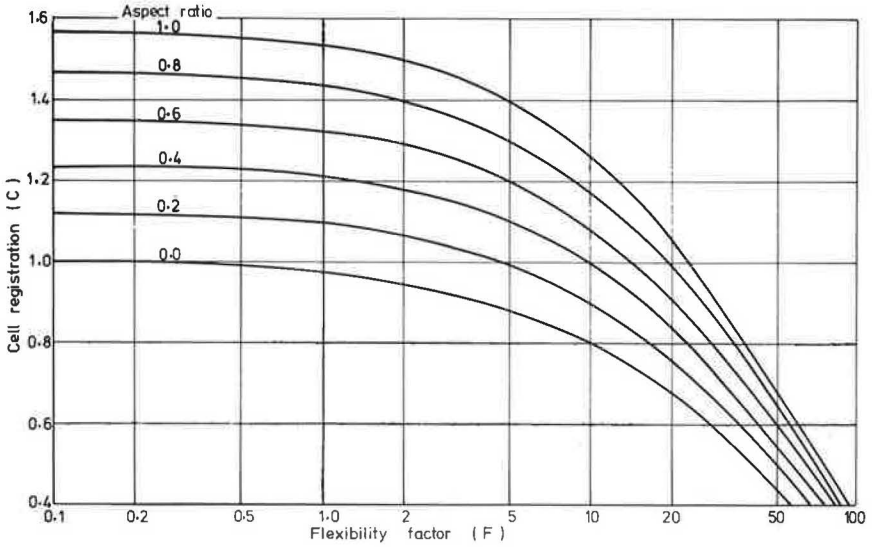

Figure 5. Theoretical cell registration for Nottingham cell based on Fossberg's theory.

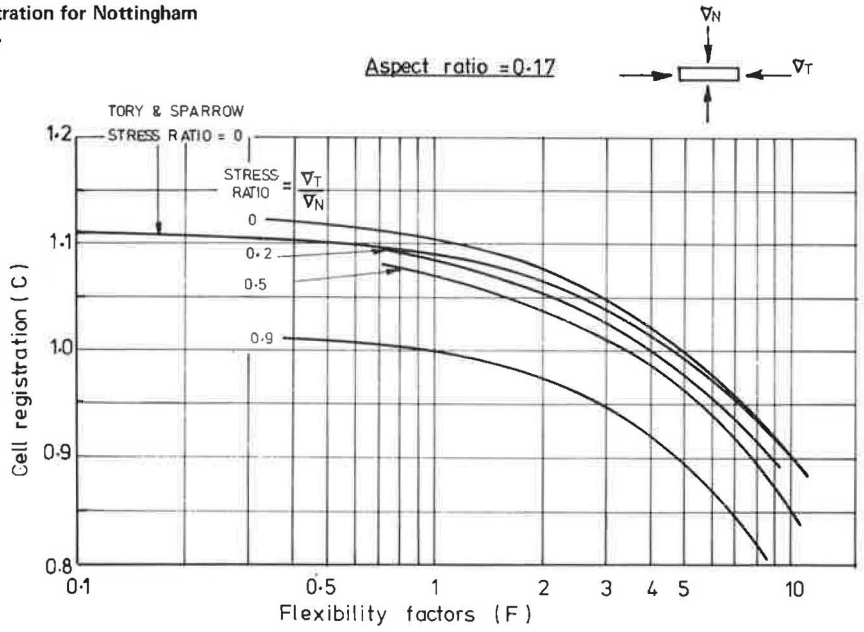

Figure 6. Comparison of theoretical pressure cell registrations for zero stress ratio.

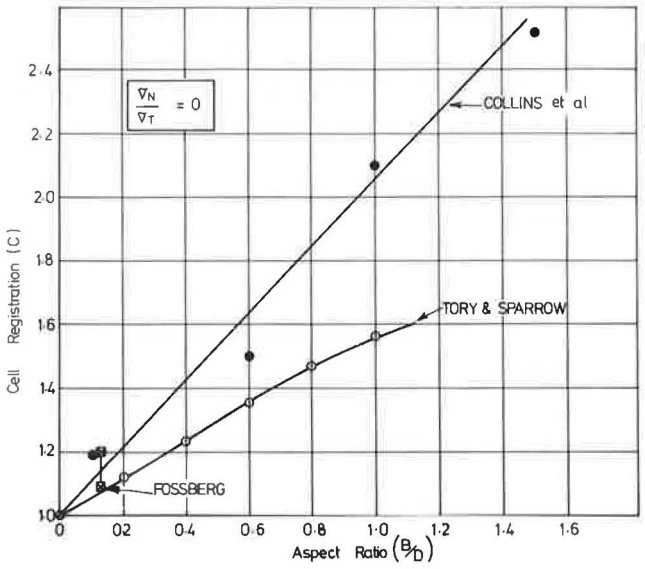

Figure 7. Comparison of theoretical pressure cell registrations at various stress ratios.

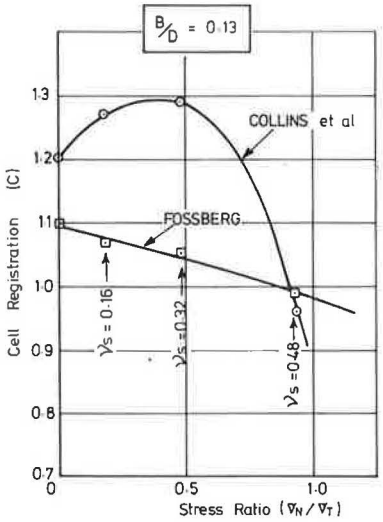

pressure cells with restrained diaphragms while the other theories are only applicable to free diaphragms. For conditions in which the diaphragm is very stiff, relative to the soil ($F \leq 1$), it is possible to compare the three sets of results. Figure 6 shows a comparison of these results for the zero stress ratio case, which is the only one dealt with by all three solutions. Collins and others (7) have shown significantly higher registrations than those shown by Tory and Sparrow. The discrepancy between both sets of registrations increased as the aspect ratio increased.

Fossberg's results were for only one aspect ratio (0.13), but he did consider lateral strains. With no lateral restraint and no correction for induced lateral tension, Fossberg's conditions were the same as Collins and others, and this agreement is shown in Figure 6. Figure 5 shows this same comparison but with Tory and Sparrow's results. Hence, it would seem that the discrepancy between Collins and others and Tory and Sparrow is because of the effect of lateral tension on the cell. Because this effect cannot be transmitted in practice, the latter results are more realistic in this particular case of zero stress ratio. Collins and others applied tensile free-field stresses in their analyses and hence the induced cross stresses were actually compressive. Both have been reversed in the above discussion for compatibility with the other solutions.

A comparison between the various stress ratios used by Collins and others and by Fossberg at the particular aspect ratio Fossberg used is shown in Figure 7. Fossberg generated different stress ratios by considering K_o conditions and varying Poisson's ratio (ν_s) for the soil. Agreement between the solutions only occurs at two points: One is the zero stress ratio previously discussed and the other is a stress ratio of approximately 1 and a Poisson's ratio of nearly 0.5. For these values, K_o conditions apply and both theories have the same assumptions regarding lateral strain. For the lower stress ratios and Poisson's ratios, the solutions by Collins and others involve the development of lateral strain and the possibility of associated tensile stresses.

This discussion has indicated that pressure cell registration is affected by the applied stress ratio and the lateral strain situation as well as the other factors noted above that are in relation to Figure 4. Of these various factors, the one that is the least well defined is the

lateral strain condition. In the ground, a pressure cell measuring vertical stress is likely to be in a K_o situation while an instrument measuring horizontal stress could experience some lateral strain. The former situation is predictable with some confidence from theory while the latter presents two difficulties. In addition to the poorly defined lateral strain condition, stress ratios greater than unity are likely to be applied.

It would seem prudent at this stage in the understanding of soil-cell interaction to try and design cells in such a way that the effects of both stress ratio and lateral strain conditions are minimized. This approach implies reducing C_T to zero in Equation 6, which has been suggested by Mills and others (8). Figure 8, derived from Collins and others (7), shows how this may be done by choosing an aspect ratio appropriate to the particular Poisson's soil ratio. Unfortunately, the required aspect ratio is sensitive to Poisson's ratio and as the latter is difficult to specify with accuracy and could also vary with stress conditions, this approach can, at best, only be approximate. Also shown is the range of aspect ratios that can be used for a particular Poisson's ratio for values of C_T between -0.05 and +0.05, which seems to be a reasonable range.

Design Considerations

The foregoing theory provides some guidelines for the design of pressure cells and an assessment of their likely registration. There are, however, a number of other design considerations, some of which have resulted from experimental investigations while others are concerned with practicalities. These considerations are outlined below and detailed information follows.

Peattie and Sparrow (9) showed that the diaphragm should not occupy more than 45 percent of the total area of the cell face. If the above limitation is observed, the high stresses shown in Figure 2 that occur at the edge of the cell would be confined to the annular ring around the diaphragm.

A stiff annular ring is also required to minimize cross sensitivity, so while Peattie and Sparrow's recommendations were aimed at free-diaphragm cells, the use of these rings would also seem advisable for restrained diaphragms. It is important to distinguish between this mechanical cross sensitivity and the effects produced by various stress ratios, as previously discussed.

The overall dimensions of the cell should be related to the soil particle size. While large particles can be kept away from the diaphragm during installation, the soil in contact with the diaphragm should not be allowed to vary greatly from that in the surroundings, otherwise further redistributions of stress are likely. Kallstenius and Bergau (10) have suggested that the diaphragm diameter should be at least 50 times that of the largest soil particle. Instruments that rely on indirect measurement of diaphragm deflection or strain are likely to be less affected by the individual point contacts of large particles than those that rely on direct measurement such as the cell in Figure 1.

In the case of free diaphragms, the requirement that a stiff diaphragm should be used conflicts with the need for an adequate electrical signal from the transducer. In these circumstances, an appropriate strain gauge or other transducer must be selected to provide an electrical output of adequate size for the available monitoring equipment.

In establishing the maximum stress that a pressure cell can be used to measure, two criteria must be considered. First, the central deflection of the diaphragm should not exceed $1/2000$ of its diameter (11), and, second, the maximum tensile stress in the cell material should not approach the yield value too closely. This maximum stress occurs in the radial direction at the built-in edge of the diaphragm on the outside of the cell.

Both diaphragm deflection and stress are dependent on the material from which the cell is manufactured. It is important that corrosion should be avoided, particularly in long-term installations, and, for this reason, three metals such as aluminium alloys, stainless steel, and titanium have been chosen most often by various investigators.

Two important practical considerations are that the cell should be waterproof and that cable entries should be strong enough to resist the stresses imposed during installation. The arrangement shown in Figure 1 has generally been satisfactory in practice but has been improved recently by screwing the cable entry into the body and by covering the cable with an additional strengthening sleeve where it passes into the metal cable entry (12).

The selection of a particular type of pressure cell will depend on various factors that will include the peripheral equipment available to drive and monitor the cells. Those cells with a simple, strain-gauge bridge only require a power pack, which balances circuitry, and a recorder for dynamic work. More expensive cells also tend to require more expensive ancillary equipment. However, the other instrumentation envisaged for a particular experiment should be taken into account in the planning stage.

Laboratory Calibration Tests

The foregoing discussion has indicated that a pressure cell will in general not register the exact field stress; however, with well-designed instruments, the error may not be very large. Experience with controlled calibration tests has often indicated errors larger than those predicted by theory. Perhaps these errors are because of the difficulty in precisely modeling the in situ conditions, particularly those resulting from placement technique.

Thus, it is clearly desirable to calibrate pressure cells under controlled laboratory conditions that reproduce, as closely as possible, the field situation. This situation implies that attention be paid to moisture content and compaction of the soil generally and in particular around the instrument; that the same installation technique is followed as on site; that the cell is subjected to the range of stresses in all anticipated directions; and that this is done at the appropriate rate of loading.

Two kinds of tests have been used for pressure cells, both employing large-diameter (225 to 950 mm) cylindrical samples with the cell installed centrally. The samples have been either tested in a rigid cylindrical container reproducing K_o conditions (2, 6, 13, 14) or as triaxial samples (15, 16, 17, 18) when the vertical and lateral stresses can be varied in different combinations.

When a pressure cell is used in a particular soil both the stress ratio and the flexibility factor can change as the stress conditions change. The magnitude of the resulting changes in cell registration has been evaluated for the U.K. Transport and Road Research Laboratory/linear variable differential transformer (TRRL/LVDT) cell (Figure 9) and the Nottingham cell (Figure 1) in two different soils, a silty clay and a fine crushed stone under a variety of stress conditions (19). The range of registrations from theoretical considerations was less than 10 percent, which, from a practical viewpoint, falls within the scatter band obtained in most experimental work. In comparing experimental results with

Figure 8. Curve for limiting cross sensitivity.

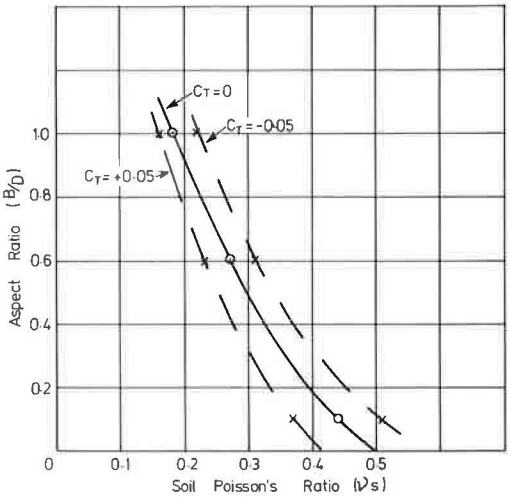

Figure 9. TRRL/LVDT pressure cell.

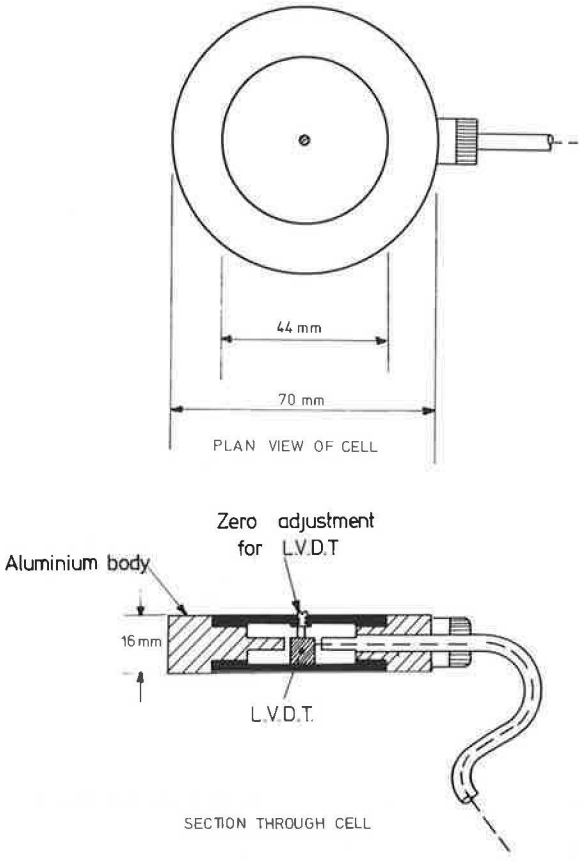

theoretical predictions, average registrations over the chosen stress range in individual calibration tests were compared with the average theoretical values. Although there was considerable scatter in the experimental cell registrations, good correlation was obtained between the mean values and those predicted from theory. Best comparison was obtained when more than six experimental results were available, which implied a fairly reliable mean value.

Hence it was concluded that the performance of pressure cells with flexible diaphragms can be predicted with some confidence, provided the anticipated stress conditions and corresponding values of soil modulus are known. It was also clear that registrations from laboratory calibration tests should be based on a reasonably large number of tests, in view of the scatter of results caused by placement technique, even when using experienced personnel. Therefore, it is even more important to obtain as many duplicate readings in a field situation as possible.

Installation Techniques

The calibration work previously summarized emphasized the need for reliable installation procedures. Experience suggests (13, 20, 21) that, for clay, a pressure cell measuring vertical stress should be installed with the diaphragm up in a precut recess in the soil surface. A trench should be provided for the cable. Care should then be taken in placing selected soil over the diaphragm to ensure that no large particles are included. After hand compacting a thin layer of such soil, the next layer of soil may be compacted by whichever site method is being used. For loose sand, Ingram (13) found that the best results were obtained by tamping the cell into the surface of the soil with a rubber-ended rod and then gently compacting the soil around the cell with a rod and a metal plate.

Details of Instruments

The instruments described in the following have been selected because they are representative of the various kinds used by different investigators; however, there are many other kinds available.

Nottingham Pressure Cell

The Nottingham pressure cell (16, 19, 20, 21) shown in Figure 1 is basically a titanium-recessed disc, the bottom of the recess forming a 2-mm thick diaphragm, with the lid enclosing the cavity. A 4-arm, active, strain-gauge bridge is bonded to the diaphragm: The gauges are arranged to reduce cross sensitivity and to give maximum output from the tension-compression characteristics of the diaphragm. The bridge is supplied by 10-V direct current (DC) and the output is fed to a galvanometer of an ultravoilet recorder. Potentiometric balance is provided across chosen arms of the bridge, and a 500 kΩ calibration resistor can be switched across one arm to simulate a fixed stress input.

The TRRL/LVDT Pressure Cell

The TRRL/LVDT pressure cell incorporates a LVDT displacement transducer set between two diaphragms that are screwed to each side of a thick annular ring, as shown in Figure 9. The core fitted to one diaphragm can be screwed to its null position in the LVDT body attached to the other diaphragm. The cell is then sealed and maintains this position under zero pressure. The cables pass through a tube with enough clearance to allow dissipation of pressure buildup in the gauge cavity. Thus, any pressure on the diaphragm is registered by the LVDT and any cross stresses are reduced by the stiff outer ring.

The TRRL Piezoelectric Pressure Cell

The TRRL piezoelectric pressure cell (22, 23) (Figure 10) uses the piezoelectric properties of quartz crystals. There are four, X-cut crystals positioned on either side of a central web (two on each side) that are connected to

Figure 10. TRRL piezoelectric pressure cells.

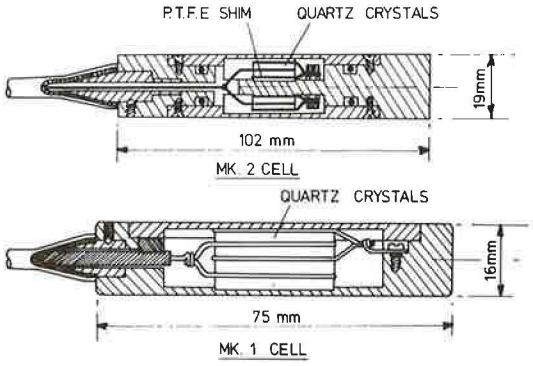

Figure 11. Kyowa pressure cell.

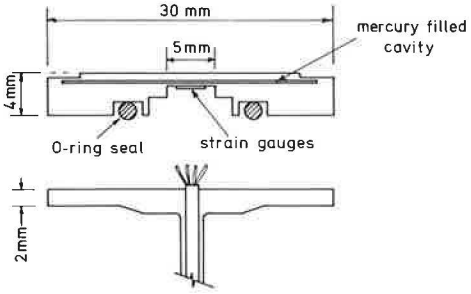

Figure 12. URS free-field stress gauge.

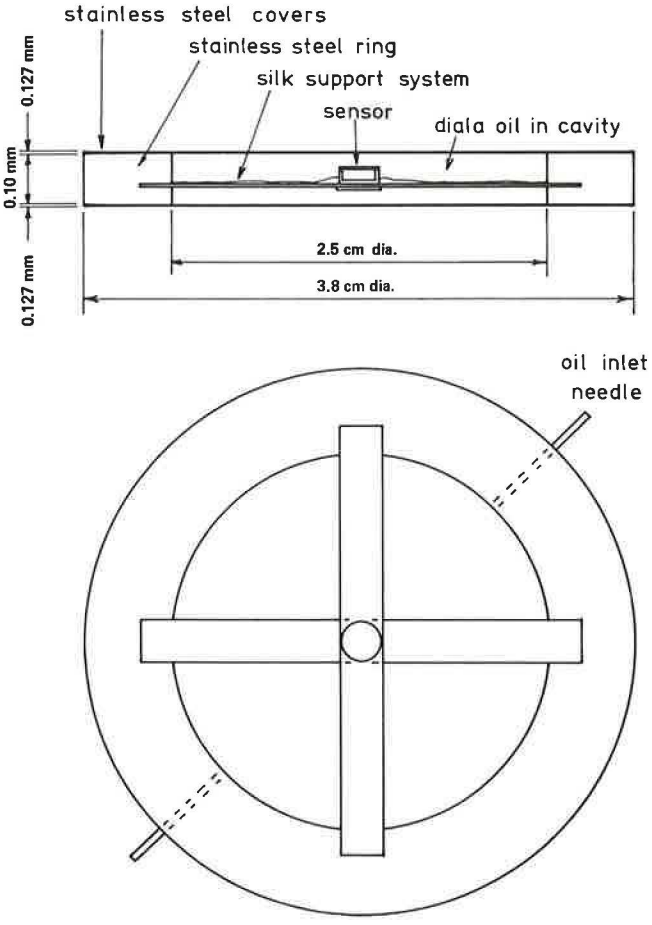

a thick annular ring. Two diaphragms are screwed to the ring in such a way that they are slightly arched by the trapped crystals. Copper shims are used to collect the charge generated across the surfaces during dynamic loading and the output is transmitted by means of a coaxial cable that is glued through a hole in the annular ring. A polytetrafluoroethylene (PTFE) sheet is inserted between the copper shims and the diaphragms to reduce the distortion caused by transmission of shear.

The Mk 1 and Mk 2 pressure cells are available to this design, the latter being of a much stiffer construction design to reduce mechanical cross sensitivity. Both cells are shown in Figure 10. The Mk 1 is only recommended for measurement of vertical stress because of its cross sensitivity. The quartz crystals of this cell only respond to changes in pressure; therefore, this cell can only be used for dynamic measurements.

Kyowa Cell

A cross section of the Kyowa cell (24) with a thin, mercury-filled cavity is shown in Figure 11. The pressure is determined by a strain-gauge bridge attached to the back of an inner secondary diaphragm with a 5-mm diameter, which is considerably smaller than the 27-mm outer diaphragm. A shortcoming in practice is the centrally situated cable entry emerging opposite the diaphragm. This arrangement has been shown to be unsatisfactory because it causes considerable disturbance to the stress regime around the cell (7). However, a normal radial edge cable entry could be incorporated without much difficulty. This cell is similar in principle to, though smaller than, the Plantema cell (25) that has an edge cable entry and the Waterways Experiment Station (WES) cell described below.

United Research Service Cell

The United Research Service (URS) cell (26) shown in Figure 12 was developed by the URS research company for the Federal Highway Administration of the U.S. Department of Transportation. It consists simply of two stainless steel discs separated by an annular ring. The central void is filled with oil and a piezoresistive transducer is mounted on crossed webbing within the oil. This cell has the advantages of low aspect ratio (0.03) and high stiffness. It is suitable for long-term static or dynamic applications. However, the cost is likely to be high.

WES Cell

A number of WES cells (29) have been developed and used by the U.S. Army Engineers at the Waterways Experiment Station over the years. These cells have varied in diameter from about 5 to 60 cm. The 15.2-cm diameter cell (27, 28, 29) that has been used successfully on a number of projects is shown in Figure 13. This cell uses the indirect diaphragm principle having a cavity filled with mercury. Details of a smaller cell (13) that incorporate twin diaphragms carrying semiconductor strain gauges are shown in Figure 14.

Summary

The above discussion about earth pressure cells was an attempt to outline the current state of the art in theory, design, and use of these instruments. A summary of the particular instruments described above is given in Table 1. This summary includes important dimensions, characteristics, usage, and relative cost of the cells and their peripheral equipment.

In general, strain-gauge bridges are suitable for

Figure 13. WES soil pressure cell.

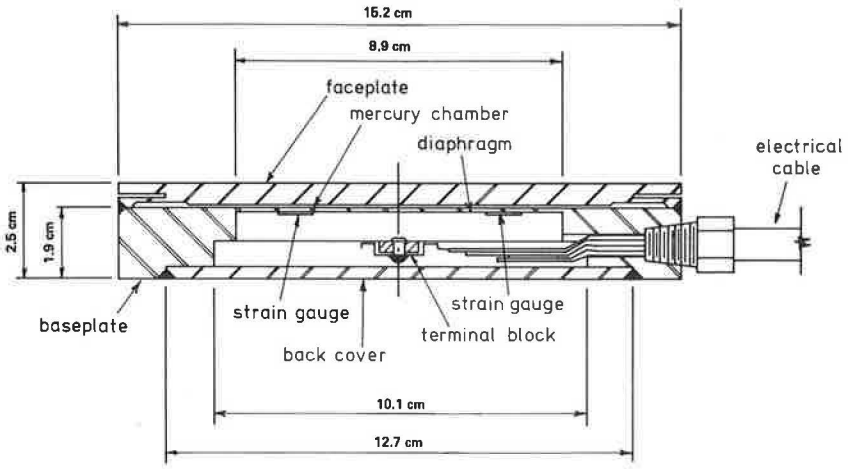

Figure 14. WES soil stress gauge.

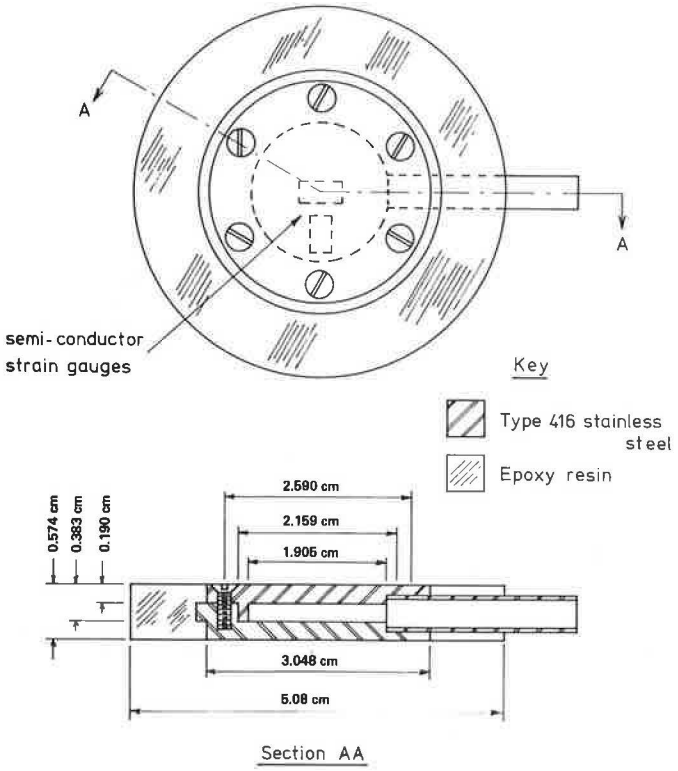

Table 1. Characteristics of various earth pressure cells.

Pressure Cell	Material	Diaphragm	Transducer	Usage	Relative Cost of Cell	Relative Cost of Peripheral Equipment	B (mm)	D (mm)	t (mm)	d (mm)	B/D	Area Ratio $=(d/D)^2$
Nottingham	Titanium	Free	Foil gauges	D, SS	Low	Low	11	64	2	38	0.17	0.35
TRRL/LVDT	Aluminum	Free	LVDT	D, SL	Medium	Medium	16	70	1.3	44	0.23	0.40
TRRL Piezo. Mk 2	Aluminum	Restrained	Quartz crystals	D	High	Medium to high	19	102	—	32	0.19	0.10
Kyowa	Steel	Indirect	Foil gauges	D, SS	Medium	Low	6	30	0.5[a] 0.1	27[a] 5	0.2	0.87[c]
URS	Stainless steel	Restrained	Semiconductors	D, SS	High	Low to medium	1.5	38	0.13	25	0.04	0.43
WES 1	Stainless steel	Indirect	Wire gauges	D, SS	Medium	Low	25	154	4.5[b]	146	0.16	0.90
WES 2	Stainless steel and epoxy	Free	Semiconductors	D, SS	Medium	Low to medium	5.7	51	1.9	19.1	0.11	0.39

Note: D = dynamic, SS = short-term static, and SL = long-term static.

[a]Outer and inner diaphragms respectively. [b]Inner diaphragm thickness varies. [c]Collar added to reduce this to 0.45.

both short-term static and dynamic applications. They are not, however, so suitable for long-term static measurements because of possible zero drift. Temperature changes contribute to this drift, but this effect can be minimized by careful matching of the resistances of strain gauges, particularly of the semiconductor type.

Temperature changes in situ will generally not be large but should not be ignored, particularly if small changes of stress are envisaged. For dynamic measurements, temperature effects and other causes of slight zero drift are not of importance, provided either a four-arm active bridge is used or dummy gauges are provided to effect temperature compensation.

Most of the cells described are not readily available through normal commercial channels. These cells were developed for particular projects, which emphasizes the need to design instruments to suit particular site situations. However, detailed procedures and design examples are given in the following for the free-diaphragm kind of cell. This cell is generally the least expensive to make and it operates for short-term static or dynamic applications.

Almost all the experience of in situ stress measurement has involved cells in soils, little work has been reported on measurements in asphalt or granular materials (21, 30, 31). The basic principles of design are the same for these materials as for soils, but, in the case of asphalt, higher stiffnesses are involved and

Figure 15. Design procedure for earth pressure cells with free diaphragms.

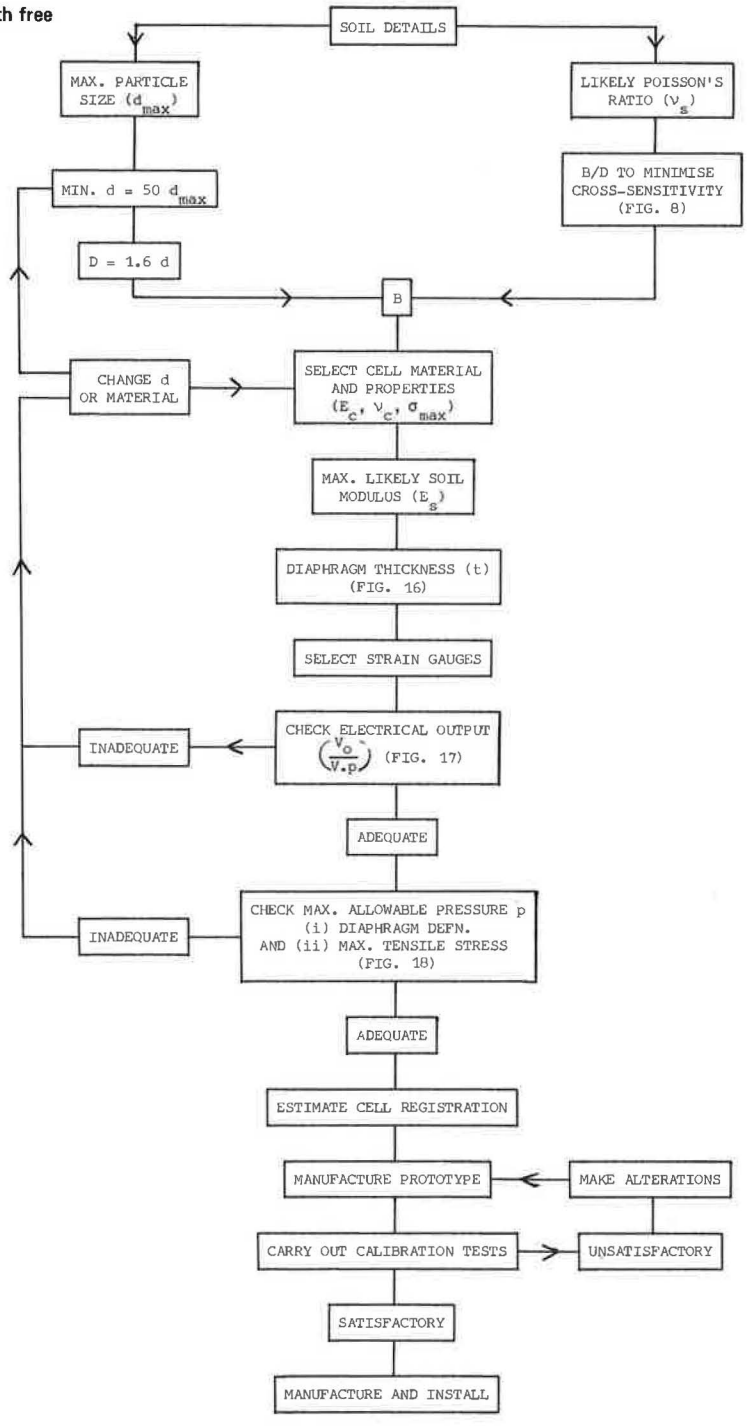

the instrument and cable will need to be resistant to the high temperatures at installation.

Design Procedure for Free-Diaphragm Earth Pressure Cells

A summary of the design procedure is presented in Figure 15. A series of graphs have been prepared and these are referred to at the appropriate points in the flow diagram to facilitate the calculations.

Thus, a desirable diameter for the diaphragm is established by considering maximum soil particle size or, in the case of fine-grained soils, factors related to the practicalities of manufacture. An initial diaphragm thickness can then be obtained by using Figure 16. This figure is based on the suggested maximum flexibility factor of unity, knowledge of the maximum soil modulus and the cell material. Aluminium, stainless steel, and titanium have been used in this graph and other graphs because they are the three most commonly used metals for pressure cells. The lines in Figure 16 are described by Equation 3, which defines the flexibility factor; Equation 3 can be rearranged as follows:

$$(d/t)^3 = (E_c/E_s)F \qquad (7)$$

Figure 16. Determination of d/t from soil modulus and cell material.

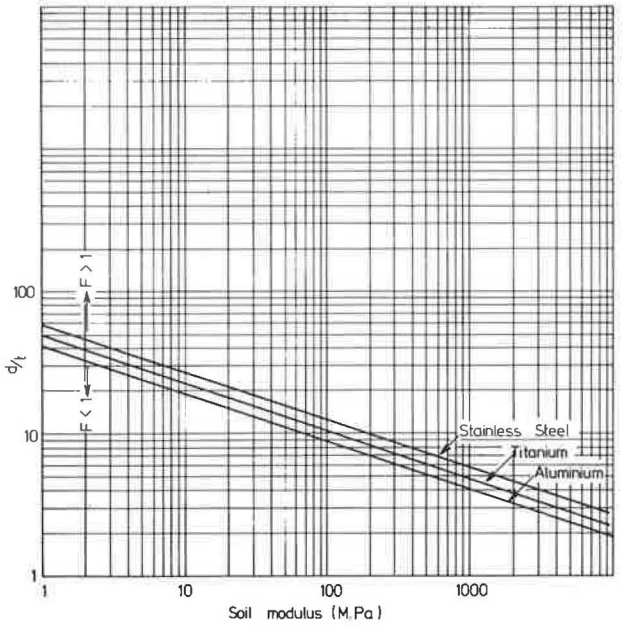

Figure 17. Determination of electrical output from d/t, cell material, and gauge factor.

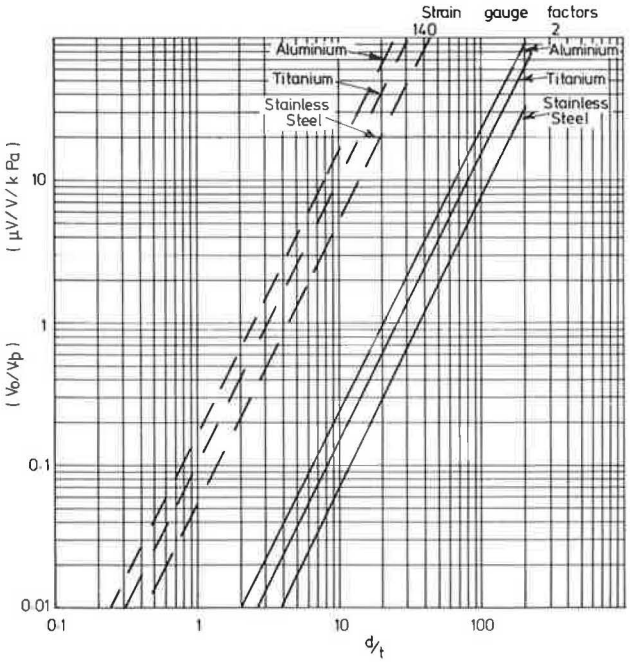

Figure 18. Determination of maximum allowable field stress from d/t and cell material.

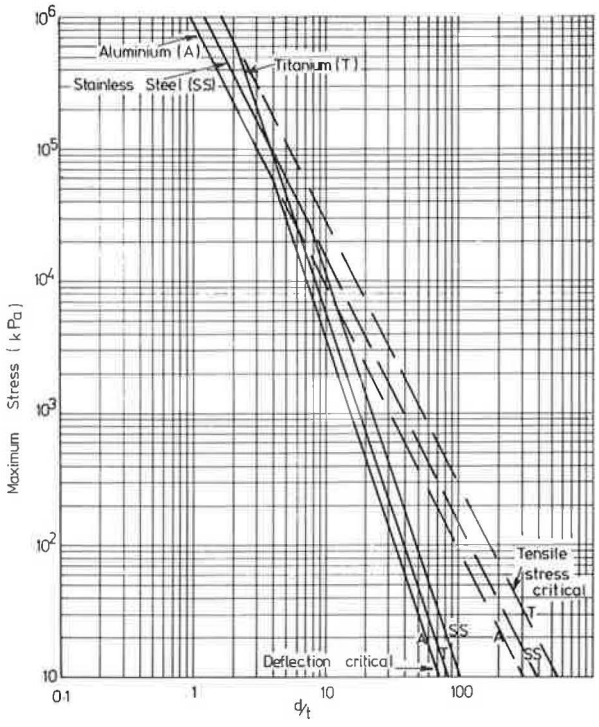

Figure 19. TRRL strain cell.

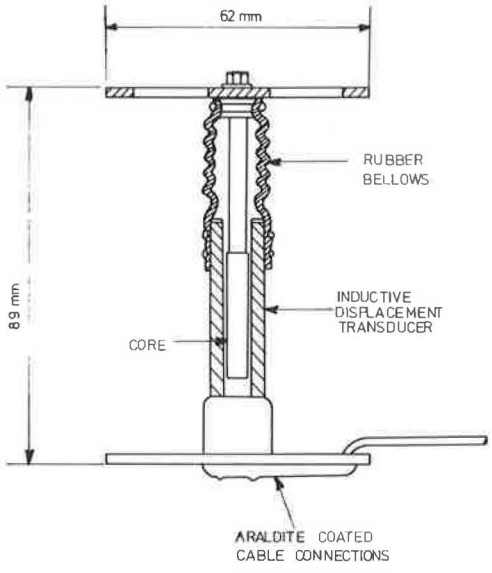

As shown in Figure 17, the electrical output to be expected from the cell can be determined in relation to the bridge voltage and stress being measured. Examples are given of foil strain gauge bridges that have gauge factors of 2 and of semiconductor bridges that have gauge factors of 140. Other lines could be established by using the following equation:

$$(d/t)^2 = (V_o/V_p)\,[32E_c/3G(1 - \nu_c^2)] \quad (8)$$

where

V_o = output voltage,
V = bridge voltage,
p = applied stress,
E_o = Young's modulus,
ν_o = Poisson's ratio of the cell metal, and
G = strain gauge factor.

The decision as to the acceptability or otherwise of a particular bridge output will depend on the minimum stress to be measured and the sensitivity of the monitoring equipment. The procedure for determining stress and sensitivity is illustrated in the design examples below.

The maximum stress to which the pressure cell can be subjected is determined from Figure 18. Thus, the diaphragm deflection and the maximum tensile stress criteria are brought together. For limiting the deflection to a diaphragm diameter of $^1/_{2000}$, the maximum pressure is determined by the following:

$$p(d/t)^3 = E_c/[23.4(1 - \nu_c^2)] \quad (9)$$

On the assumption that the maximum stress in the metal should not exceed half the yield stress (σ_y), this criterion gives the following:

$$p(d/t)^2 = 2.67\sigma_y \quad (10)$$

Figure 18 shows that the deflection criterion is critical except for cells with relatively thick diaphragms. The deflection criterion is only relevant to the performance of the cell in situ but the maximum stress criterion is also applicable during the so-called scragging process carried out after strain gauging and before the instrument is used. This process involves the cyclic application of stresses that at least covers the range expected in practice so that the stresses built into the metal during manufacture can be relieved.

Once a satisfactory cell has been designed, it is desirable that calibration tests be carried out in the soil involved in the investigation. A theoretical estimate of cell registration may also be obtained from Figure 4 or from the following equation based on C values for $F \leq 1$.

$$C = 1 + 0.56(B/D) \quad (11)$$

Strain Gauge Arrangement

A satisfactory arrangement of strain gauges on the cell diaphragm to provide a four-arm active bridge is indicated in Figure 1. This arrangement will result in approximately equal tensile and compressive strains from the gauges. The equation for radial strain is as follows:

$$\epsilon_r = (3a^2 p/8t^2 E_c)\,(1 - \nu_c^2)[(3r^2/a^2) - 1] \quad (12)$$

where

a = diaphragm radius (d/2) and
r = radius to the particular point.

From Equation 12, it can be shown that the compressive strain at r = 0.82a is numerically equal to the tensile strain at r = 0. Since the strain gauge measures the average strain over its gauge length, this equality will occur for a gauge length of 0.36a when the arrangement of Figure 1 is used. This figure is reasonable for many strain gauges. The perpendicular arrangement of both pairs of gauges is to minimize mechanical cross sensitivity. Circular strain gauge arrangements specially designed for diaphragms are available as an alternative, but the calculation procedure would differ from that indicated above.

DESIGN EXAMPLE 1

The soil data include silty clay with a maximum particle size of 0.1 mm, a maximum E_s of 100 MPa, and a ν_s of 0.4. The material to be used is titanium. As shown in Figure 8, B/D is 0.2, which minimizes cross sensitivity. However, the minimum d is 5 mm (50 × 0.1), which is impracticable. Therefore, for adequate cable entry, it is assumed that the minimum B is 6 mm, D is 30 mm (6/0.2), and d is 18.8 mm (30/1.6). As shown in Figure 16, maximum d/t is 10.5; therefore, t is 1.79 mm. By using conventional strain gauges (G = 2), Figure 17 shows the electrical output as 0.17 μV/V/kPa. It is assumed that the minimum resolution on the monitoring equipment is 10 μV, the minimum stress to be measured is 3 kPa, and the required bridge voltage is 19.7 V [10/(0.17 × 3)]. Because the maximum allowable current through most strain gauges is 20 mA, the bridge current will be 40 mA and the gauge resistance will be 492 Ω [19.7/(40 × 10^{-3})]. Thus, for instance, 600 Ω gauges and a 20-V supply are used. As shown in Figure 18, the maximum stress that can be measured is 4500 kPa, and the maximum allowable stress during scragging is 25 000 kPa. The cell registration is then estimated from Equation 11 as C = 1 + (0.56 × 0.2) = 1.11.

DESIGN EXAMPLE 2

The soil data include sand with a maximum particle size of 2 mm, a maximum E_s of 500 MPa, and a likely ν_s of 0.2. The material to be used is stainless steel. As shown in Figure 8, B/D is 0.9, which minimizes cross sensitivity. However, the minimum d is 100 mm (50 × 2); therefore, D is 160 mm and B is 144 mm. As shown in Figure 16, the maximum d/t is 7.3; therefore, t is 13.7 mm. As shown in Figure 17, V_o/V_p is 0.037 μV/V/kPa. For a V of 24, V_o/p is 0.89 μV/kPa. For a minimum resolution of 10 μV, the minimum p is 11.2 kPa. However, if this is unsatisfactory, then semiconductor strain gauges are used. As shown in Figure 17, V_o/V_p is 2.8 μV/V/kPa for a G of 140 and this is satisfactory. As shown in Figure 18, the maximum stress is 13 000 kPa. The cell registration is then estimated from Equation 11 as C = 1 + (0.56 × 0.9) = 1.5.

SOIL STRAIN CELLS

Basic Principles

Stress gauges need to be stiff for reliable performance; however, strain cells need to be of low stiffness so that their operation does not reinforce the soil or impede its deformation. The instrument must move with the soil and provide a minimum of interference. Deformation is measured over some known gauge length to determine strain. This implies that the instrument must determine the relative movement of two points in the soil.

Figure 20. Bench calibration of strain coils.

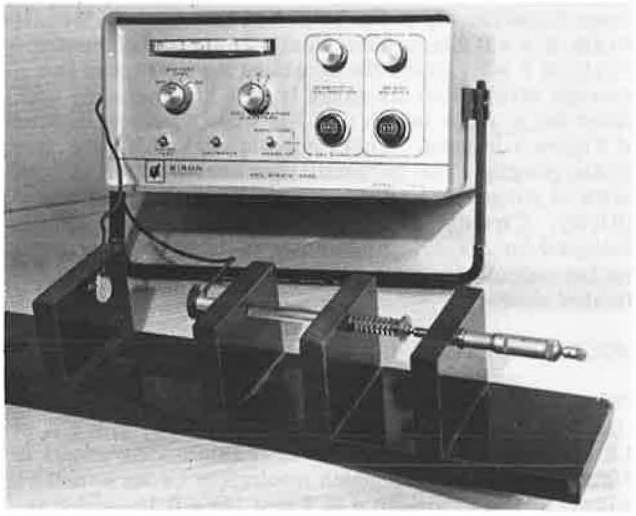

Figure 21. Strip gauge used by NIRR.

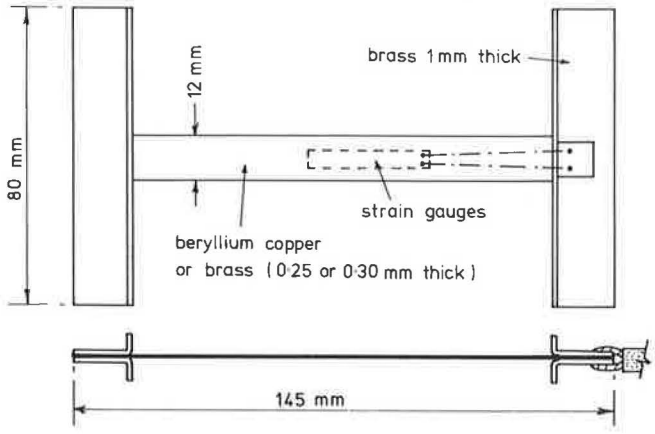

Relatively little attention has been given to soil strain measurement but some satisfactory instruments have, none the less, been developed.

Instruments

Basically, two kinds of instruments are available. One works on the principle of the TRRL version shown in Figure 19 in which the two end discs move relative to each other; the movement being determined by a built-in displacement transducer. This kind of instrument relies on a satisfactory shear break developing to provide a transition from the uniform deformation in the soil between the end plates and the concentrated movement of the instrument at one end. This movement is achieved by greasing and particularly by using the rubber bellows over the parts where relative movement takes place. The bellows also prevent soil from inhibiting free mechanical movement. The soil core between the end plates is prevented from being compressed unduly by using one end plate with an open section, which is shaped like a steering wheel.

The main shortcoming of this instrument is the mechanical linkage between the ends of the gauge length. This linkage causes problems of installation and friction that inhibit free movement (15). These problems are overcome in the other kind of instrument that consists of a pair of strain coils (32).

Generally, the two wire-wound induction coils are placed, coaxially but they can be used in a coplanar or orthogonal mode. An alternating current (AC) set up in one coil induces a current in the other coil, the magnitude of which depends on the coil spacing. The coils and the operating equipment are available commercially from Bison Instruments and field use has been reviewed by Selig (33).

Coil spacing can be up to 4-coil diameters and various sizes of from 2.5 to 35.6 cm in diameter have been used in a variety of projects. This instrument is suitable either for dynamic or static work and long-term stability is good. They have been used in asphalt materials as well as soil (21, 34, 35).

A problem does arise with strain coils when they are used near metal objects, which interfere with the flux linkage between the coils. This interference is particularly important when the metal moves such as when a wheel is over a test pavement and it comes within about five times the gauge length of the coils. Attempts have been made to overcome this difficulty by shielding the coil with a layer of aluminium foil on the pavement surface (35). However, this interference problem only affects dynamic measurements.

The coils are relatively inexpensive, but the electronic unit required to monitor a single pair of coils is quite expensive. For static measurements, switching between pairs of coils overcomes this restriction, but, if simultaneous dynamic readings are required, then several units are needed. For dynamic measurements, strains 0.003 percent can be resolved and for long-term measurements the percentage is about 0.1 (33).

The bench calibration of strain coils is carried out in an apparatus of the kind shown in Figure 20 wherein the spacing of coils can be accurately related to the electrical signal. If the medium in which the cells are to be used is likely to contain ferrous metal ions, special calibration may be required by placing the coils in samples of the material. An indication of the need for this can be obtained by placing a sample of the material between the coils when they are set up in the calibration apparatus shown in Figure 20 (21, 36). The coils are fairly tolerant to errors caused during installation or subsequently thereafter, which involve movements in directions other than the one in which measurements are being taken (33, 36).

The installation of coils in soil is a relatively easy process. An electrical technique can be used to position a second coil over a first coil that is already buried. The coil is moved until a maximum output is recorded, i.e., when exact coaxiality is achieved (33).

STRAIN GAUGES FOR BOUND LAYERS

The strain measuring devices that have been used in bitumen or cement-bound pavement layers are of three types: foil-strain gauges cemented to carrier blocks or directly placed on an exposed surface; strip gauges (24) of the type shown in Figure 21; and the strain coils previously described. When working in bituminous layers, high temperature resistance is required of both the instruments and the electrical cables, if placement is to be undertaken during paving operations, as is generally the case.

Care should be taken to ensure that carrier blocks have a stiffness that is less than the material in which they are to be placed so that the blocks do not reinforce the layer, which would cause low strains to be recorded.

Foil Strain Gauges

Foil strain gauges (37, 38, 41) may be used for measuring either vertical or horizontal strains and experience has been confined to bituminous layers. Horizontal strain at the bottom of a bituminous layer can be successfully measured by a strain gauge cemented to a carrier block. This block is let into the underlying layer so that the surface carrying the gauge is flush with the top of this layer. Subsequent paving over this arrangement results in the gauge adhering to the bottom of the bituminous layer. Care is taken to remove large aggregate particles from the mix placed immediately over the strain gauge.

Vertical strain gauges have to be placed on carrier blocks and good results are obtained by sandwiching the gauge between two blocks, for protection, and then placing the block on the surface before paving. This surface can either be the underlying layer or an intermediate bituminous layer.

Strip Gauges

The TRRL version of the strip gauge (23) consists of two 6.3-mm square steel bars connected by a thin strip of aluminum that carries a foil strain gauge on either side. The South African version of the strip gauge used by the National Institute for Road Research (NIRR) (24) is shown in Figure 21. Protection of the gauges can be provided by molding polyethylene around each gauge before installation or simply by wrapping each gauge with polyvinyl chloride tape.

The instrument is laid on the surface below the bituminous or cement-bound layer and paving takes place over that layer so that a measure of horizontal strain at the bottom of the layer may be subsequently obtained. The instrument may alternatively be cast into a block of the bound material that is then placed face down on the surface before paving.

These gauges are rather stiff and this would seem to violate the basic principle of in situ strain measurement. In view of this, it is surprising that hardly any relevant calibration tests seem to have been performed with these gauges. Bohn (as related through private conversation) has shown from tests with various gauges placed at the bottom of asphalt beams that their stiffness relative to the asphalt is very important and should be minimized. He used some gauges with a plastic strip having a modulus of elasticity 25 times lower than that for aluminum, but even these tended to underregister the true strain, even when the asphalt modulus was relatively high. Calibration tests with this type of strain-measuring device are therefore strongly recommended before installation in a test pavement.

Strain Coils

When used in bituminous material, the coils may be attached to an intermediate layer by using a tack coat or they can be mounted on carrier blocks. In the latter case, care should be taken to ensure that the block is not moved unduly because the mix is compacted above and around the block. Hand compaction of material around the carrier block before paving can help. An alternative procedure (36) for placing coils slightly below the current level of construction is to cut a circular hole and place the coil in a hot mastic mix. A similar technique can be used for placing a pair of horizontally aligned coils.

Intereference by moving metals is particularly marked for coils that are to be used in surfacing layers. In addition, the minimum resolution of about 0.003 percent strain could be a problem in stiff bound layers.

DEFLECTION GAUGES

Measurement of transient surface deflection of pavements is carried out extensively in connection with overlay design. However, the standard methods involving the Benkelman beam or Lacroix deflectograph involve slow speeds and equipment at the surface, which does not provide particularly accurate measurements. It is an advantage, therefore, in full-scale trials to have in situ, deflection-measuring equipment that can provide not only surface measurements but also interface deflections. Three basic kinds of equipment appear to be available for this purpose.

Displacement Transducers

The principle of the method of displacement transducers (23, 29, 33) is that a rod is driven into the subgrade at a sufficient depth to be beyond the zone of influence of wheel loads (about 2 m), and an LVDT or similar transducer attached to the top of the rod registers movements of the particular level in the pavement relative to these data. Alternatively, the datum could be at an interface; therefore, deflection of one or more layers above this point could be determined. The disadvantage of this method is that a hole has to be made through the pavement to accommodate the rod, and the hole has to be lined so that the rod is free from the surrounding material; otherwise, it would reinforce the pavement and make the datum ill-defined.

An advantage is that the displacement transducer can be screwed into the top of the rod when measurements are required and replaced afterwards by a blank plate at the surface. In addition, both permanent and transient deflections can be determined.

Optical Method

An optical method has been developed by Hofstra (private conversation) in which a 1.5-mm laser beam was used. This beam is passed through a thin rectangular metal tube (4 by 5 mm) cemented in an indentation on the asphalt surface. The beam is partly intercepted by a thin blade positioned vertically in the tube beneath the wheel track. Application of a wheel load changes the blade position and hence affects the intensity of light reaching the other end of the tube. The intensity of light is measured by a photoelectric cell and can be related to the surface deflection after suitable calibration.

This arrangement has yet to be used on a full-scale trial but a similar system has been used successfully in Holland (39). A light beam was projected along a tube to two photoelectric cells located in the road surface. The output from the cells was changed by their movement under passing wheel loads and the deflection determined from prior calibration.

Accelerometers

The use of accelerometers is attractive because installation is simple and no rods or tubes are required, only the usual electrical connections. Electronic integrators are available to convert the acceleration measurements to deflection though this process requires that the output is zeroed before each wheel pass, which could present a problem if a train of wheel loads is involved. This technique would seem to be better for the determination of peak deflections than for defining the shape of the deflection bowl and only applies to transient measurements.

OTHER INSTRUMENTS

Equipment for Wheel Load Determination

The loading applied to a test pavement is an important parameter; therefore, correct evaluation is essential. If the experiment is to be loaded by using special trucks with a known wheel load, then no special provision is required for monitoring loads during testing. However, if tests are to be conducted on a public road using actual traffic, measurements of wheel loads are essential. Two basic kinds of equipment have been used for this purpose: One is the dynamic weighbridge (40), which is a major permanent installation, and the other is a portable, axle-weight analyzer (41).

The weighbridge developed by the British TRRL consists of a rigid platform supported by load cells and set so that its top is flush with the road surface. Its width (in the direction of the traffic) has to be sufficient to support the largest anticipated tire contact area and its length will depend on whether wheel or axle loads are to be determined. The arrangement must be rigid to prevent resonance interfering with the load cell signals.

The electronics associated with a weighbridge can count the numbers of loads in a series of load ranges, which produces an axle load spectrum. The active part of the weighbridge can be designed to be removable so that a dummy platform may be installed when measurements are not required.

The axle-weight analyzer developed by the South African NIRR has been designed to be portable so that information can be obtained from a variety of sites. It consists of a thin rubberized pad that contains two layers of metal foil separated by a soft rubber. This arrangement acts as a capacitor, the capacitance depending on the pressure applied by the wheel load.

The analyzer is stuck to the road surface by using hot bitumen and has a thickness of about 7 mm. A flat road surface is required for best results and care has to be taken over calibration. Detailed information on this piece of equipment has been described by Basson and others (41).

When taking in situ measurements of stress, strain, or deflection, it is important to know the position as well as the magnitude of the load, and various techniques have been used for determining these. Again, the procedure is easier if special loading trucks are used. For those cases, a metal detector strip is set in the pavement surface and can be used in conjunction with a pair of pickups on the truck, which are a simple visual guide for the driver. Alternatively, a row of photoelectric cells can be used to detect reflected light from the white marks on the pavement surface. For real traffic, a triggering mechanism is located in line with the instrumentation so that wheels proceeding down this line will register on the instrumentation.

Pore Pressure Transducers

Earth pressure cells register total stresses; therefore, it is desirable to be able to evaluate pore pressures so that effective stresses can be calculated. The measurement of long-term changes in pore pressure is relatively straightforward and has been done in earthworks by using piezometers of various kinds for many years. For the pavement test section application, a simple instrument has been developed at the Waterways Experiment Station (29). A porous stone allows the pore fluid to enter a small cavity that is protected from the influence of effective stresses by a strong surrounding. The changes of fluid pressure in the cavity, and, hence pore pressure, are monitored by a small pressure transducer. With modern technology, it should be possible to produce an instrument smaller than the one currently used that is based on the same principles.

The WES instrument was used to measure general changes in pore pressure during the test period, but the system has the potential for measuring transient changes caused by individual wheel loads. There are many problems in measuring these changes satisfactorily but the principal one is the need for a very stiff measuring system to reduce flow into the cavity to a minimum. The pore size of the filter element has to be small enough to prevent blockage by soil but large enough to allow adequate flow (20). These problems are particularly marked in fine-grained soils but dynamic pore pressure measurement has not been developed to the stage in which it can be reliably used in full-scale trials.

Temperature Transducers

When dealing with asphalt materials, it is important that the in situ temperature conditions be accurately determined. This parameter influences the behavior of the asphalt and, hence, often that of the entire pavement. Fortunately, temperature can be easily measured with thermocouples (42) or thermistor probes (29). These instruments can be placed after construction by drilling and filling the hole with bitumen, but less interference to the structure results from installation during construction. In the latter case, high temperature resistant wire is needed.

Soil Suction Measurements

In partially saturated soils occurring in regions with low water tables, the evaluation of soil suction has a significance exactly analogous to that of pore pressure measurement in saturated or nearly saturated soils. Satisfactory results can be obtained by using the psychometric technique (43, 44, 45, 46).

This method is used for measurements in situ or on samples. The soil suction (the measurement includes any osmotic contribution as well as capillary contributions) is determined from measurements and an empirical calibration curve. Continuous recording is not possible with the psychometric technique but repeated measurements may be made at intervals as short as 15 min. A variation of this technique called the Dew Point Method has been developed commercially and permits continuous measurement and recording.

When the instrument is in equilibrium with the soil, an accuracy of about 100 kPa over the range 0 to -5 MPa is normal. The wide range makes this instrument particularly useful in measurements related to pavement studies in most areas with low water tables.

Limitations of the method are that independent measurement of solute suction (osmotic contribution) is needed if measurements are to be related to pore pressures. The calibration is temperature dependent, and diurnal soil temperature changes prevent in situ operation within about 300 mm of the surface. The relatively low absolute accuracy is acceptable in pavements where soil suction is a significant factor and considerable practical use can be made of the technique (47).

ACKNOWLEDGMENTS

The gestation period for this report has been longer than I wished; however, this allowed time for the receipt of valuable information from persons experienced in the use of field instrumentation in various parts of the world.

I, therefore, acknowledge with gratitude the assistance rendered by the following in preparing this paper: R. G. Ahlvin, R. D. Barksdale, A. Bohn, J. Delcour, F. N. Finn, A. Hofstra, W. D. O. Paterson, J. F. Potter, B. G. Richards, A. J. Scala, E. T. Selig, and J. F. Shook. In addition, valuable discussions have been held with B. V. Brodrick at the University of Nottingham, England.

REFERENCES

1. E. T. Selig. A Review of Stress and Strain Measurement in Soil. Proc., Symposium on Soil-Structure Interaction, Univ. of Arizona, 1964, pp. 172-186.
2. G. E. Triandafilidis. Soil-Stress Gage Design and Evaluation. Journal of Testing and Evaluation, ASTM, Vol. 2, No. 3, 1974, pp. 146-158.
3. D. W. Taylor. Pressure Distribution Theories, Earth Pressure Cell Investigations, and Pressure Distribution Data. Soil Mechanics, U.S. Army Engineer Waterways Experiment Station, Vicksburg, Miss., 1947.
4. G. E. Monfore. An Analysis of the Stress Distribution in and Near Stress Gauges Embedded in Elastic Solids. Bureau of Reclamation, U.S. Department of Interior, Res. Rept. SP-26, 1950.
5. A. C. Tory and R. W. Sparrow. The Influence of Diaphragm Flexibility on the Performance of an Earth Pressure Cell. Journal of Scientific Instruments, No. 44, 1967, pp. 781-785.
6. P. E. Fossberg. Load Deformation Characteristics of Three-Layer Pavements Containing Cement-Stabilized Base. Univ. of California, PhD thesis, 1970.
7. R. Collins, K. J. Lee, G. P. Lily, and R. A. Westmann. Mechanics of Pressure Cells. Experimental Mechanics, Vol. 12, No. 11, 1972, pp. 514-519.
8. K. G. Mills, S. Matthews, and B. G. Richards. An Investigation of Diaphragm Earth Pressure Cells. Proc., 7th Australian Road Research Board Conference, Adelaide, 1974.
9. K. R. Peattie and R. W. Sparrow. The Fundamental Action of Earth Pressure Cells. Journal of Mechanics and Physics of Solids, No. 2, 1954, pp. 141-155.
10. T. Kallstenius and W. Bergau. Investigations of Soil Pressure Measuring by Means of Cells. Proc., Royal Swedish Geotechnical Institute, No. 12, 1956.
11. Soil Pressure Cell Investigation. U.S. Army Engineer Waterways Experiment Station, Vicksburg, Miss., Technical Memo., No. 210-1, 1944.
12. J. Delcour, J. L. Jansen, and W. G. Jansen. Gronddrukmetingen onder Hoogovenslakken voor de Oosterscheldedrempel: Vervaardiging Nottingham/TPD-dozen. Calibratie, Technisch Physische Dienst TNO-TH, Rept. 409.380-1, Delft, Holland, 1975.
13. J. K. Ingram. Development of a Free-Field Soil Stress Gauge for Static and Dynamic Measurements. U.S. Army Engineer Waterways Experiment Station, Vicksburg, Miss., Technical Rept. No. 1-814, 1968.
14. A. A. Williams and S. F. Brown. The Use of Earth Pressure Cells in Some Road Experiments. Proc., 5th Regional Conference for Africa on Soil Mechanics and Foundation Engineering, Luanda, Angola, 1971, pp. 5.15-5.21.
15. S. F. Brown and P. S. Pell. Subgrade Stress and Deformation Under Dynamic Load. Journal of Soil Mechanics and Foundations Division, ASCE, Vol. 93, No. SM1, Jan. 1967, pp. 17-46.
16. S. F. Brown. The Performance of Earth Pressure Cells for Use in Road Research. Civil Engineering and Public Works Review, Feb. 1971, pp. 160-165.
17. G. F. Buck. An Investigation of Earth Pressure Cell Response and the Stress Distribution in Test Pavement Subgrades. Univ. of Alabama, Birmingham, PhD thesis, 1963.
18. J. R. Morgan and C. M. Gerrard. Free-Field Measurements of Stresses and Strains in Soils. Proc., 4th Australian Road Research Board Conference, 1968, pp. 1743-1760.
19. S. F. Brown. The Measurement of in Situ Stress and Strain in Soils and Discussion. Field Instrumentation in Geotechnical Engineering, 1973, pp. 38-51 and 543-545.
20. S. F. Brown and B. V. Brodrick. The Performance of Stress and Strain Transducers for Use in Pavement Research. Science Research Council, Univ. of Nottingham, England, Res. Rept., 1973.
21. S. F. Brown, C. A. Bell, and B. V. Brodrick. Permanent Deformation of Flexible Pavements. Univ. of Nottingham, England, Final Rept., 1977.
22. A. C. Whiffin and S. A. Morris. Piezoelectric Gauge for Measuring Dynamic Stresses Under Roads. The Engineer, No. 213, April 1962, pp. 741-746.
23. J. F. Potter, H. C. Mayhew, and A. P. Mayo. Instrumentation of the Full-Scale Experiment on A1 Trunk Road at Connington, Hunts. British Road Research Laboratory, Rept. LR 296, 1969.
24. W. D. Paterson and L. S. de Vletter. The Characteristics and Performance of Strainmeters, Pressure Cells, and Deflection Gauges in Use in 1974. National Institute for Road Research, Council for Scientific and Industrial Research, South Africa, Technical Note TP/46/74, 1974.
25. G. Plantema. A Soil Pressure Cell and Calibration Equipment. Proc., 3rd International Conference on Soil Mechanics and Foundations, Vol. I, 1953, pp. 283-298.
26. D. Walter, A. R. Kriebel, and K. Kaplan. URS Free-Field Soil Stress Gauge—Design, Construction, and Evaluation. United Research Service, Rept. 785-6, 1971.
27. Investigations of Pressures and Deflections for Flexible Pavements—Homogeneous Clayey-Silt Test Section. U.S. Army Engineer Waterways Experiment Station, Vicksburg, Miss., Rept. 1, Technical Memo., No. 3-323, 1951.
28. Investigations of Pressures and Deflections for Flexible Pavements—Homogeneous Sand Test Section. U.S. Army Engineer Waterways Experiment Station, Vicksburg, Miss., Rept. 4, Technical Memo., No. 3-323, 1954.
29. Multiple-Wheel Heavy Gear Load Pavement Tests. U.S. Army Engineer Waterways Experiment Station, Vicksburg, Miss., Technical Rept., Vol. IIIA, No. 5-71-17, 1971.
30. S. F. Brown and P. S. Pell. An Experimental Investigation of the Stresses, Strains, and Deflections in a Layered Pavement Structure Subjected to Dynamic Loads. Proc., 2nd International Conference on the Structural Design of Asphalt Pavements, Ann Arbor, Mich., 1967, pp. 487-504.
31. S. F. Brown and D. I. Bush. Dynamic Response of Model Pavement Structure. Journal of Transportation Engineering, ASCE, No. TE4, Nov. 1972, pp. 1005-1022.
32. E. T. Selig and O. H. Grangaard. A New Technique for Soil Strain Measurements. Materials Research and Standards, Vol. 10, No. 10, 1970, pp. 19-36.
33. E. T. Selig. Soil Strain Measurement Using Inductance Coil Method. ASTM, Symposium on Performance Criteria and Monitoring for Geotechnical Construction, 1974.
34. W. D. Paterson. Deformations in Asphalt Con-

crete Wearing Courses Caused by Traffic. Proc., 3rd International Conference on the Structural Design of Asphalt Pavements, Vol. I, London, 1972, pp. 317-325.
35. E. Stuart, Y. Miyaoka, E. L. Skok, and N. C. Wenck. Field Evaluation of an Asphalt Stabilized Sand Pavement Design Using the Elastic-Layered System. Proc., AAPT, 1974, pp. 77-109.
36. W. D. Paterson. Measurement of Pavement Deformation Using Induction Coils. Road Research Unit, National Roads Board, New Zealand, Bulletin 13, 1972.
37. A. J. Klomp and T. W. Niesman. Observed and Calculated Strains at Various Depths in Asphalt Pavements. Proc., 2nd International Conference on the Structural Design of Asphalt Pavements, Ann Arbor, Mich., 1967, pp. 671-688.
38. A. Hofstra and C. P. Valkering. The Modulus of Asphalt Layers at High Temperatures: Comparison of Laboratory Measurements Under Simulated Traffic Conditions With Theory. Proc., 3rd International Conference on the Structural Design of Asphalt Pavements, London, 1972, pp. 430-443.
39. L. W. Nijboer. Testing Flexible Pavements Under Normal Traffic Loadings by Means of Measuring Some Physical Quantities Related to Design Theories. Proc., 2nd International Conference on the Structural Design of Asphalt Pavements, Ann Arbor, Mich., 1967, pp. 689-705.
40. J. J. Trott and J. W. Grainger. Design of a Dynamic Weighbridge for Recording Vehicle Wheel Loads. British Road Research Laboratory, Rept. 219, 1968.
41. J. E. Basson, G. L. Dehlen, and E. R. Beulink. The Use of the Axle Weight Analyzer Model WA2. National Institute for Road Research, Council for Scientific and Industrial Research, South Africa, Rept. RP/8172, 1972.
42. R. H. Williamson and W. T. Kirby. Measurement of Pavement and Air Temperatures: A Basic Discussion. National Institute for Road Research, Council for Scientific and Industrial Research, South Africa, Rept. RP/10/70, 1970.
43. L. A. Richards. Physical Condition of Water in Soil. In Methods of Soil Analysis (C. A. Black and others, eds.), American Society of Agronomy, Madison, Wisc., 1965, pp. 128-152.
44. B. G. Richards. Psychometric Techniques for Measuring Soil Water Potential. Division of Soil Mechanics, Australian Commonwealth Scientific and Industrial Research Organisation, Technical Rept. 9, 1969.
45. S. L. Rawlins. Some New Methods for Measuring Components of Water Potential. Soil Science, Vol. 112, 1971, pp. 8-16.
46. B. G. Richards. Psychometric Techniques for Field Measurement of Negative Pore Pressure Soils. Proc., Australian-New Zealand Conference on Geomechanics, Vol. 1, Melbourne, 1971, pp. 387-394.
47. B. G. Richards and R. Gordon. Prediction and Observation of the Performance of a Flexible Pavement on an Expansive Clay Subgrade. Proc., 3rd International Conference on the Structural Design of Asphalt Pavements, London, 1972, pp. 133-143.

Publication of this paper sponsored by Committee on Strength and Deformation Characteristics of Pavement Sections.

Field Observations of Rutting and Their Practical Implications

N. W. Lister and R. R. Addis, Transport and Road Research Laboratory, U.K. Department of the Environment, Crowthorne, England

Observation of a series of full-scale road experiments in the United Kingdom indicates that, after an initial period of deformation, reflecting compaction, and moisture changes, permanent deformation and rutting can be related to ranges of cumulative equivalent standard axles of 82 kN (18 000 lb). Cracking of structural significance seldom occurs until ruts have developed to a depth of 10 mm (0.4 in). After the cracking occurs, deformation behavior is more difficult to predict; continuity of the relation of the cumulative equivalent standard axles is most likely on stronger pavements. The marked influence of temperature and subgrade strength on deformation is demonstrated by results from the AASHO Road Test in the United States and from road experiments in the United Kingdom. Essentially similar behavior was observed in both countries, and differences can be related to differences in climatic conditions. Accelerated pilot-scale testing under controlled conditions of wheel load and temperature in a circular road machine has quantified the contributions of these two factors to deformation behavior. The link demonstrated between this type of testing and actual road behavior indicates its potential for developing and validating predictive models of deformation behavior.

Road deterioration under the action of traffic takes two main visible forms: cracking of the road surface and deformation in the wheel paths along which the great majority of heavy vehicles pass. The appearance of either form is not necessarily accompanied immediately by the other. Cracking at the pavement surface is normally a fatigue phenomenon originating either in the surface itself or in a cement- or bituminous-bound base beneath. Cracking that originates in the surface is associated with underdesigned pavements having bituminous materials of the asphalt concrete type or thin rolled-asphalt surface layers. Once cracking has become general, rutting will occur because the lower layers of the pavement or the subgrade or both are consequently overstressed and because those elements of the road are weakened by the ingress of water. Prediction of road behavior after general cracking has taken place is difficult, and in many cases the onset of general cracking must be taken as the effective end of the life of the road without structural maintenance.

Rutting can develop over many years without cracking taking place, particularly if the rutting is associated

with a fault in the surfacing laid on an otherwise structurally adequate pavement. When cracks finally occur, they tend to be confined to the wheel path and may or may not accelerate the development of rutting to an unacceptable failure condition.

Deterioration of the riding quality of a road will take place as a consequence of increasing rutting and, to a minor extent, as a direct consequence of cracking. Ultimately the pavement will require strengthening or resurfacing to prevent structural failure, to improve the riding quality, or to eliminate splash and spray resulting from ponding of water in pavement ruts. The development of rutting therefore plays a central role in determining the overall performance of pavements.

DEVELOPMENT OF RUTTING

In the United Kingdom, roads designed to carry moderate to heavy traffic are surfaced with bituminous material at least 75 mm (3 in) thick. The wearing course is of rolled asphalt. Pavement deterioration appears as rutting in the wheel paths and is followed by cracking of the asphalt as the road continues to deform, until, at failure, pavements are generally both cracked and deformed. The onset of critical conditions, which define the optimum time for extending pavement life by overlaying, is normally characterized by moderate rutting and little or no visible cracking. Thus in most British pavements deformation behavior is of prime importance; this is reflected in the present design recommendations for flexible pavements in the United Kingdom (1). The recommendations were developed from systematic observations of the surface behavior of a series of full-scale road experiments (2, 3). In these experiments different combinations of pavement materials were laid in a range of thicknesses on as uniform a subgrade as was practically possible. The performance of the experimental sections under normally mixed traffic was assessed primarily in terms of the development of deformation of the road in the wheel paths (3). The deformation was measured by precise optical leveling. The results are presented in terms of an equivalent rut under a 1.8-m (6-ft) straightedge so that comparisons can be made with results of other studies normally given in terms of rut depth.

Figure 1 shows a typical transverse road profile on the full-scale road experiment at Alconbury Hill (4). The greatest deformation is along the wheel paths of the lane carrying the greatest proportion of heavy vehicles (5). Deformation and rutting develop rapidly in the early life of the road. On roads that do not fail at this stage subsequent deterioration occurs at a slower rate, but progress to final failure is normally accompanied by a rapid increase in the rate of deformation and rutting. A typical history of rutting or deformation is shown in Figure 2. In addition to being influenced by the basic deformation behavior of the road layers, the form of the initial phase is also influenced both by the compacting effect of traffic on granular layers and by the moisture changes in the subgrade after the disturbance of the construction period.

The development of rutting and deformation in those sections of the Alconbury Hill experiment (4) constructed with crushed-slag, wet-mixed bases is shown in Figure 3. In section D, the thinnest, which is grossly underdesigned for the intensity of commercial traffic, the initial phase leads straight to early failure. As thickness increases, the initial deformations and ruts decrease, and the rate of increase thereafter also decreases. In section C the onset of surface cracking (marked by an arrow) is followed by a rapid increase in rutting to failure; however, in section B, which has a thicker base, the development of rutting was unaffected by cracking, and a much longer life resulted. The behavior of section A, the strongest section, was similarly unaffected by cracking. The results are shown on a logarithmic scale in Figure 4. After about 500 000 equivalent standard axles of 82 kN (18 000 lb), the development of both rutting and deformation in the thicker sections can be related to a power index, at least up to the stage at which surface cracking occurs. The index is based on the equivalent standard axles to some power (in this case times 10^6). Data in Figure 5 from three sections of different thicknesses having lean concrete bases show a similar trend for both deformation and rutting. Sections with rolled-asphalt bases, although following the same pattern for rutting, appear to diverge from any simple power index relation when deformation is considered (Figure 6). Because cement-bound bases do not compact under traffic, the initial movement in pavements containing them was, as expected, smaller. The considerable compaction experienced by the sand subbase, equivalent to about 112 kg/m^3 (7 lb/ft^3) during the whole experiment, accounted for the large initial movements; these were about twice as great as observed elsewhere.

The pattern that emerges from the observation of a series of full-scale experiments is this: After the initial period, the deformation and rutting can be related in cumulative traffic by power index values between 0.2 and 0.5, at least up to the point at which surface cracking is evident. Values of 0.4 to 0.5 are most commonly observed; the lowest index values are normally associated with pavements having considerably thick bituminous bases. Cracking seldom occurs until ruts have developed to depths of at least 10 mm (0.4 in). After cracking, the relation is not necessarily predictable; the precracking trend may continue, or rutting and deformation may increase at a much faster rate. The stronger the pavement is the less is the likelihood that surface cracking is associated with the change in the trend.

INFLUENCE OF ENVIRONMENTAL FACTORS

Although the curves indicate systematic development of deformation and rutting, closer examination indicates the strong influence of seasonal factors. The limited accuracy of leveling measurements dictated the installation in the road of deformation gauges to measure those factors (6). Figure 7 shows the strongly seasonal cycle of movement superimposed on the deformation developing in a pavement with a rolled-asphalt base. In this section the bituminous layers and the clay subgrade contribute virtually all the significant measured deformation, and both pavement elements show the same pattern of seasonal movement. Figure 8 shows in greater detail the deformation behavior related to the temperature conditions within bituminous layers during the second year the road carried traffic. The maximum rate of deformation in both layers took place after the onset of high temperatures in the late spring when the water-table level in the subgrade was still high.

Seasonal changes in the strength of the clay subgrade are reflected in the annual cycle of wetting and expanding in winter and drying in summer. These changes are superimposed on an overall increase with time in subgrade deformation, which is also seasonal. The stresses transmitted to the subgrade are sufficient to bring about deformation within it under repeated loading only at high temperatures, when the bituminous pavement is at its weakest. The rate of deformation was highest in late spring and early summer when the subgrade was weak and lowest later in the year as drying occurred.

As expected, the rate of deformation in the bituminous

Figure 1. Typical mean transverse profile at four levels of traffic.

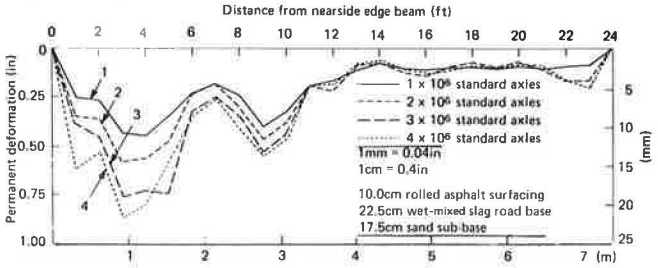

Figure 2. Typical development of rutting.

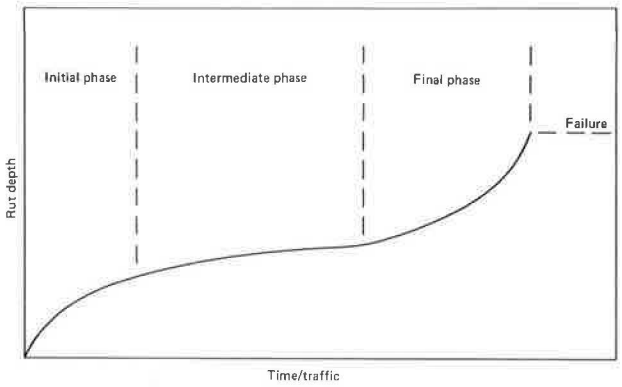

Figure 3. Development of rutting and deformation in pavement constructed with crushed-slag, wet-mixed bases at Alconbury Hill.

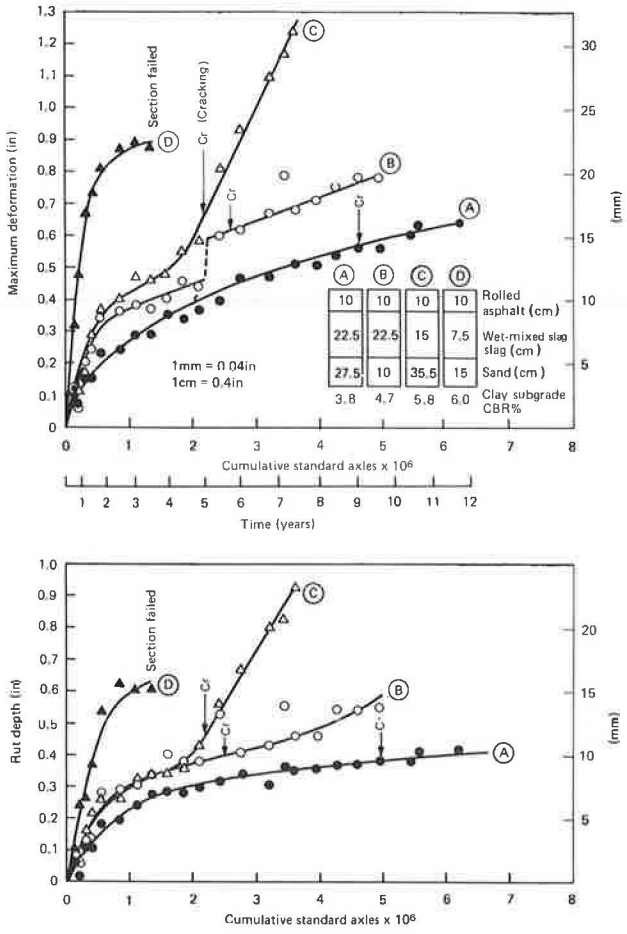

layers was closely related to the high temperatures of the late spring and summer. The apparent recovery from deformation in winter is harder to explain and may possibly be a consequence of the nonuniform distribution of heavy wheel loads across the wheel-path zone. Pavements with crushed-stone bases showed the same pattern of deformation behavior and the same seasonal dependence (7).

Extensive information on rutting behavior in the United States was obtained during the AASHO Road Test (8). Accelerated trafficking tests were made during a 2-year period under climatic conditions that produced frost penetration of the subgrade for periods of about 2 months each winter. These conditions are much more severe than are encountered in the United Kingdom, where frost penetrates below formation level on major roads every 15 years or so. (The effect of one such year is shown in Figures 3, 4, and 5 at about 2.2 million standard axles.)

In the AASHO Road Test the maximum rutting rate in pavements with granular bases occurred during and immediately after the thaw; considerable movement continued through spring and summer. In the United Kingdom, where subgrades are in a relatively stronger condition in the early spring, movement begins only when temperatures rise in the late spring. In the AASHO Road Test pavements with bituminous bases deformed more slowly in the early spring when those layers at low temperatures were stiff enough to protect the greatly weakened road foundation. In the United Kingdom temperature is also the dominant factor for roads with bituminous bases and, as we have seen, the maximum rate of deformation takes place in the late spring and early summer in pavements built with both bituminous and crushed-stone bases.

The rutting behavior of cement-bound bases in the AASHO Road Test is broadly typical of their behavior as observed in the United Kingdom. Rutting is less for a pavement of a given thickness than for other base types; that is, in pavements that have cemented bases

Figure 4. Logarithmic presentation of data shown in Figure 3.

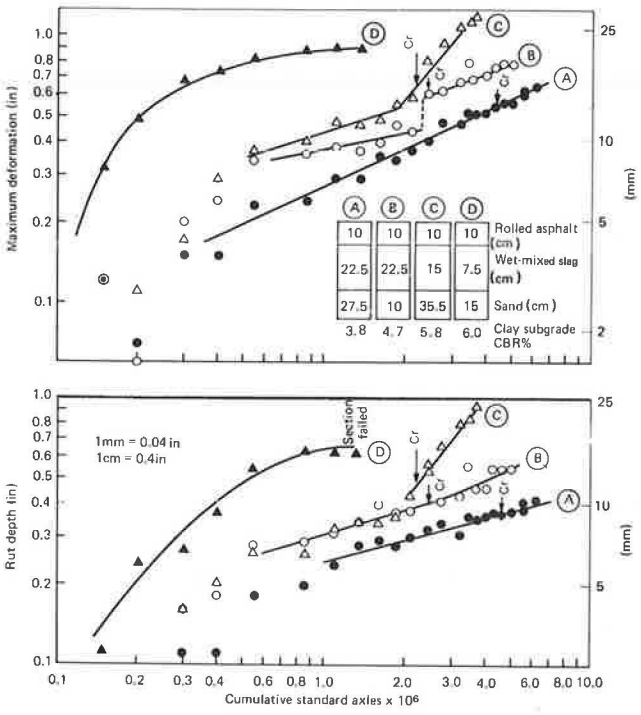

sufficiently thick to remain substantially uncracked, rutting is confined to the bituminous surfacing alone. When the base breaks up, rutting behavior is similar to that of pavements with granular bases.

DEVELOPMENT OF RUTTING UNDER CONTROLLED CONDITIONS

The importance of temperature in determining the development of rutting under traffic load has been demonstrated. Although both size and distribution of wheel loads and temperatures are measured on full-scale road experiments, the damage potential of various wheel loads under different temperature conditions cannot be distinguished. The distinction is being examined in a circular road machine at the Transport and Road Research Laboratory, where we are repeatedly testing experimental pavements with different combinations of wheel loads and surfacing temperatures. Details of the experimental technique used and method of analysis of results obtained are given in another report (7).

Figure 9 shows the development of rutting in a pavement with a crushed-stone base trafficked while mean surfacing temperatures were 25, 35, and 45°C (77, 95, and 113°F); each mean temperature represents testing

Figure 5. Development of rutting and deformation in pavement constructed with lean concrete bases at Alconbury Hill.

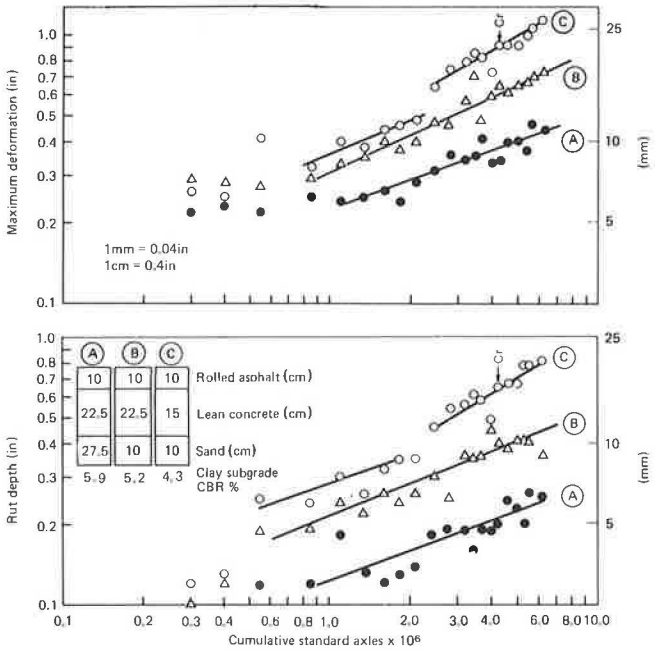

Figure 6. Development of rutting and deformation in pavement constructed with rolled-asphalt bases at Alconbury Hill.

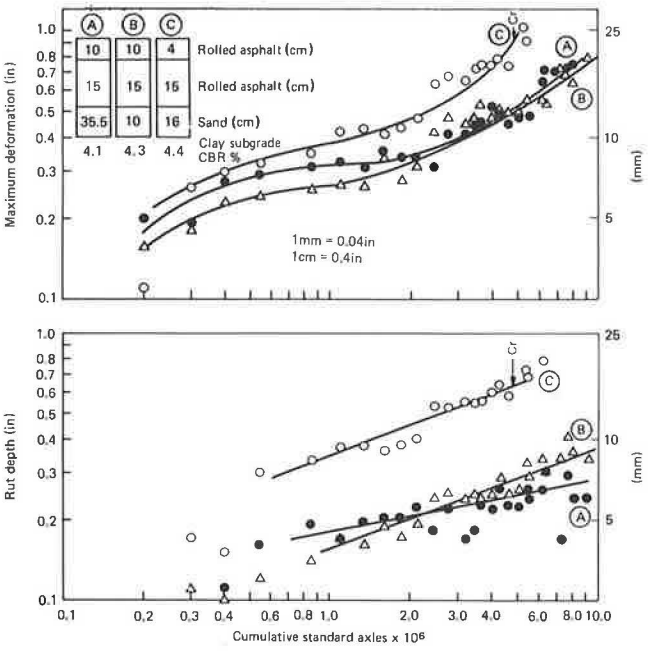

Figure 7. Development of deformation in pavement constructed with rolled-asphalt base at Conington Lodge.

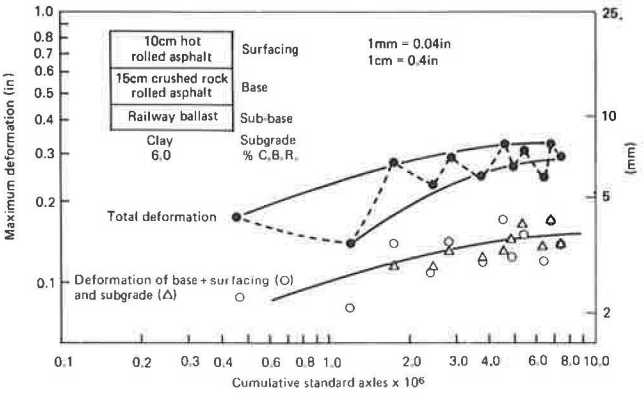

Figure 8. Relation of development of deformation in rolled-asphalt pavement and its subgrade to temperature.

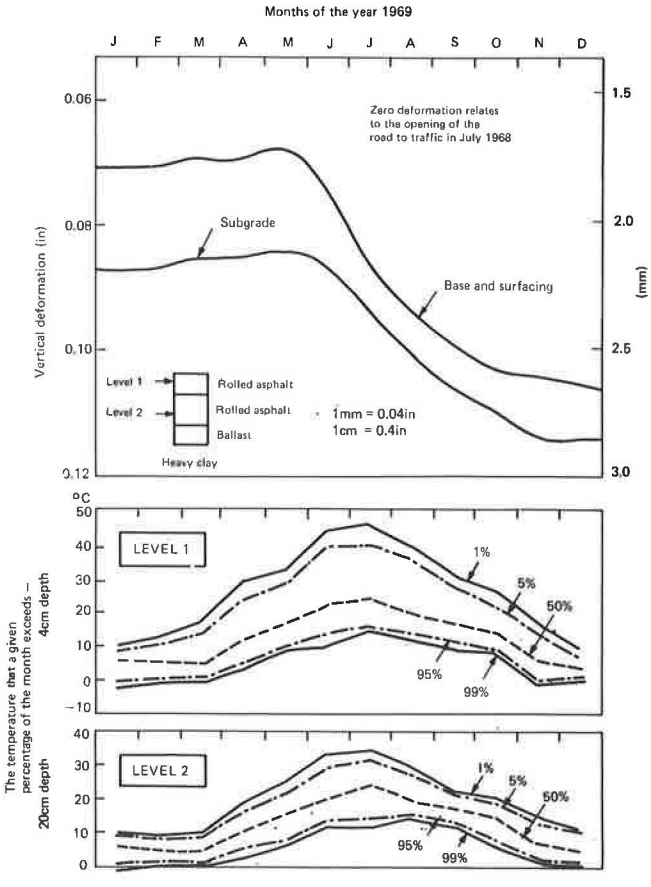

Figure 9. Development of rutting under controlled wheel loads and temperature.

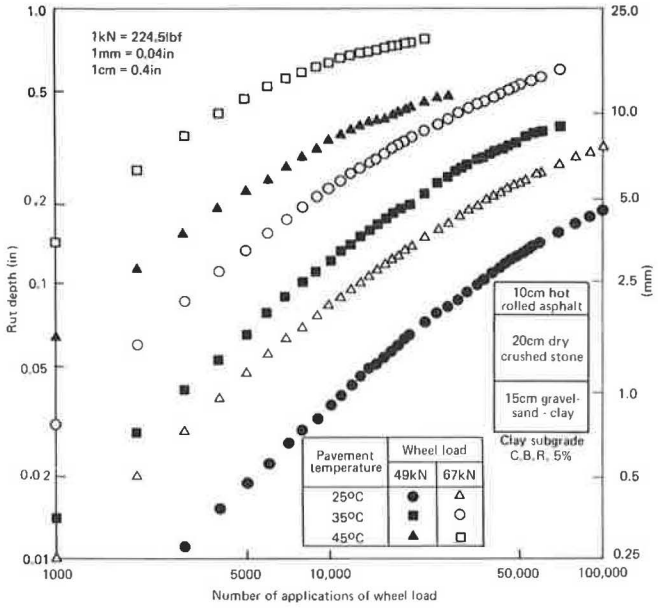

Figure 10. Comparison of development of rutting in granular-based pavement occurring under actual traffic and predicted from road-machine test results.

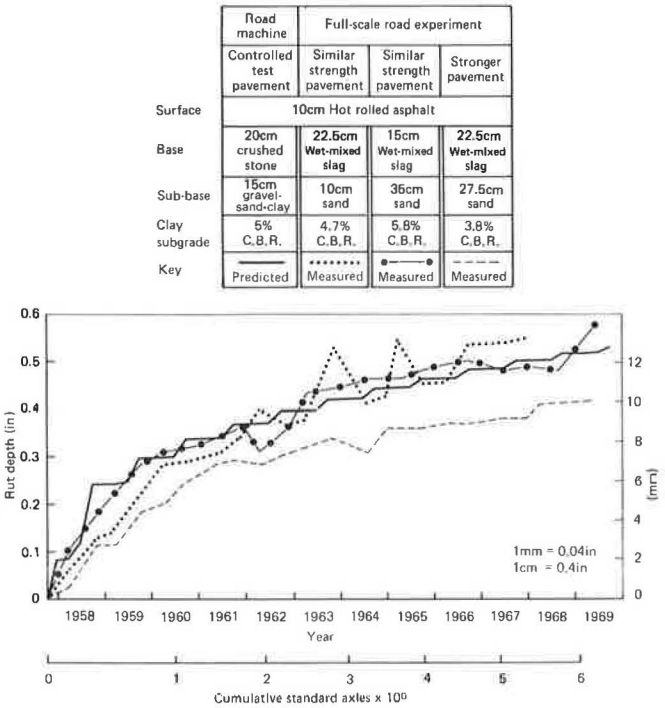

under a series of cooling cycles starting 5°C (41°F) above the mean and finishing 5°C below it. The marked influence of temperature and wheel load on the rate of surface rutting is shown; during the first 10 000 repetitions of load at 45°C, mean rates were about 10 times those at 25°C. The relatively small change in the size of wheel load from 49 to 67 kN (11 000 to 15 000 lb) resulted in a doubling of the rate, indicating the great importance of wheel-load size in the development of ruts.

The model describing rutting behavior under constant wheel-load and temperature conditions developed from these tests was used to predict the relation that could be expected between rutting and load repetitions in the test pavement when subjected to the wide spectra of wheel loads and surfacing temperatures of an actual road. Results using load and temperature data obtained at the Alconbury Hill experiment (4) were used to compute the development of rutting that could be expected under those conditions during the 12-year life of the experiment. In the computations, the increments of rut were assumed to be additive; that is, the additional depth of rut produced by the application of a particular combination of wheel load and temperature was a function only of that wheel load and temperature and of the rut depth at the time of its application.

The marked seasonal variations predicted are shown on linear scales in Figure 10; nearly all the predicted rutting developed in the three warmest months of each year (June, July, and August). Figure 10 also shows the development of rutting at the Alconbury Hill site on three experimental pavements built with granular bases. Although none is identical with the pavement tested in the road machine, good agreement was obtained with the two that can be considered to be similar in strength. The third pavement, which was definitely stronger, rutted less.

The results also indicate the great importance of large wheel loads in combination with high temperatures in the development of rutting. Out of a total rut of 14.2 mm (0.56 in) developed in 12 years of traffic, 2.54 mm (0.1 in) was contributed by the 0.003 percent of wheel loads greater than 82 kN (18 000 lb) that traversed the road when surfacing temperatures were higher than 30°C (86°F), that is, in a period corresponding to only about 4.5 percent of a normal year.

IMPLICATIONS FOR STRUCTURAL DESIGN OF PAVEMENTS

Structural methods of pavement design based on an understanding of the stress-strain behavior of pavements and subgrades are being developed worldwide. Such methods are essential to enable road designers to respond to changing technical and economic circumstances.

Essential to such methods are procedures for predicting the deformation behavior of roads from mathematical models and from experimental data on the dynamic and long-term behavior of pavement materials and soils. However, the laboratory test regimes that are practically possible do not simulate real road conditions at all closely, and the behavior of the materials themselves is complex.

Test methods and computation techniques must therefore represent a considerable degree of simplification and compromise with reality, and a link is required between the predictive procedures and the road. The link is needed for both the development and the validation of the procedures. Information from full-scale experiments on real roads cannot be used because of their mixed loading and temperature conditions.

Figure 10 suggests that the testing of pilot-scale pavements under controlled conditions of wheel loading and temperature can be used to predict the deformation of real roads. This form of testing, therefore, has potential both for developing and validating prediction procedures under simplified conditions of constant wheel load and temperature and for providing the essential extension of the validation process to the road itself.

Figure 11. Typical transverse pavement profiles superimposed on 1:40 cross slope.

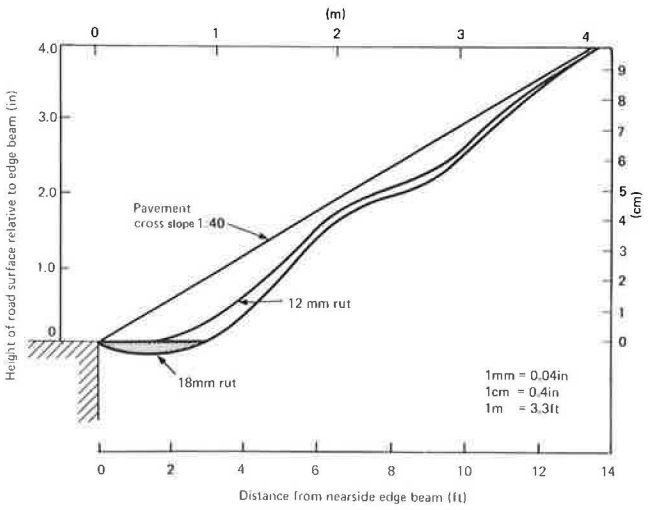

PRACTICAL IMPLICATIONS OF RUTTING

In well-designed, well-constructed roads in the United Kingdom, ruts as deep as 10 mm (0.4 in) are unlikely to be associated with cracking of structural significance. Measurements of the change of deflection with time and traffic indicate that at that stage the pavement has retained most of its overall structural strength (10) but that the development of cracking and the loss of structural strength once this critical condition is reached are less predictable. For preventive road strengthening by overlaying, United Kingdom recommendations use deflection criteria that should ensure that the rutting not exceed 12.5 mm (0.5 in) in depth and that structural cracking be confined to isolated instances (11). The equivalent value of present serviceability index is estimated to be between 3.1 and 3.3.

In the absence of strengthening measures, the road will deteriorate to failure. The criterion of pavement failure generally accepted in the United Kingdom is rutting to a depth of 18 to 19 mm (0.75 to 0.8 in) under a 1.8-m (6-ft) straightedge. At this stage rutting normally increases rapidly; water ponded in the ruts penetrates the road structure through surface cracks; and the condition of the pavement requires reconstruction of at least the base and surfacing.

PONDING OF WATER

When rutting becomes deep enough to allow ponding of water, the safety of the road user is adversely affected. Visibility in wet weather is reduced by increased splash and spray. Skid resistance in the wheel paths is reduced and aquaplaning is also a danger. In the United Kingdom in 1971, 25 000 injury accidents on wet roads were attributable to reduced skid resistance, to impaired visibility from splash and spray, and to glare at night (12).

The standard cross slope or cross fall on new construction in the United Kingdom is 1:40, or 2.5 percent. Figure 11 shows two typical transverse profiles having rut depths of 12.5 and 18 mm (0.5 and 0.75 in) superimposed on this cross fall; the shape of the ruts is distorted by the scales adopted. The potential extra hazards associated with ponding occur when ruts deeper than about 12.5 mm (0.5 in) are present, and at a failure condition the ruts may retain about 3.75 mm (0.15 in) of water. In practice rut profiles seldom follow exactly the smooth profiles shown in the figure, and actual variations will inevitably cause localized areas of ponding at depths shallower than 12.5 mm (0.5 in). Rutting confined to the surface, because of its relative thinness, may also cause ponding at depths much shallower than 12.5 mm (0.5 in). The timing of overlay placement recommended in the United Kingdom should virtually prevent ponding in most situations and greatly limit it in the remainder.

CONCLUSIONS

1. Flexible roads in the United Kingdom deteriorate primarily by rutting in the wheel paths. The development of rutting in relation to cumulative traffic can be characterized by a power index, at least up to the stage when cracking appears in the road surface at rut depths greater than 10 mm (0.4 in).
2. Development of rutting in the pavement layers and the subgrade is related primarily to the effect of high road temperatures, which increase the deformability of bituminous pavement layers and reduce their load-spreading ability.
3. Pilot-scale tests carried out with a circular road machine have quantified the effects of wheel loading and temperature on the development of rutting in a pavement with a granular road base. The results have been used to predict successfully the development of rutting in broadly similar pavements in a road experiment subject to a known mix of wheel loading and pavement temperatures. The results indicate the potential of pilot-scale testing in the development and validation of structural methods of road design.
4. Recommendations for structural strengthening in the United Kingdom are designed to ensure that ruts in pavements do not exceed 12.5 mm (0.5 in), at which safety problems associated with ponding of water in ruts are largely eliminated.

ACKNOWLEDGMENTS

The work described in this paper forms part of the program of the U.K. Transport and Road Research Laboratory, and the paper is published by permission of the director.

REFERENCES

1. A Guide to the Structural Design of Flexible and Rigid Pavements for New Roads. U.K. Transport and Road Research Laboratory, Crowthorne, England, Road Note 29, 1970.
2. G. F. Salt. Recent Full-Scale Flexible Pavement Design Experiments in Britain. Proc., 2nd International Conference on the Structural Design of Asphalt Pavements, Univ. of Michigan, Ann Arbor, 1967.
3. P. D. Thompson, D. Croney, and E. W. H. Currer. The Alconbury Hill Experiment and Its Relation to Flexible Pavement Design. Proc., 3rd International Conference on the Structural Design of Asphalt Pavements, Univ. of Michigan, Ann Arbor, 1972.
4. E. W. H. Currer. Commercial Traffic Studies. U.K. Transport and Road Research Laboratory, Crowthorne, England, TRRL Rept. 628, 1974.
5. D. Croney and J. A. Loe. Full-Scale Pavement Design Experiment on A1 at Alconbury Hill, Huntingdonshire. Proc., Institution of Civil Engineers, Vol. 30, Feb. 1965, pp. 225-270.
6. N. W. Lister and A. P. Mayo. A Gauge for the Measurement of Transient and Long-Term Displacements in Road Pavements. British Road Research Laboratory, Crowthorne, England,

BRRL Rept. 353, 1970.
7. N. W. Lister. The Transient and Long-Term Performance of Pavements in Relation to Temperature. Proc., 3rd International Conference on the Structural Design of Asphalt Pavements, Univ. of Michigan, Ann Arbor, 1972.
8. The AASHO Road Test: Report—Pavement Research. HRB, Special Rept. 61E, 1962.
9. A. H. Wilson. Distribution of Temperatures in Experimental Pavements at Alconbury-By-Pass. U.K. Transport and Road Research Laboratory, Crowthorne, England, TRRL Rept. LR719, 1976.
10. N. W. Lister. Deflection Criteria for Flexible Pavements. U.K. Transport and Road Research Laboratory, Crowthorne, England, TRRL Rept. 375, 1972.
11. P. J. Norman, R. A. Snowdon, and J. C. Jacobs. Pavement Deflection Measurements and Their Application to Structural Maintenance and Overlay Design. U. K. Transport and Road Research Laboratory, Crowthorne, England, TRRL Rept. LR571, 1972.
12. P. J. Codling. Weather and Road Accidents. Symposium on Climatic Resources and Economic Activity. University College of Wales, Aberystwyth, 1972.

Publication of this paper sponsored by Committee on Strength and Deformation Characteristics of Pavement Sections.

Viscoelastic Deformations in a Two-Layered Paving System Predicted From Laboratory Creep Results

G. Battiato and C. Verga, Chemistry Institute, Milan Polytechnic, Italy
G. Ronca, Snamprogetti, Milan, Italy

A new viscoelastic method developed to calculate deformations in a two-layered flexible pavement system subjected to both single and repeated moving loads is described. On the basis of laboratory creep experiments the rheologic behavior of all asphalt-bound materials can be represented in viscoelastic equations by a simple analytical expression for creep compliance. The mathematical analysis is performed by (a) calculating the viscoelastic deformations (vertical, transverse, and longitudinal strains) around the moving load and (b) predicting the repeated load effect, considering the effects of velocity and waiting time between two consecutive loads. The theory is applied to the asphalt pavement design for a steel slab bridge on an Italian motorway. Calculated deformations are compared with actual deformations, measured by means of strain gauges incorporated into the asphalt layers. Temperature for tests and calculations was 40°C (104°F). Both the theoretical predictions and the experimental results show that recovery is considerably delayed for the vertical and the transverse elongational deformations only. No delay was observed for the longitudinal deformation. The contribution of delayed viscoelastic deformations to total deformations was found to be relevant under some actual traffic conditions.

Elastic methods in pavement design can be used to predict the fatigue behavior of flexible pavements and generally to determine maximum deformation from the passage of a single load. These methods provide no useful information regarding the onset of permanent deformation that may be largely due to viscoelastic effects associated with the deformation from repeated loads. However, adequate methods for calculating viscoelastic deformations in layered systems are not currently available.

Some authors have provided interesting solutions to viscoelastic problems (1, 2), and even for multilayered systems (3), but these consider repeated application of static loads. This simplification may lead to a substantial underestimation of deformability in the lowest layer of a paving system, since the diffusion of stresses gives rise to an effective load time that increases with depth if the load moves on a viscoelastic system. Experimental results (4) confirm that load time relates to the load velocity and to the depth of the point under examination. For this reason viscoelastic models dealing with repeated application of a static load underestimate the deformation at greater depths. Therefore, a theoretical method was developed for predicting the viscoelastic behavior of a two-layered system subjected to repeated moving loads (5).

A two-layered, incompressible asphalt pavement system subjected to a sequence of moving loads is examined. On the basis of laboratory experiments (6), asphalt-bound materials can be characterized rheologically in terms of Equation 1, where J(t) is the viscoelastic creep compliance function.

$$J(t) = \alpha_1 J_1 \tau_o^{\alpha_1} \gamma(\alpha_1, t/\tau_o) \quad (1)$$

When a single or only a few load passages are being considered, Equation 1 reduces to the simpler formula

$$J(t) = J_1 t^{\alpha_1} \quad (2)$$

for short time periods, generally <10 s ($t << \tau_o$).

In Equation 1 $\gamma(\alpha_1, t/\tau_o)$ is the incomplete gamma function of α_1 and t/τ_o:

$$\gamma(\alpha_1, t/\tau_o) = \int_o^{t/\tau_o} u^{\alpha_1 - 1} e^{-u}\, du \quad (3)$$

Equation 2 takes slope α_1 as a straight line on a log-log plot. We assume that characteristics of the subgrade can also be described by Equations 1 or 2, provided we choose suitable values for the parameters. We observed, also, that putting $\alpha = 0$ in Equation 2 gives us the elastic behavior.

Creep tests carried out in the laboratory on a large class of asphalt concretes show that the order of magnitude of τ_o is nearly 1 000 to 10 000 s at a temperature of 20°C (68°F) and nearly 10 to 100 s at a temperature of 40°C (104°F).

The circular load function has been expressed, according to general Hankel transform methods, as a superposition of Bessel functions of order zero having a continuous spectrum of "wavelengths." The problem for a "Bessel-like" load moving on the surface of a viscoelastic double layer has been solved first.

The viscoelastic problem is then reduced to an equivalent elastic problem by means of a Fourier transformation over the time variable.

The Fourier transform of the relaxation modulus of the materials is easily obtained in an analytic form from Equations 1 and 3. Fortunately, the time-dependent load condition corresponding to a moving Bessel-like load has a Fourier transform that can also be calculated analytically.

As a consequence, general results for stresses and deformations around a moving load can be expressed via a double integral (Fourier antitransformation and integration over the wavelength spectrum of the applied load). Although we have considered a two-layered system, this conclusion applies to systems containing any number of layers.

If we are interested in calculating the viscoelastic deformation still present long after the passage of the load, the Fourier antitransformation integral can be asymptotically evaluated in a closed form, and we are left with the single integration over the Hankel wavelength spectrum. Our calculations show that appreciable accumulation effects from multiple loads are to be expected in connection with the deformation components ϵ_z, ϵ_y, and γ_{yz}. For one load passage, our viscoelastic calculations show that elastic methods predict deformations with an accuracy that is satisfactory for the first layer only. If the response of the second (subgrade) layer is not competely elastic, the methods underestimate the deformability of the lower layer by a factor that increases with the depth.

For accumulated, recoverable viscoelastic deformation from repeated loads, we show that these deformations can be as significant as those of single loads under some traffic conditions. Furthermore, when the subgrade behavior is either elastic or characterized by a viscoelastic response time substantially shorter than that of the asphalt concrete surface layer, the deformation accumulated in the surface layer is independent of the subgrade stiffness.

To predict the onset of permanent deformations from high total deformations (single load + accumulation), some experimental distress criteria are still required.

However, even if the material behaves linearly, permanent deformations may occur after each load passage if one of the rheologic models representing the mechanical characteristics of the two layers contains a Maxwell element in series. In this case only can we correlate permanent deformation with the number of load passages. On the other hand, permanent deformations in asphalt-bound layers may occur if there is a limiting deformation value above which the material undergoes irreversible viscoelastic yielding.

LABORATORY TESTING TECHNIQUES

The viscoelastic properties of asphalt-bound material can be adequately investigated by unconfined creep tests, since it has been shown (7) that the rheologic behavior of asphalt concretes is linear within a range of deformations, e.g., <1200 $\mu\epsilon$ for axial compressive strain in unconfined tests at 21°C (70°F) and <600 $\mu\epsilon$ at 38°C (100°F).

Consequently, the viscoelastic function is independent of test type if the deformations are not too great. For this reason, we think that at the present time linear isotropic viscoelasticity is the only practical approach for characterizing asphalt materials. The viscoelastic parameters of creep compliance can be measured by creep tensile tests at the required temperature. Laboratory creep tests are done with an electrohydraulic system. A step load-controlled function is applied to a cylindrical specimen. The axial strain can be measured 0.1 s after load application with two strain gauges cemented on diametrically opposite sides. A carrier frequency amplifier and a photographic galvanometer recorder are used for strain output measurements.

Specimens are prepared to ensure uniform bulk density. Samples are compacted by the application of static loading at the two ends of a cylindrical mold by means of two free, opposing plungers (8). The distribution of the bulk density inside the cylindrical specimen is checked by means of gamma ray absorption equipment (9).

THEORETICAL RESULTS FOR A TYPICAL TWO-LAYERED SYSTEM

For a sequence of circular loads moving on the surface of a double viscoelastic layer, the following model parameters were chosen:

- A = thickness of first layer of asphalt concrete = 30 cm (12 in);
- R = load radius = 12.16 cm (4.8 in);
- P = load value corresponding to a uniform pressure of 686.4 kPa (99.5 lbf/in^2) = 3250 kg (7165 lb);
- α_1 = parameter of creep compliance for first layer at 20°C (68°F) = 0.3;
- J_1 = parameter of creep compliance for first layer at 20°C (68°F) = 6.8 mm^2/N·s$^{-\alpha}$ (0.047 in^2/lbf·s$^{-\alpha}$);
- τ_o = parameter of creep compliance for first layer at 20°C (68°F) = 10 000 s;
- α_2 = parameter of creep compliance for second layer = 0;
- J_2 = parameter of creep compliance for second layer = 33.6 mm^2/N·s$^{\alpha}$ (0.23 in^2/lbf·s$^{\alpha}$);
- τ_o = parameter of creep compliance for second layer = 0;
- v = load velocity = 10 km/h (6.2 mph); and
- t_o = waiting time between two consecutive loads = 2 s.

For the sake of simplicity the second layer was assumed to be elastic ($\alpha_2 = 0$), and all materials were assumed to be incompressible (Poisson's ratio = 0.5).

Figure 1 shows depth versus the total vertical strain localized along the axis of the Nth moving load, for N = 1, 100, and 1000.

THEORETICAL RESULTS OF VISCOELASTIC THEORY ON A ONE-LAYERED SYSTEM WITH RIGID SUPPORT

Our viscoelastic theory was applied to the design of an asphalt pavement for a steel slab bridge on an Italian motorway.

The thickness of the asphalt-bound material was 10 cm (3.9 in). We assumed that there were no friction interface conditions between steel and asphalt layer, because of the presence of a thin [2 mm (0.08 in)] layer of asphalt waterproofing. The steel was assumed to behave rigidly.

The creep compliance of asphalt concrete was measured in our laboratory at 20 and 40°C (68 and 104°F) (Figure 2). The aggregate gradation for the asphalt concrete composition is given below, where 1 μm = 39 μin.

Figure 1. Accumulation of vertical deformation versus depth along center of mass of load system.

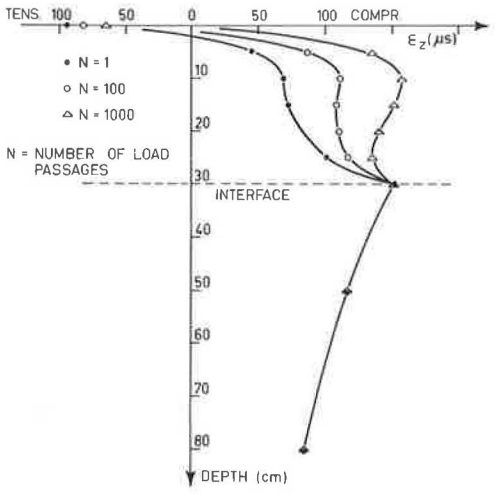

Figure 2. Creep compliance of asphalt concrete measured in laboratory.

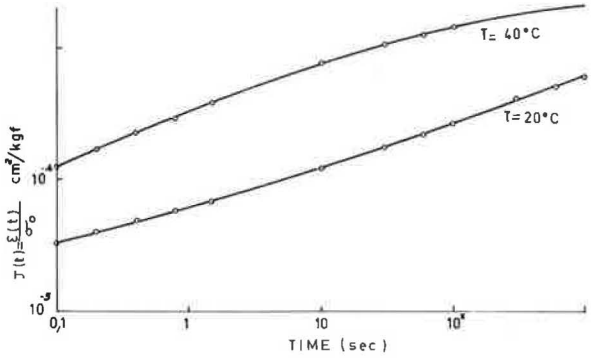

Figure 3. Experimental load parameters.

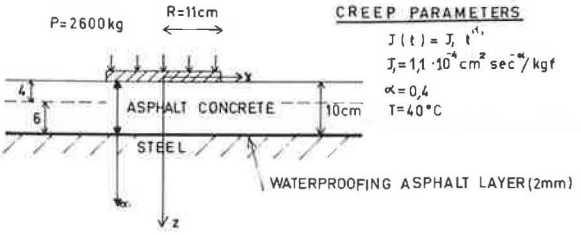

Sieve Size (μm)	Percent Passing by Weight	Sieve Size (μm)	Percent Passing by Weight
12 500	100	850	23.5
9 500	89.3	425	17.0
6 300	70.0	180	12.1
4 000	53.5	75	9.0
2 000	34.5		

The percentage of asphalt by weight of total mix (60 to 70 penetration) was 5.5; the bulk density was 2.29 g/cm^3 (0.082 lb/ft^3); the percentage of voids was 6.3; and the specific gravity of aggregate was 2.66 g/cm^3 (0.096 lb/ft^3).

The viscoelastic deformations were calculated at 40°C for velocities and experimental load parameters shown in Figure 3.

Vertical deformations relative to distance from the load center at a fixed depth of 4 cm (1.6 in) and velocity of 5 km/h (3.1 mph) are shown in Figure 4. Positive distances correspond to instants of time preceding load passage. The lack of symmetry of the curves with respect to time reversal should be noted. The same configuration can be seen for the transverse (Figure 5) and the longitudinal deformations (Figure 6).

The influence of velocity is clearly shown in Figure 7, where the maximum tensile longitudinal strain is reported as a function of velocity. It must be pointed out that the calculations show a considerable delay in recovering from deformation for the vertical and the transverse deformations only, which experience accumulation when the paving system is subjected to repeated moving loads.

Longitudinal and transverse deformations in the asphalt pavement were measured at depths of 4 and 10 cm (1.6 and 3.9 in) by means of strain gauges incorporated into the concrete during the laying operations (Figure 8). Ordinary strain gauges glued between thin kapton foil and HBM-DD 1 strain gauges were used for the measurements. A typical measured longitudinal deformation profile is shown in Figure 9. The transverse deformation is shown in Figure 10. Measurements refer to 40°C (±2°C) (104°F). In conformity with theoretical predictions, no accumulation was observed for the longitudinal strain.

Calculated and measured amounts were correlated for the transverse strain and are shown in Figure 11, and in Figure 7 for the maximum longitudinal strain. The comparison between experimental and theoretical values for longitudinal strain (at a depth of 4 cm) is fairly good with reference to the velocity dependence of deformation. Actual experimental figures are 15 to 20 percent larger than the calculated ones.

Figure 4. Viscoelastic solution for a moving load: vertical deformation.

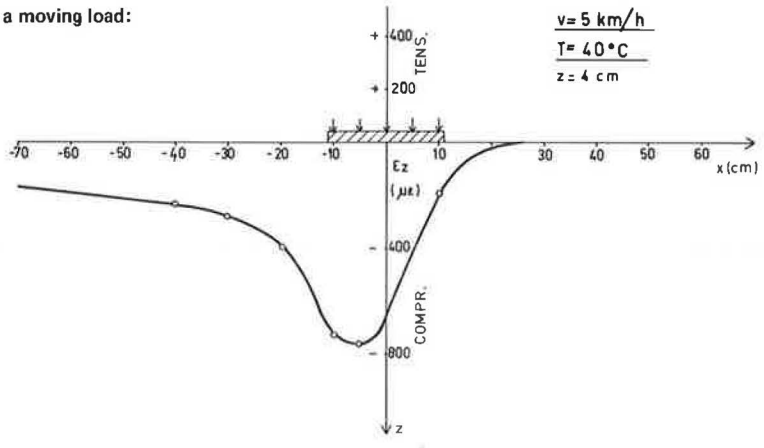

Figure 5. Viscoelastic solution for a moving load: transverse deformation.

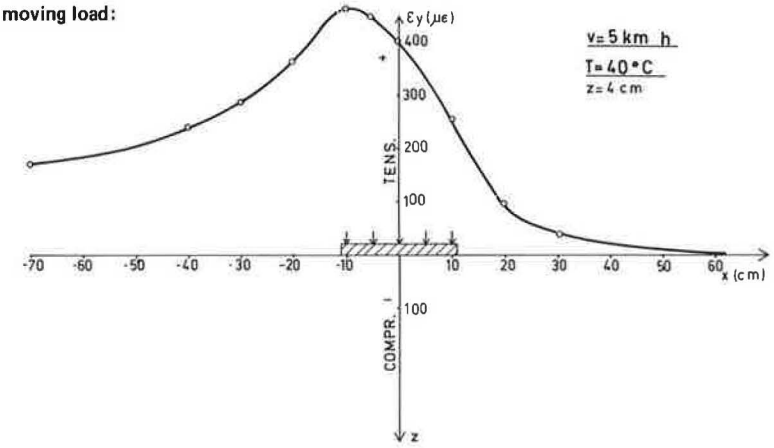

Figure 6. Viscoelastic solution for a moving load: longitudinal deformation.

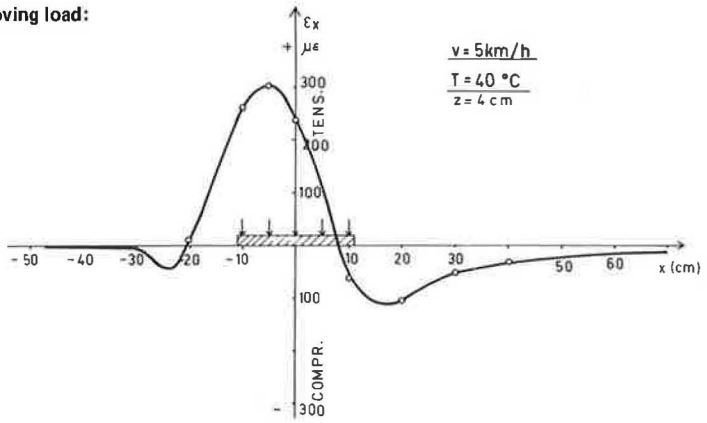

Figure 7. Longitudinal deformation versus load velocity.

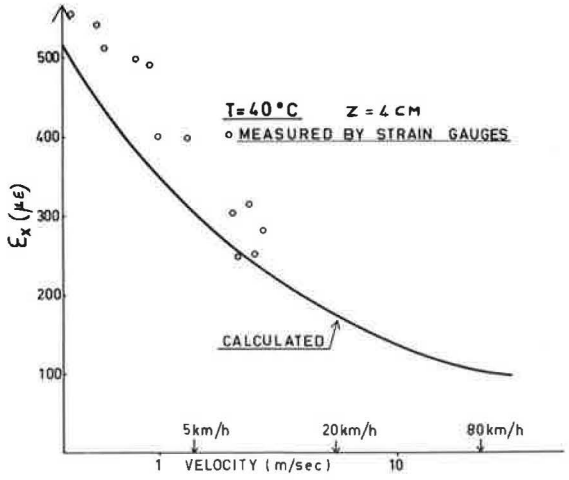

Figure 8. Strain gauges for measuring transverse and longitudinal deformation.

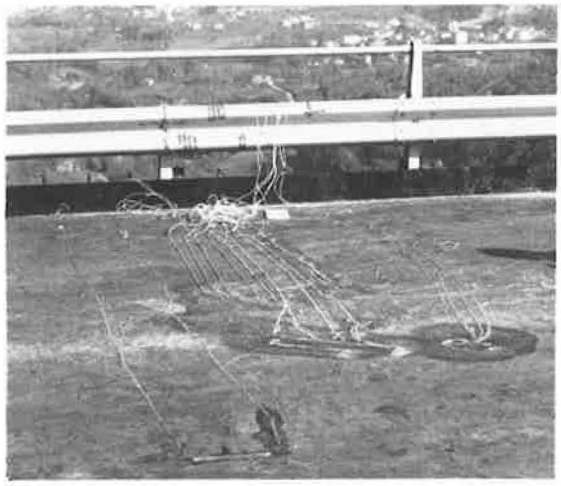

Figure 9. Experimental longitudinal deformation.

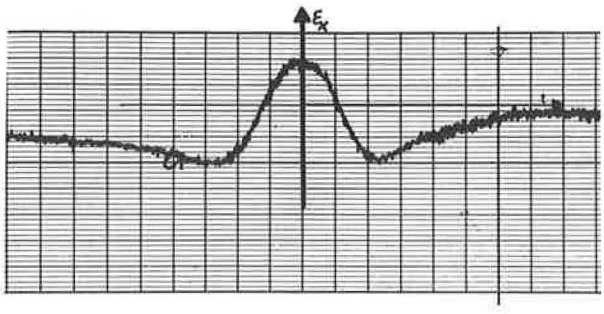

Figure 10. Experimental transverse deformation.

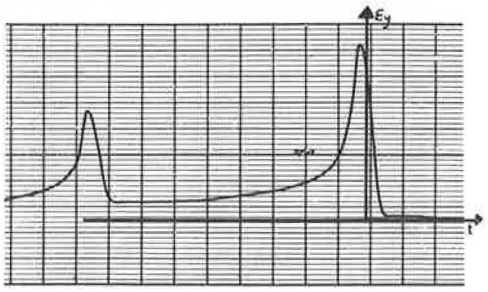

Figure 11. Calculated and experimental transverse deformation.

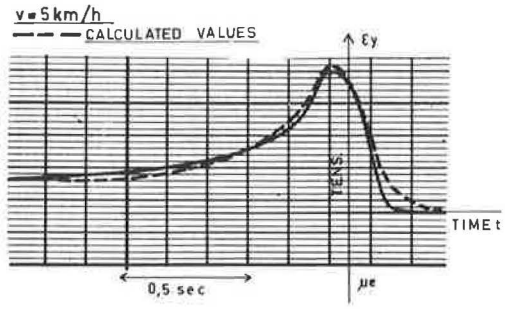

Figure 12. Accumulation of vertical and transverse deformation.

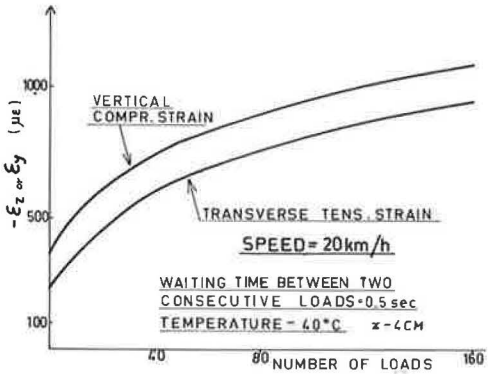

Theoretical calculation of accumulated deformation was performed for vertical and transverse strains; the fixed waiting time between two consecutive loads was 0.5 s (this is adequate when considering a large number of loads) and velocity was 20 km/h (12.4 mph). The strain accumulation is shown according to the number of loads in Figure 12; N = 40 represents five heavy trucks with trailers (under Italian traffic conditions).

The increase in vertical and transverse deformations is significant: After N = 20 passages, the transverse deformation is two times greater than that for a single passage.

Experiments are being conducted to validate our predictions concerning the repeated load effect.

GENERAL CONCLUSIONS

On the basis of the viscoelastic analysis of a two-layered system subjected to moving loads, the following can be said:

1. The calculations show considerable accumulation of deformations for the vertical and the transverse strains, but not for the longitudinal strain;
2. Strain measurements carried out in the asphalt layers on a steel bridge of an Italian motorway confirm the theoretical predictions;
3. Those viscoelastic parameters for the asphalt layers used in our viscoelastic model can be measured by simple uniaxial laboratory creep tests; and
4. The accumulation of deformations in asphalt pavements cannot be adequately investigated by repeated application of static loads, for with moving loads the loading time is related to load velocity and also depends on depth.

REFERENCES

1. F. Moavenzadeh and J. F. Eliott. A Stochastic Approach to Analysis and Design of Highway Pavements. Proc., 3rd International Conference on Structural Design, London, 1972.
2. D. B. McLean and C. L. Monismith. Estimation of Pavement Deformation in Asphalt Concrete Layers Due to Repeated Traffic Loading. TRB, Transportation Research Record 510, 1974, pp. 14-30.
3. W. J. Kenis. Response Behavior of Flexible Pavements. AAPT, Minneapolis, 1973.
4. S. F. Brown, C. A. Bell, and B. V. Brodrick. Permanent Deformation of Flexible Pavements. Univ. of Nottingham, 1973; U.S. Army Corps of Engineers.
5. G. F. Battiato, G. Ronca, and C. Verga. The Viscoelastic Analysis of a Two-Layer Paving System Subjected to Repeated Moving Loads: The Contribution of Residual Deformations. Proc., 8th International Congress on Rheology, Gothenburg, August 23-27, 1976.
6. G. Battiato, G. Ronca, and C. Verga. On the Deformability of Flexible Pavements Subjected to Repeated Moving Loads. TRB, Transportation Research Record 572, 1976, pp. 97-110.
7. K. Nair and others. Applicability of a Linear Viscoelastic Characterization for Asphalt Concrete. Proc., 3rd International Conference on Structural Design, London, 1972.
8. C. Verga, G. Battiato, and C. La Bella. Laboratory Evaluation of Rheological Behavior of an Asphalt Concrete Containing an SBR Elastomer. TRB, Transportation Research Record 515, 1974, pp. 104-113.
9. G. Battiato. Gamma Ray Equipment for Density Measurements in Asphalt Concrete Specimens. Snamprogetti, Milan, Italy, 1975.

Publication of this paper sponsored by Committee on Strength and Deformation Characteristics of Pavement Sections.

Field Measurements of Lateral Earth Pressures and Movements on Retaining Walls

H. M. Coyle and R. E. Bartoskewitz, Texas Transportation Institute, Texas A&M University

Field data were obtained and analyzed from two instrumented full-scale retaining walls. The data presented in this paper cover a period of 1156 d for a cantilever wall founded on H-piles and a period of 769 d for a precast panel wall founded on drilled piers. The data consist of pressure cell and movement measurements from both walls. For the precast panel wall, the force transmitted from the panel to the supporting pilasters was measured with force transducers. Analysis of the data indicates that movements near the bases of both walls were not large enough to develop active pressures. Earth pressure measurements near the bases of both walls were close to at-rest pressures. Earth pressures changed with seasonal variations in temperature. Pressure changes occurred as a result of construction equipment activity both during and after backfilling. Vehicular traffic after completion of construction did not produce measurable pressure changes during the time periods covered by this study.

Since the publication in 1932 of earth pressure tests on large-scale retaining wall models by Terzaghi (10), designers have accepted Terzaghi's conclusion that a small yield of the structure will cause shear resistance to develop in a sand backfill. When sufficient movement has occurred, the developed shear stress reduces the earth pressure on the wall to the active state.

Using the principles of limiting equilibrium, wall design is based not on a determination of the expected forces but on an analysis of the forces that would exist if the wall started to overturn or slide outward (5). Terzaghi observed during his large-scale model tests (10) that the lateral earth pressure existing after backfilling and before the wall yielded "undoubtedly depends to a considerable extent on the method of compaction." Terzaghi and Peck (11) observed that for rigid structures the magnitude of earth pressure depends to a large extent on the methods of placing the fill. Casagrande (1) cited the results of field measurement that revealed that even light compaction could result in the development of greater than active earth pressures. Lambe and Whitman (5) pointed out that "if the thrust against a retaining wall were greater than the active value it would not mean that potentially the wall was in trouble. On the contrary it would mean that the soil underlying the wall is much stronger than it need be." They further observed that "long before a wall can fail, it must move enough to mobilize the shear strength of the soil and to drop the thrust to its active value." The term "failure" refers to foundation failures, i.e., to overturning or sliding outward.

The designer is concerned with limiting equilibrium mechanics analysis used for foundation design and with the maximum loads that the structure will be required to support at any time. As previously stated, lateral pressures greater than those predicted by limiting equilibrium analysis may exist immediately after backfilling. Once established, these pressures will continue until outward movement occurs. This movement develops shear stresses in the backfill. As shear stresses increase, the pressure reduces, until at pending failure the active state exists. The total design of a retaining structure must consider both the effects of residual stress caused by placement of the fill and the earth pressures existing at failure.

A 5-year research study was begun at Texas A&M University in 1970 to measure lateral earth pressures in the field on full-scale retaining walls. The first year was devoted to selecting earth pressure cells that would provide both accuracy and long-term reliability. Nine cell types were considered, four of them field tested (2). Two types, Terra Tec and Geonor, were used for installation in the cantilever test wall (3) during the second year of the study. Terra Tec cells were used for installation in the precast panel wall (6) during the third year of the study. During the fourth and fifth years of the study, field data were collected and analyzed for both the cantilever and the precast panel walls. This paper presents the results and analysis of the data collected for 3 years on the cantilever wall and for 2 years on the precast panel wall.

CANTILEVER TEST WALL

Test Wall

The instrumented cantilever retaining wall was located near the intersection of US-59 and I-45 in Houston, Texas. A total of seven cantilever retaining walls were constructed at this site. One panel in a retaining wall supporting an access road was selected for instrumentation.

The test wall is of typical cantilever retaining wall design, except that it was founded on steel H-piles. A cross section of the cantilever test wall is shown in Figure 1. The test panel was approximately 4.9 m (16 ft) high and 9.2 m (30 ft) long. The significant dimensions of the cantilever wall and the location of the pressure cells are shown in Figure 2. The groundwater table was located below the footing of the wall. Weep holes were provided to allow drainage and thus prevent hydrostatic forces from building up behind the wall. The wall was instrumented in March 1972, and the backfilling operation was completed in April 1972. Paving of the access road began in May 1973. Vehicular traffic began in October 1974.

Instrumentation

The cantilever wall was instrumented with four Terra Tec and two Geonor cells, located as shown in Figure 2. The four Terra Tec cells were placed in a vertical row to measure pressure distribution behind the wall. The Geonor cells were located adjacent to the upper and lower Terra Tec cells. The cells were grouted flush with the back of the wall. A thermocouple was installed at each pressure cell location. Connecting cables and wires were secured with a strip of raw tread rubber, and a steel box on top of the wall protected the cable ends.

Results of pressure cell calibration revealed that, with no pressure applied, initial zero cell readings vary with temperature. These calibration studies are

described in detail in other reports (2, 3). Calibration tests were performed at the test site after the wall was instrumented and before it was backfilled. Pressure cell temperature variations from 21 to 32°C (70 to 90°F) were observed. Temperature correction curves were developed for each cell, and these were used to correct measured pressures. Pressure measurements were made at approximately 1-month intervals. The field measurements included cell pressure and temperature from the adjacent thermocouple. Sources of measurement error include nonlinearity, hysteresis, read-out resolution, and reading stability with temperature change. Initial calibration indicated that the cell response, i.e., pressure change measured in accordance with pressure applied, was linear within 1 percent. The effect of installation by grouting into a wall was investigated, and no effect on pressure cell response was indicated. Hysteresis was also found to be negligible. Read-out resolution of the Terra Tec cells was improved by replacing the 1724-kPa (250-lb/in^2) gauge on the read-out device with a more sensitive 241-kPa (35-lb/in^2) gauge. Read-out resolution error was 0.345 kPa (0.05 lb/in^2). Temperature corrections were made based on field calibration data. The estimated maximum error of pressure cell measurements with temperature corrections made from the field calibration was ±3.45 kPa (0.5 lb/in^2).

Wall movement was determined by two measurements: lateral translation and offset from a vertical line. Lateral translation was determined by measuring the change in distance from a fixed point on a bridge bent column to a reference point on top of the wall. The change in distance was measured to the nearest 0.51 mm (0.0017 ft) by using an engineer's scale and a steel tape. The steel tape was always pulled with the same tension, and a correction was made for tape temperature variation.

Offset measurements from a vertical reference line were used to determine relative movements of six points aligned in a vertical row. The reference line was established by suspending a plumb-bob from a permanent frame at the top of the wall. Offsets were measured

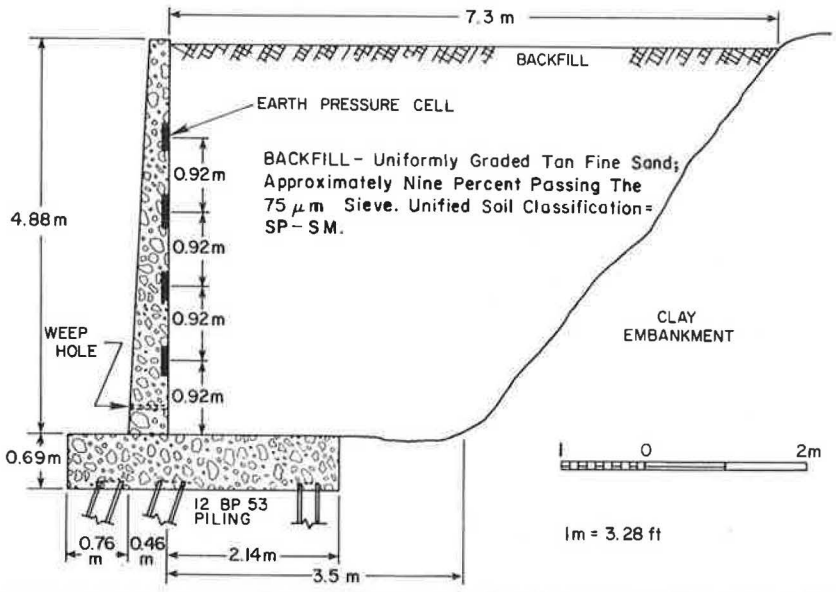

Figure 1. Cross section of cantilever wall.

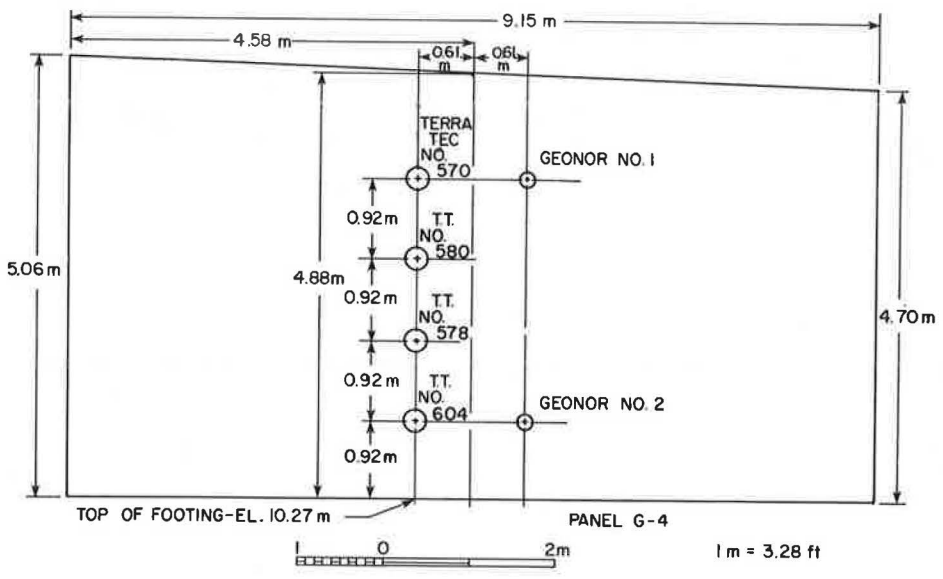

Figure 2. Location of earth pressure cells, cantilever wall.

horizontally from the reference line to each of the wall points. Initial offsets were obtained before backfilling. Accuracy of the wall-movement measurements was limited by the constraints of the test site. Continual construction required the establishment of the fixed reference point above ground level on a bridge bent column, but this resulted in possible error in establishing the horizontal movement of the wall. The relatively high flexibility of the wall reduced the accuracy of the offset measurements. The combination of these factors undoubtedly affected the accuracy of the horizontal movement computation. Thus, the long-term relationship between horizontal movement and time is of questionable accuracy. The only conclusions that can be drawn concern the amount of movement occurring during backfilling because these movements were relatively large. The offsets were measured to 0.079 cm ($\frac{1}{32}$ in).

PRECAST PANEL TEST WALL

Test Wall

The test site for the precast panel test wall was in northwest Houston, Texas. The freeway portion of US-290 is being extended in that area, and the test site was located at the intersection of the freeway extension and Dacoma Street.

This retaining wall differs in design from the cantilever wall in that it is founded on a series of drilled shafts placed at regular intervals. Footings were constructed on the drilled shafts, and T-shaped pilasters were formed on the footings. Precast panels were then placed between the pilasters and rested on neoprene bearing pads. The flange of the T-shaped pilasters supported the panels after the backfill was placed. At the test panel location the drilled shafts were 0.91 m (3 ft) in diameter, 6.10 m (20 ft) deep, and spaced at 3.66-m (12-ft) intervals. The wall was 3.05 m (10 ft) high and the footings were 0.97 m (3 ft 2 in) square and 0.4 m (16 in) high. Figures 3 and 4 show the retaining wall and its construction elements.

In Figures 3 and 4 there are several items of interest that should be noted. Fill was placed against the fronts of all walls except the instrumented panel to a height of 0.9 m (3 ft). A timber barrier was placed against the pilasters on which the instrumented panel was placed. This prevented the development of earth pressure on the front face of the instrumented panel. All panels except the instrumented one were grouted to the pilasters. A concrete gutter was placed on the backfill behind the wall, and 2 months after completion of the sand backfill a clay surcharge was placed above it at a 3:1 slope and varied in thickness from 15.2 cm (6 in) near the wall to 76.2 cm (30 in) near the top at the embankment. A drain for the backfill was placed directly behind the lower row of pressure cells.

The instrumented panel was supported at six points. Vertical support was provided by the footings through the neoprene pads, which measured 12.7 by 25.4 cm (5 by 10 in) and were 0.95 cm ($\frac{3}{8}$ in) thick. Lateral support was provided at four points on the front face of the panel. Two force transducers were installed between the pilasters and the panel on each side. The location of the force transducers and the neoprene pads is shown in Figure 5.

Instrumentation

Lateral earth pressures acting on the panel were measured by two methods. Nine Terra Tec pressure cells placed symmetrically in three rows as shown in Figure 5 measured the lateral earth pressures on the back of the panel. The second measurement method used force transducers located between the panel and the supporting pilasters (also shown in Figure 5). The transducers measured the force transmitted by the panel to the supporting pilasters.

The pressure cells and the force transducers were both installed in cavities, made during forming, in the panel for the pressure cells and in the pilasters for the force transducers. In the field the force transducers were grouted into the pilasters before the panel was installed. The precast panel was then seated against the transducers. After the panel had been installed, the pressure cells were grouted into the back of the panel flush with the surface, and a thermocouple was placed at the location of each pressure cell and force transducer. Temperature was recorded when the pressure cell and force transducer readings were taken. Connecting cables and wires were secured to the wall by strips of raw tread rubber. A steel box at the top of the wall protected the cable ends.

Terra Tec cell calibration studies (6) had shown that with no applied load the pressure readings varied with temperature. Additional calibration tests were performed after instrumentation and before backfilling. The gauge readings with no force applied were recorded over a temperature range of 7 to 23°C (45 to 74°F). A temperature correction curve for each cell and transducer was developed from these data.

Regular monthly cell pressure and temperature measurements were taken during the course of this study. The correction for zero-offset with temperature was made. The accuracy of the Terra Tec cells has been discussed previously, and based on calibration tests the accuracy of the cells installed in the panel wall was estimated to be ±3.45 kPa (0.5 lb/in^2). Calibration of the force transducers revealed negligible errors caused by nonlinearity, hysteresis, and read-out resolution. The zero-force reading versus temperature relationship was established in a manner similar to that used for the earth pressure cells; the force was calculated by correcting the field reading for temperature; and the difference was then multiplied by the transducer's calibration factor to obtain the actual force indicated by the transducer. Calibration tests indicated that the force transducer's accuracy was ±445 N (100 lbf).

Wall-movement measurements were made in a manner similar to that used for the cantilever wall. Lateral translation was determined by measuring the distance from a fixed point on a curb to a reference point on the panel. Offset measurements from a vertical reference line (suspended plumb-bob) were used to determine relative movements of seven points in a vertical row at the center of the panel. Construction activities did not interfere with our study. The fixed reference point was close to the panel wall, and the panel was very rigid. Therefore, the accuracy of the panel wall measurements was considered better than that of those made on the cantilever wall.

PRESENTATION AND ANALYSIS OF RESULTS

Cantilever Wall

Presentation of Results

The pressure cell measurements corrected for temperature are plotted versus time in Figure 6. The upper three cells were not covered until near the end of the backfilling operation on days 5 and 6. As shown in Figure 7, cell pressures increased rapidly on days 6

Figure 3. Cross section of panel wall.

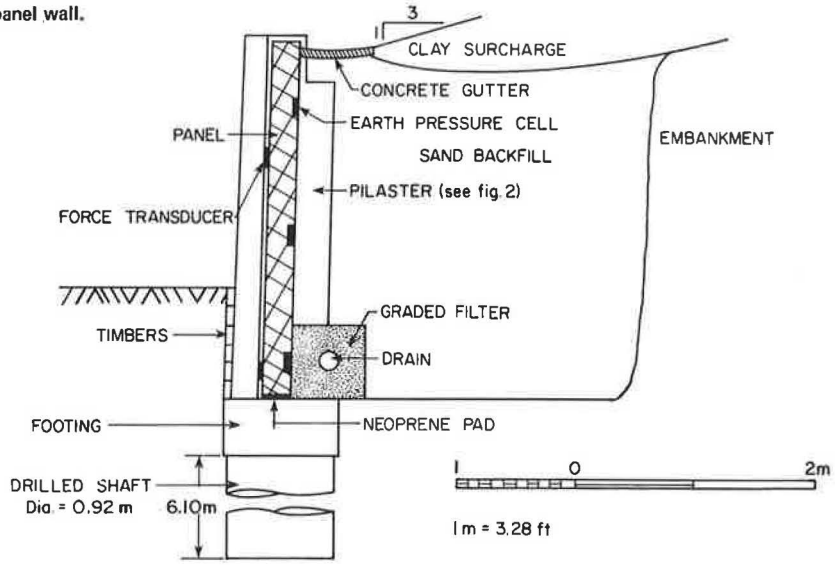

Figure 4. Front view of panel wall.

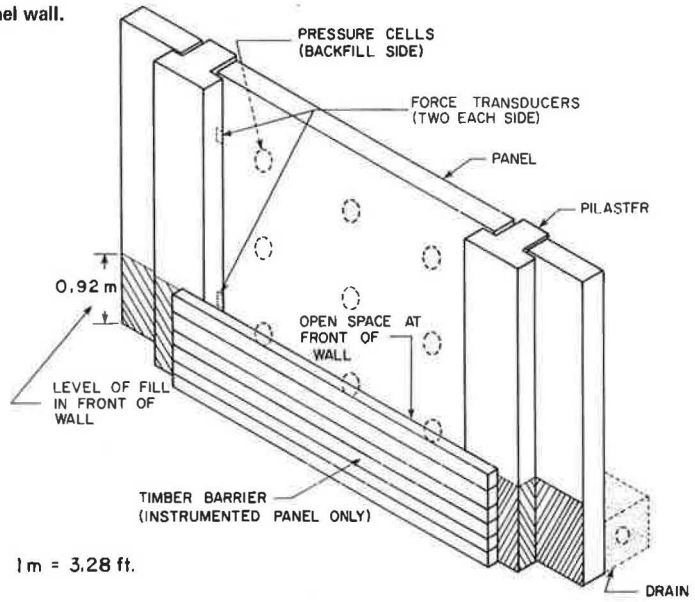

Figure 5. Location of earth pressure cells and force transducers, panel wall.

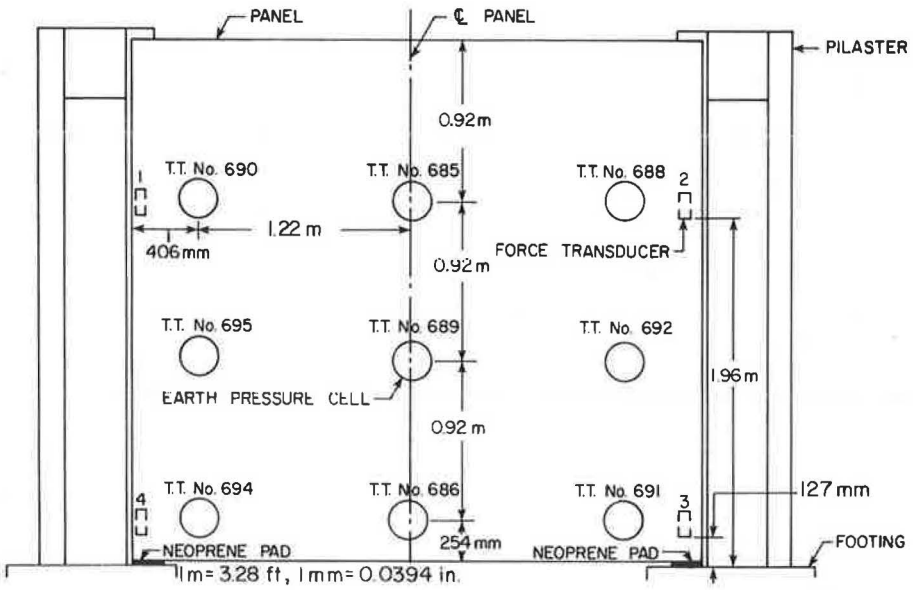

Figure 6. Measured earth pressures for cantilever wall.

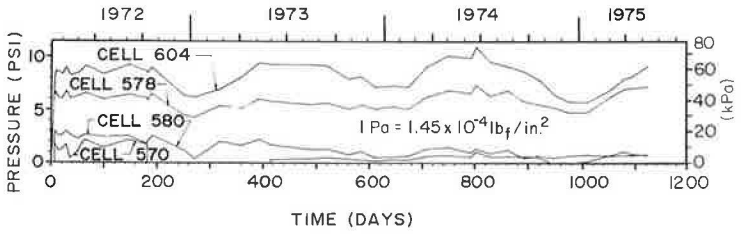

Figure 7. Pressure changes during backfilling.

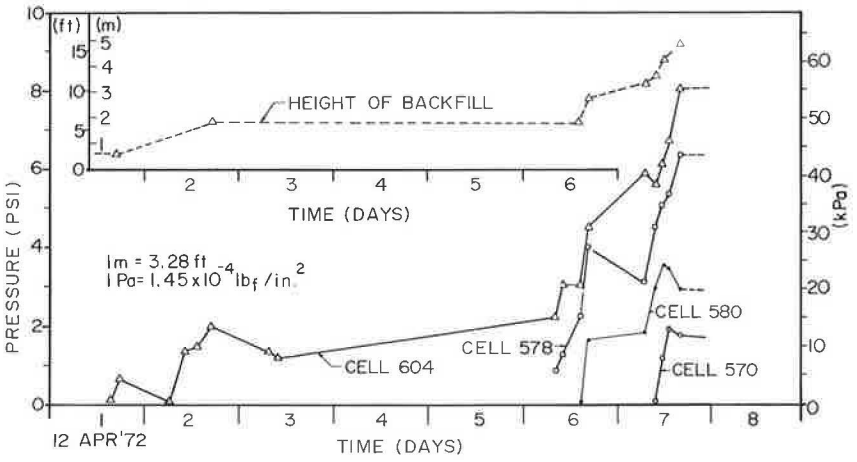

Figure 8. Typical displacements, cantilever wall.

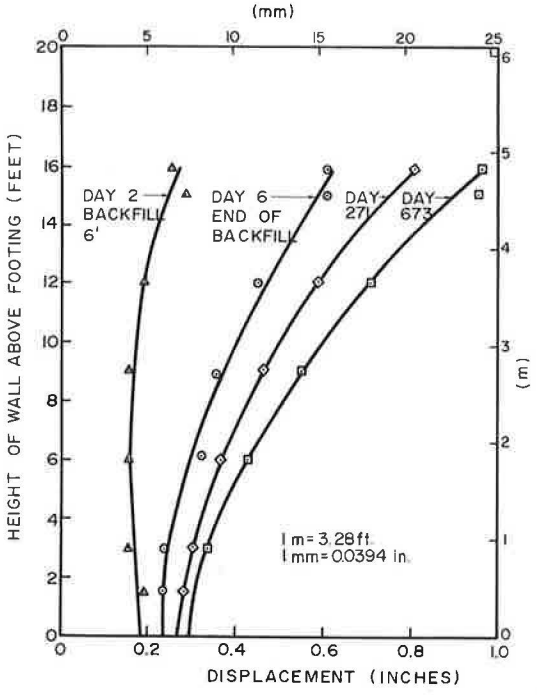

and 7. At the end of backfilling the two middle cells, 578 and 580, attained pressures near the maximum measured during the entire study. The upper cell, 570, reached a pressure within 3.45 kPa (0.5 lb/in^2) of its maximum. The lower cell, 604, was 59.3 kPa (8.6 lb/in^2) at the completion of backfilling. This was exceeded seasonally.

Obvious seasonal variations of cells 604 and 578 are shown in Figure 6. These cell pressures were lower in the winter and reached peak values during the warm months of June, July, and August. Sharp drops began in September or October; lowest readings were recorded in December or January; and recovery occurred in early spring. The range of the seasonal variation of cell 604 was approximately 24.1 kPa (3.5 lb/in^2), corresponding to 40 percent of the mean pressure, which is about that established at the end of backfilling.

Cell 570 was uncovered on day 181. The temperature calibration for zero-offset was checked and found to be unchanged. The backfill was replaced, but significant pressures were not measured for 234 d. This cell became active again on day 415. Since road surfacing work above the wall was in progress at this time, these pressure changes may have resulted from arching.

The wall-movement instrumentation system was limited by the physical constraints of the site. The movement associated with each cell is not precisely known. Analyses of these data were limited to characterizing and quantifying the movements. Typical wall displacements are pictured in Figure 8. The large deflections and horizontal movements during backfilling and the high flexibility near the top of the wall are all quite evident.

Analysis of Results

The saturated condition of the backfill material and the lack of compaction near the wall resulted in a zone of loose soil along the wall. The average total unit mass of 1623 kg/m^3 (101.3 lb/ft^3) when compared with those typical of fine sands indicated that the density was loose to medium.

The coefficients of earth pressure at rest (K_o) at the end of backfilling were computed and are shown in Figure 7. Terzaghi and Peck (11) reported that if backfilling involves no artificial compaction by tamping the value of K_o ranges from about 0.40 to 0.50 and that tamping in layers may increase K_o to about 0.8. K_o for the lower two cells, 578 and 604, are somewhat higher than 0.80. The soil at this level of backfill was allowed to drain between days 2 and 6 and was probably denser than

the soil at cells 580 and 570, where the measured K_o was slightly lower than 0.80.

Terzaghi (8) reported that at the end of construction the coefficient of lateral earth pressure depends on the relative density of backfill material, the method of compaction, and the wall movements during backfilling. As stated previously, the measurement scheme used in this study was not sufficiently accurate to allow correlation of individual pressure cell readings with movements. Movement occurred as the backfill, which was saturated at that time, was being placed. As a result, the compacted soil had a soft, plastic consistency and could have moved with the wall as compaction continued. Movements slowed abruptly when backfilling was completed.

The seasonal variations in pressure readings probably result from temperature changes in the backfill. As shown in Figure 9, these variations correlate with the seasonal changes in temperature. Pressure cell calibration tests indicated that the variations are not the result of instrument error. Water pressure buildup was not possible because the cells were located above weep holes from which frequent drainage was observed. Also, maximum pressures occurred during the summer months when rainfall was lowest.

The wall tilt required to obtain the Rankine pressure distribution was determined by Terzaghi (9) to be 0.005 times the wall height. For movements less than this the coefficient of earth pressure lies between the at-rest coefficient (K_o) and the active coefficient (K_a). The pressure distribution for an interim state is unknown but depends on wall movements.

The measured wall movement of approximately 0.76 cm (0.3 in) at the top of the wall was not sufficient to obtain the Rankine active pressure distribution over the entire height of the wall. However, pressure reductions to the active Rankine values did occur in the upper cells. These pressure reductions probably resulted from movements associated with the higher flexibility of the wall in that region. The lower two cells showed seasonal variations but on the average maintained at-rest pressures.

Precast Panel Wall

Presentation of Results

All of the pressure cell measurements corrected for temperature for the panel wall are presented in Figure 10. The cells were grouped into vertical rows. Figure 10 illustrates the pressure distribution on the left, center, and right portions of the wall.

Cells located near the pilasters exhibited similar pressure increases after the completion of backfilling. The lower cells, 694 and 691, at the panel ends recorded a rapid rise in pressure through day 38. Between days 29 and 58 a clay surcharge was added to the sand backfill, and the lower cells followed different trends during this time. These changes are depicted in Figures 11 and 12. The lower right cell (691) pressure began to register a steady decrease, dropping below the Coulomb active value about day 240; by day 560 its output had become steady at about a third of the calculated active pressure. The lower left cell (694) continued to show an increase that reached a peak about day 65, after which it exhibited a seasonal pressure variation similar to the lower cell of the cantilever wall. The seasonal variation was about 20.7 kPa (3 lb/in^2) as compared with 24.1 kPa (3.5 lb/in^2) for cell 604 of the cantilever wall. The pressures of other cells at the edges of the panel have consistently measured smaller than Coulomb active pressures.

The vertical row of cells at the center of the panel showed a different pressure distribution pattern. The upper and lower cell pressures were erratic but generally increased during the first 38 d. During the surcharge period the upper cell pressure dropped below that of the lower cell pressure and continued to remain slightly lower. Except for a brief period during the winter of 1974, the upper cell pressure has been above the Coulomb active value. The lower cell (686), despite readings higher than those of the upper cell, has shown near active pressures since day 58. The middle cell in the center vertical row has consistently shown the lowest pressure.

The movement measurement system was not sufficiently accurate to determine wall movement at specific cell locations. Since measurements were restricted to the center of the panel, determination of the estimated wall movements at the base near the pilasters was based on an analysis of the support restraints.

Unlike the cantilever wall, the panel was relatively thick in comparison to its height. Very little curvature due to flexure was detected. The base of the wall was located 0.91 m (3 ft) below ground level and was not accessible for measurement, but horizontal movement at the base was estimated. Observations with regard to wall tilt were that

1. Less than 20 percent of the tilt occurred during backfilling;
2. Tilt increased rapidly after backfilling, reaching a constant value about day 150; and
3. Tilt has not shown consistent increasing or decreasing trends.

Observations with regard to horizontal movement at base were that

1. About 30 percent of the movement occurred during backfilling and
2. Two periods of increasing movement were from backfilling to day 100 and from day 300 to day 500.

Displacement plots for some of the data are shown in Figure 13. The rotational and translational nature of early movements as well as the predominantly lateral translation later in the program are evident.

Analysis of Results

The panel-wall data indicate that increases in earth pressures after backfilling are not in agreement with the earth pressure theories of Coulomb or Rankine, who predicted that lateral earth pressures will be highest at the completion of backfilling if the wall moves outward from the backfill and external loads are not added to the backfill.

The study data show that a general trend of outward movement and increasing pressure took place between backfilling and day 38, when the clay surcharge was being placed on the backfill. Although this activity may have accounted for part of the increase, it was not responsible for the early pressure increases. There was no construction activity on the backfill from completion to day 29.

After day 38 the changes in pressures were similar to those that occurred on the cantilever wall after backfilling. Most cell pressures remained near their day-38 level. Some cell pressures decreased while others entered a seasonal cycle. In general, a steady-state condition with no long-term trends had been reached. The pressure distribution over the panel as a whole was complex.

For a typical dense sand Taylor (7) gave rough quantitative values of amounts of yield needed for two types of active cases:

1. If the mid-height point of the wall moves outward a distance roughly equal to 1/20 of 1 percent of the wall height, an arching-active case is attained. This criterion holds whether or not the wall remains vertical as it moves; however, the exact pressure distribution depends considerably on the amount of tilting of the wall.
2. If the top of the wall moves outward an amount roughly equal to ½ of 1 percent of the wall height, the totally active case is attained. This criterion holds if the base of the wall either remains fixed or moves outward slightly.

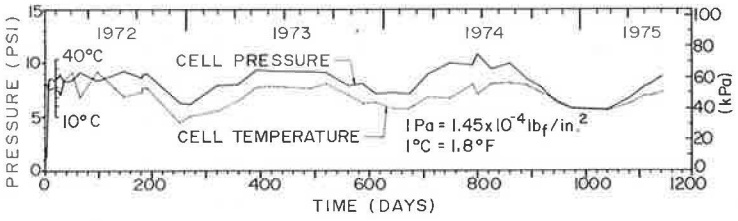

Figure 9. Temperature and pressure relationship, cell 604, cantilever wall.

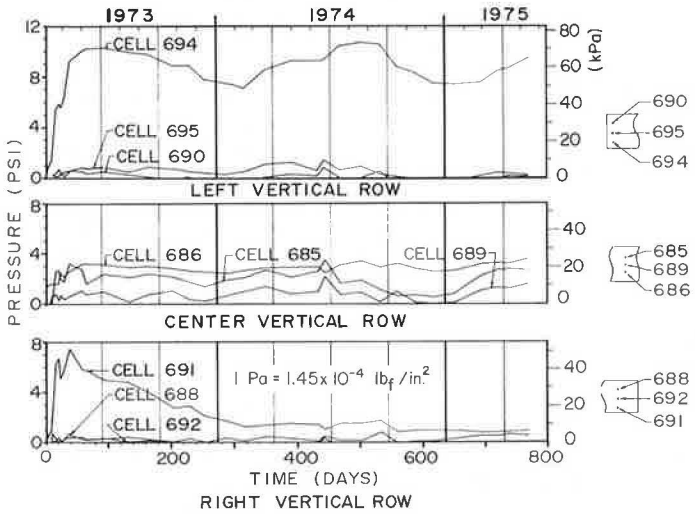

Figure 10. Pressure variations with time, panel wall.

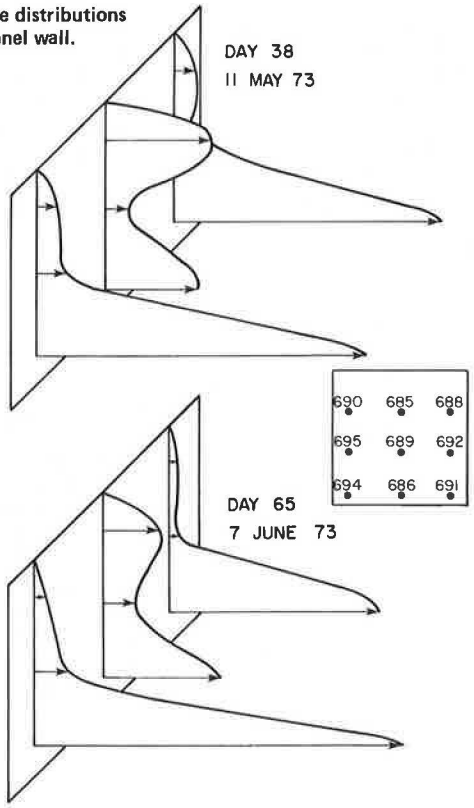

Figure 11. Pressure distributions days 38 and 65, panel wall.

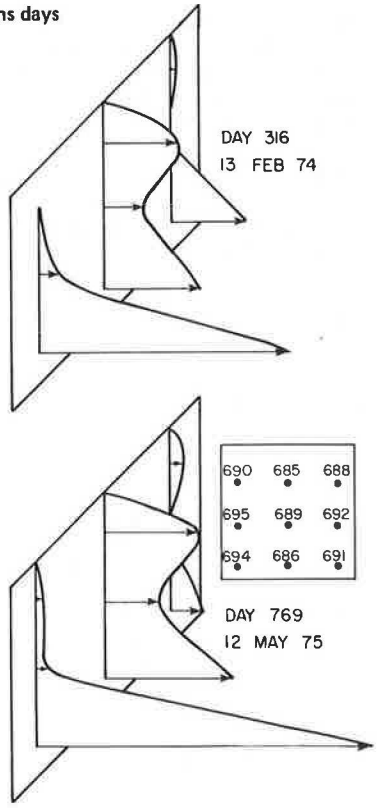

Figure 12. Pressure distributions days 316 and 769, panel wall.

For the panel wall 1.50 cm (0.59 in) of movement at the top would be required to attain a hydrostatic, totally active pressure distribution. Only 0.074 cm (0.029 in) of movement at the midheight would be required to attain the arching active case. As pointed out by Taylor (7), essentially the same total thrust on the wall occurs for both active cases. The pressure distribution for the arching active case is not hydrostatic.

If the effective yield is considered to be the movements since completion of backfilling, an estimated 1.40 cm (0.55 in) of the movement occurred at the top of the wall by day 150. This movement further increased to about 1.65 cm (0.65 in) between days 325 and 425. The smaller yields required for the arching active case occurred within 5 d after backfilling. These early movements were not accompanied by pressure reductions, and hydrostatic pressure distributions were not attained.

Lack of agreement with Taylor's estimates suggests that the state of stress in the backfill was affected by other factors as significant as movement. This was also indicated by the continuing increase in earth pressure after backfilling. The average force on the wall reached a maximum on day 38, but construction activity on this day probably caused stress changes. Pressure cell readings stabilized or began dropping at this time. The wall movements associated with the stabilized and dropping pressures were those recorded after day 38. If the effective yield is taken as the movement since day 38, the movements are not sufficient to reduce the pressures to the hydrostatic distribution of the totally active case. The reductions in total force associated with the arching active case could occur.

The force transducer data shown in Figure 14 indicate that the panel was probably not bearing evenly. Highest forces were measured by the transducers located diagonally on the lower left (4) and upper right (2) of the panel. Lowest forces were measured at the other diagonal corners. Highest forces were measured by transducer 4. Pressure cell 694 was located 35.6 cm (14 in) from transducer 4. Pressure changes of cell 694 closely correspond with force changes for transducer 4. This suggests that transducer 4 was in good contact with the wall after backfilling.

The measured forces on the upper right transducer (2) were about two-thirds of those measured on transducer 4. The total force measured by transducers 2 and 4 accounts for 70 to 75 percent of the total measured force. Although high forces were measured at transducer 2, small pressures, less than 6.9 kPa (1 lb/in^2), were measured at the closest pressure cell (688). Forces could have been transferred to transducer 2 through the panel from areas of higher pressure near the center of the panel. Transducer 3, with was located at the lower right panel corner, was close to pressure cell 691. Comparison of measured values between force transducer 3 and pressure cell 691 indicate that the large pressures measured by cell 691 during the first 29 d after backfilling were not transferred to force transducer 3. After day 38 a steady decrease in pressure was measured on cell 691. The force measurements from transducer 3 increased about 3.56 kN (800 lbf) after day 38 and remained fairly constant. The data from transducer 1 does not indicate a sharp rise associated with backfilling. This may be an indication that the panel was not bearing against this force transducer until afterward. The forces measured from transducer 1 were about 10 percent of the total for the four transducers.

As noted previously, movement measurements were made at the middle of the panel. The movements at the base of the wall, near the pilasters at the location of the neoprene support pads, were not measured directly. Since shear forces that could be developed in the pads were not accounted for in the original force computations, a test was conducted to determine the magnitude of these shear forces and is discussed in another report (6). A displacement of 0.25 cm (0.1 in) produced a shear force of about 8 kN (1800 lbf). The movements at the force transducers were estimated to be less than 0.25 cm (0.1 in). This estimate was based on a consideration of the restraint conditions in this area of panel. Since the transducers responded immediately to the placement of backfill, it was assumed that no displacement of the wall was required to engage the transducer. Thus, based on the neoprene pad shear test and the estimated movements, the forces developed in these pads were probably less than 10 percent of the approximate average of 89 kN (20 000 lbf) measured by the force transducers.

The panel wall data also suggest that earth pressure changes seasonally. The changes in earth pressure cell readings correlate with the temperature changes measured adjacent to the cells as shown in Figure 15. The force cell measurements follow a similar trend. We must emphasize again that the results of calibration studies have shown that when temperature corrections are made, the pressure cell data are accurate to within ±3.45 kPa (0.5 lb/in^2).

Arching and apparent cohesion of the backfill material could have affected the distribution of earth pressures. The phenomenon of arching provides a convenient means of explaining pressure transfer in the backfill soil and could account for both the variations in pressure cell readings across the panel and the pressure changes resulting from construction on the backfill on day 38.

Apparent cohesion can be caused by capillary forces in the sand backfill, for example, with the periodic percolation of runoff water through the backfill. An increase in effective cohesion increases the shear strength of the soil, thus reducing the lateral earth pressures on the wall. This phenomenon could also explain the seasonal reductions in earth pressures. Arching and apparent cohesion could not be measured, and the magnitude of their effect, if any, is not known.

The pressure cells and the force transducers provided independent methods of obtaining the total earth pressure forces acting on the panel. These forces were computed and are presented in Figure 16. Total forces measured by the transducers were computed by adding the force transducer readings for each set of measurements. Total forces measured by the pressure cells were determined by integration of the pressures over the entire panel.

As shown in Figure 16, there was good agreement between the cells and the transducers after about day 200. Differences were within the accuracy of the pressure cell readings and the pressure distribution assumptions. Between day 24 and day 200 the forces computed from the pressure cells were greater than the forces computed from the force transducers because cell 691 pressures were initially very high. These high pressures were not measured by the closest force transducer (3). The reasons for lack of agreement between cell 691 and transducer 3 have been discussed. The total force plot as shown in Figure 16 suggests that cell 691 pressures were not transferred to other force transducers. The reasons for these discrepenacies are not known.

SUMMARY AND DISCUSSION OF RESULTS

The test study results apply only to retaining walls of the two types tested. The most significant similarity between these structures is that they were founded on deep foundations, i.e., H-piles and drilled shafts. An important aspect of this test study is the opportunity to compare results from two structures with similar instrumentation and consistent measurements over a long period of time. Analysis of the data from both walls has shown areas with similarities in results and areas with significant differences.

Figure 13. Displacement of panel wall.

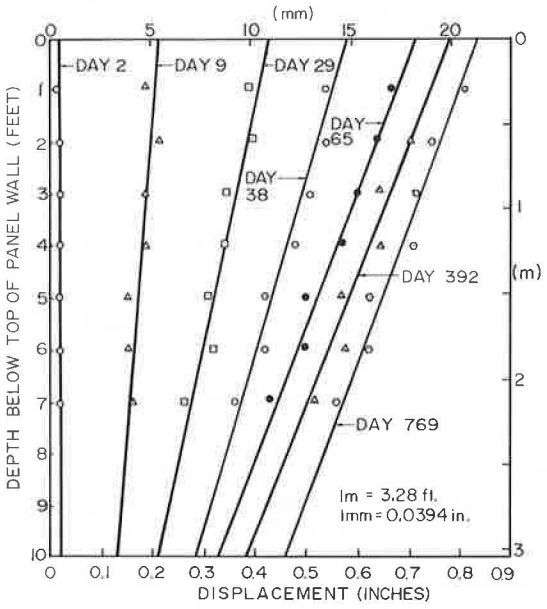

Pressure Increases After Backfilling

Earth pressures continued to increase after backfilling the panel wall. In contrast, the pressures on the cantilever wall essentially leveled off at the end of backfilling. The pressure changes after backfilling may be related to the method of compaction of the fill, as suggested by the difference in compaction procedures used for the two walls. The heavy compaction of the panel wall backfill material may have resulted in the development of residual shear stresses that continued to increase the pressures after backfilling. Placement of the clay surcharge on the panel wall around day 38 could have resulted in a redistribution of stresses in the backfill and a corresponding change in pressure at that time. On the other hand, the lighter compaction at high moisture content may not have caused residual stress to build up on the cantilever wall. The argument that residual shear stresses can cause pressure changes of the type measured is subjective. Additional field data or laboratory tests or both are required.

Earth Pressure Distributions

Four vertical distributions of earth pressure were mea-

Figure 14. Force variation with time, panel wall.

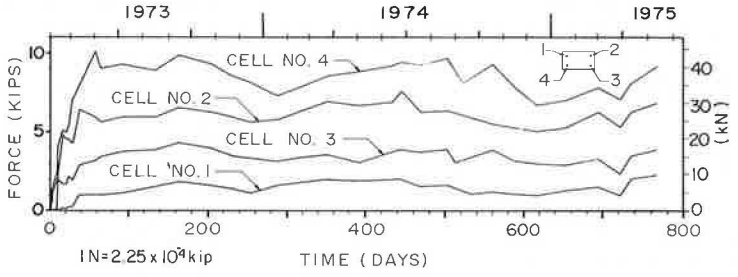

Figure 15. Temperature and pressure relation, cell 694, panel wall.

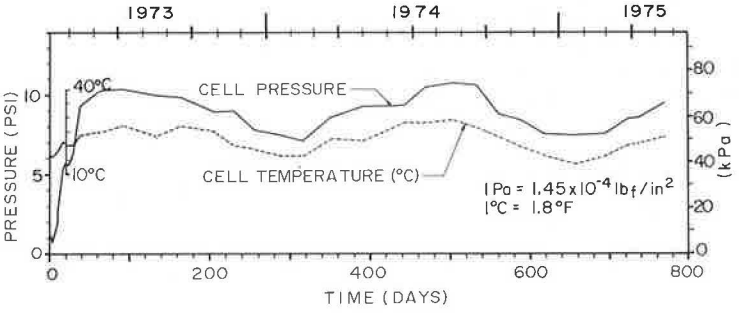

Figure 16. Total force on panel wall.

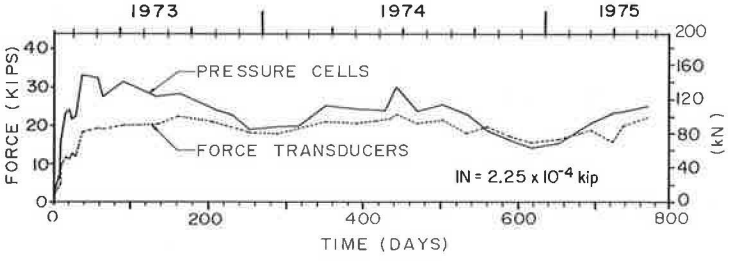

sured: three on the panel wall and one on the cantilever wall. After backfilling, earth pressures near the base of the cantilever wall and on the panel wall at the bottom of the panel near each pilaster were approximately equal to the at-rest values reported by Terzaghi and Peck (11) for dense sands compacted by tamping in layers. The pressures near the top of the wall for these distributions were lower than the at-rest values. Two of these distributions changed only slightly throughout the test study, but the lower cell at the right side of the panel wall began to decrease after day 38. Although the movements of the panel wall near the pilasters were not measured, the restraint condition at these locations was similar to that of the cantilever wall. In contrast to the center of the panel, the ends were directly bearing on the pilasters that were formed on drilled shafts. This produced the same kind of restraint as the H-piles of the cantilever wall. The principal difference was that the massive pilasters provided higher resistance to tilting. The rigidity of the pilasters was probably not important because the measured earth pressures above the lower cells at both ends was well below even the Coulomb active value. For walls founded on drilled shafts or piles the amount of yield required to effect a reduction in pressure can probably be attained only on the upper portions of the wall. This would depend on the stiffness or flexibility of the stem.

According to Kezdi (4) this type of pressure distribution may result from simple tilting about the top of the wall. Kezdi contended that the displacements required to produce frictional forces along a plane from the base of the wall to the backfill cannot be produced. Such a plane surface of sliding is assumed in the Coulomb and Rankine earth pressure theories. Kezdi therefore suggested that, based on the results of model tests, the surface of sliding originates some distance above the base. The result is that the earth pressures will remain at rest, as they have during this test study, below the point of intersection of the plane of sliding and the wall.

Effects of External Loads

Construction loads during and after backfilling did have an effect on the pressure cell readings, but vehicular traffic did not produce noticeable changes in earth pressures measured on the cantilever wall.

During the backfilling period sharp random increases and decreases in cell pressures occurred until the backfill was a few feet above the cells. This suggests that the increase in pressure as the backfill rises is accompanied by complex stress changes in the backfill caused by compaction.

Two instances of pressure changes resulting from construction after the completion of backfilling were observed: the revival of cell 570 on the cantilever wall and the high pressures occurring on the panel wall on day 38. Both of these events were associated with the movement of heavy construction equipment on the backfill near the wall.

Vehicular traffic was active on the cantilever wall for the last 239 d of the test. Cell pressures during this period followed their established pattern of pressure reduction during the winter months. Only the upper cell tended to remain constant. The panel wall was open to traffic just prior to the last set of measurements. Pressures continued to show their usual seasonal increase during early summer. The number of measurements is not large enough, however, to evaluate the effects of vehicular traffic on the panel wall.

Seasonal Pressure Variations

The most striking long-term characteristic of the study data was the seasonal increase and decrease of lateral earth pressure. These seasonal pressure variations were measured on both walls. The variations correlated closely with temperatures measured near the pressure cells and could not be accounted for by instrument error. On the panel wall, earth pressure variations were measured simultaneously by force transducers and pressure cells. These variations in pressure on both walls probably resulted from a temperature-related phenomenon occurring in the backfill material. The cause of these variations was not determined and will require additional study.

ACKNOWLEDGMENTS

The data reported in this paper were obtained during a cooperative research study sponsored by the Texas State Department of Highways and Public Transportation and the Federal Highway Administration, U.S. Department of Transportation. Receipt of this research support is gratefully acknowledged. William V. Wright did much of the analysis reported in the paper as partial fulfillment of the requirements for the master of science degree at Texas A&M University.

The contents of this paper reflect only our views, and we are responsible for the facts and the accuracy of the data presented. The contents do not necessarily reflect the official views or policies of the sponsors.

REFERENCES

1. L. Casagrande. Comments on Conventional Design of Retaining Wall Structures. Journal of the Soil Mechanics and Foundations Division, ASCE, Vol. 99, No. SM2, Feb. 1973, pp. 181-198.
2. A. Corbett, H. M. Coyle, R. E. Bartoskewitz, and L. J. Milberger. Evaluation of Pressure Cells Used for Field Measurements of Lateral Earth Pressures on Retaining Wall. Texas Transportation Institute, Texas A&M Univ., Res. Rept. 169-1, Sept. 1971.
3. H. M. Coyle, R. E. Bartoskewitz, and L. J. Milberger. Field Measurements of Lateral Earth Pressures on a Cantilever Retaining Wall. Texas Transportation Institute, Texas A&M Univ., Res. Rept. 169-2, Sept. 1972.
4. A. Kezdi. Earth Pressure on Retaining Wall, Tilting About the Toe. Proc., Conference on Earth Pressure Problems, Brussels, Vol. 1, 1958, pp. 116-132.
5. T. W. Lambe and R. V. Whitman. Soil Mechanics. Wiley, New York, 1969, pp. 33-162.
6. D. M. Prescott, H. M. Coyle, R. E. Bartoskewitz, and L. J. Milberger. Field Measurements of Lateral Earth Pressures on a Pre-Cast Panel Retaining Wall. Texas Transportation Institute, Texas A&M Univ., Res. Rept. 169-3, Sept. 1973.
7. D. W. Taylor. Fundamentals of Soil Mechanics. Wiley, New York, 1948, pp. 480-502.
8. K. Terzaghi. Anchored Bulkheads. Trans., ASCE, Vol. 119, 1954, pp. 1243-1277.
9. K. Terzaghi. Fundamental Fallacy in Earth Pressure Computations. Journal of Boston Society of Civil Engineers, April 1936; reprinted in Contributions to Soil Mechanics, 1925 to 1940, Boston Society of Civil Engineers, pp. 277-294.
10. K. Terzaghi. Large Retaining Wall Test. Engineering News—Record, Vol. 112, Feb. 1932, pp. 136-140.
11. K. Terzaghi and R. B. Peck. Soil Mechanics in

Engineering Practice. Wiley, New York, 2nd Ed., 1967, pp. 188-373.

Publication of this paper sponsored by Committee on Foundations of Bridges and Other Structures.

Permeability and Related Properties of Coal Refuse

C. Y. Chen, Michael Baker, Jr., Inc., Beaver, Pennsylvania
A. G. R. Bullen and James E. Vitale, University of Pittsburgh
H. A. Elnaggar,* Orbital Engineering, Englewood, Colorado

Perpetual treatment of acid water from coal waste dumps or from embankments constructed with coal refuse may be uneconomical. The only practical and economical method available for controlling this pollution problem appears to be the isolation of acid-generating ingredients such as pyrite from the other reagents, oxygen and water. Accordingly, controlling the permeability and air content of mine waste has become one of the most important measures in achieving this purpose. This paper focuses on the permeability of coal refuse. Data from both foreign and domestic sources were used to determine the relationship between the permeability found in the laboratory and the various index properties and to assess the effect of the reduction in void ratio caused by compaction, or other means, on the permeability of coal refuse. Traditional relationships between permeability and void ratio of soils were examined for coal refuse. Better regression models between permeability and other properties for both coarse and fine refuse were developed by using stepwise regression analysis. Some established relationships for soils were found to be unsuitable for coal refuse. Good models were developed for both coarse and fine refuse, despite the fact that the data obtained for the analyses were widely scattered in range.

Increased coal production, since the energy crisis, has generated more coal refuse, which in turn creates many environmental problems and sometimes tragic events (2, 3). Large-scale utilization of coal waste material in engineering construction and properly planned economical transformation of disposal areas into reclaimed land are believed to be the most effective measures to ameliorate the coal waste disposal problem.

In addition to the conventional engineering aspects of earthwork design, the following special considerations in using coal mine waste as a construction material should be observed: degradation, combustion, and pollution. Degradation and combustion problems have been discussed by Elnaggar, Chen, and Bullen (4, 5). The pollution problem is greatly affected by permeability. Consequently this paper focuses on the permeability of coal refuse by (a) determining the relationship between the permeability found in the laboratory and various index properties and (b) by assessing the effect of the reduction in void ratio, caused by compaction or other means, on the permeability of coarse and fine coal refuse.

NOTATION

The following notation is used in this paper:

C.I. = confidence interval,
R^2 = coefficient of determination of sample,
$\overline{R}^2$ = coefficient of determination corrected for degree of freedom,
s = standard deviation of sample,
S_{yx} = standard error of estimate,
t = t-statistic assuming null hypothesis is true,
K = number of regressors,
k = permeability,
e = void ratio,
F = fine fraction,
D_{50} = average size, and
D_{10} = effective size.

SOURCES OF DATA

A total of 57 sets of laboratory permeability results with void ratios and gradation curves were obtained from four different sources for coarse refuse (6, 7, 8, 9). Thirty-eight sets of laboratory permeability results with void ratios and gradation curves for fine refuse were also obtained from two different sources (9, 10).

ANALYSIS AND DISCUSSION

As a first step toward determining the effect of void ratio on permeability, the straight-line relationships between k and e^2 and between log k and e (11, 12, 13) were examined for both coarse and fine refuse. For coarse refuse, the linear relationship was found to have an $R^2 = 0.023$ for k versus e^2 and an $R^2 = 0.068$ for log k versus e, indicating that these two models lack explanatory power. Other statistics of these analyses further support this conclusion. As for fine refuse, a similar analysis for both models showed even poorer results. The equations obtained from regression analyses suggest two intuitively incorrect models; i.e., k decreases as e increases. Consequently, those models suggested in the literature for soils do not apply to coal refuse, particularly fine refuse.

Considering prior knowledge from soil mechanics regarding the influence of void ratio and grain size on permeability (11, 12, 13, 14), the variables used in establishing regression models for k versus void ratio and various grain sizes for mill tailings (15), and study conducted on tailing sands (16), we decided that the void ratio, average size, fine fraction, and their various products would be used as independent variables in regression analyses for coarse refuse. Subsequently, simple regression analyses were performed by using ln(k) as the dependent variable and $\ln(eD_{50})$, ln(e/F), ln(F), ln(e), $\ln(D_{50})$, and $\ln(e^2D_{50})$ as independent variables.

The results of those simple regression analyses revealed that the model with $\ln(e^2D_{50})$ as an independent variable was the best model among those six tested, as indicated by the highest t and R^2 and the lowest S_{yx}. Further analyses using step-wise multiple regression were performed. The models that showed the independent variables to be collinear were discarded, and these analyses revealed a "best" regression model with two independent variables, ln(e) and $\ln(D_{50})$. This best model confirms that the previous model having one independent variable of $\ln(e^2D_{50})$ is a very good one. A third model of these two independent variables, e and D_{50}, when expressed in nonlinear form, is

$$k = 483\, e^{3.257} D_{50}^{1.594} \quad (1)$$

This third model is shown in Figure 1, which also shows the comparison between calculated and measured ln(k). For coarse refuse, the model given by Equation 1 is the best model obtained in this study. Although the R^2 is 0.449 and the $\bar{R}^2$ is 0.429, it is a good model considering the wide variability and scatter in the permeability results (range = 0.31 to 16 000 Nm/s, average = 1837 Nm/s, and standard deviation = 3275.1 Nm/s) obtained from four different sources in two different countries.

Regression analyses were also performed for 38 sets of fine refuse data. A procedure similar to that used for coarse refuse was followed to select variables and models in performing the regression analyses. In addition to the parameters, e, D_{50}, and F, D_{10} (the effective size or the size at which 10 percent is finer) was also used (D_{10} was not used in analyzing the coarse refuse because of insufficient data).

A total of eight independent variables, $\ln(eD_{50})$, $\ln(e/F)$, $\ln(F)$, $\ln(eD_{10})$, $\ln(D_{10})$, $\ln(e)$, $\ln(D_{50})$, and $\ln(e^2D_{50})$, were regressed on ln(k) individually. Among those eight bivariate regression models, the results indicate that the best model is the one with $\ln(eD_{10})$ as the independent variable. It has the highest t and R^2 and the lowest S_{yx}. The regression equation is

$$\ln(k) = 8.709 + 1.033\ln(eD_{10}) \quad (2)$$

or

$$k = 6057(eD_{10})^{1.033} \quad (3)$$

To find a better regression model, multiple regression analyses using the step-wise method were performed. When the models whose independent variables are collinear are discarded, the model with two independent variables of ln(e) and $\ln(eD_{50})$ is considered to be the best for fine refuse. The regression equation of the best model for fine refuse, therefore, is

$$\ln(k) = 7.617 + 3.486\ln(e) + 1.235\ln(D_{50}) \quad (4)$$

This model is shown in Figure 2, which also displays the comparison between the calculated and measured ln(k). This model is considered to be a good one, given that the permeability results (range = 3 to 8860 Nm/s, average = 634.06 Nm/s, and standard deviation = 1601.52 Nm/s) obtained and used in the analysis are quite scattered.

The model for predicting the permeability of mill tailings as developed by Bates and Wayment (15) was not pursued in this study because of apparent structural problems and the resulting multicollinearities that developed when the refuse data were analyzed. Besides, Bates and Wayment's model deals only with the mill tailings, which are cohesionless, free of clays and micas, and have a well-defined grain size distribution.

The results of the following analyses, for both coarse and fine refuse, strongly indicate that of all those index properties selected and used in the regression analyses the void ratio appears to be the most important. This is clearly shown in Figure 1 for coarse refuse and in Figure 2 for fine refuse.

The results of multiple regression analyses also indicate that the coefficients of determination are generally higher for fine refuse than for coarse refuse. This might be attributed to the fact that the data for coarse refuse were obtained from four different sources including the data from England, whereas the data for fine refuse were obtained only from two different sources, both of which represent Appalachian coal refuse. Be-

Figure 1. Calculated versus measured permeability for coarse refuse.

$\ln(k) = 6.180 + 3.257\ln(e) + 1.594\ln(D_{50})$
(or $k = 483e^{3.257} D_{50}^{1.594}$)
$R^2 = 0.449$ $\bar{R}^2 = 0.429$
t = 4.200 for coef. of ln(e) (95% C.I. = ± 1.551)
t = 5.855 for coef. of $\ln(D_{50})$ (95% C.I. = ± 0.545)
n = 57

$Syx = \sqrt{\frac{\Sigma(Y_i - \hat{Y}_i)^2}{n-K-1}} = 2.481$ (s = 3.254)

(K = 2)

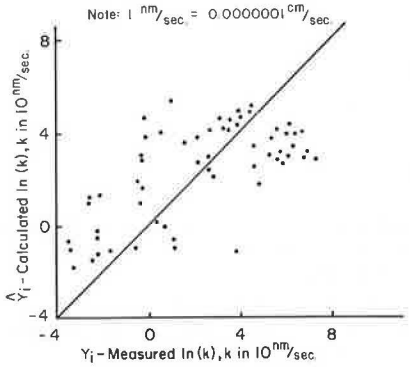

Figure 2. Calculated versus measured permeability for fine refuse.

$\ln(k) = 7.617 + 3.486\ln(e) + 1.235\ln(D_{50})$
(or $k = 2033e^{3.486} D_{50}^{1.235}$)
$R^2 = 0.695$ $\bar{R}^2 = 0.678$
t = 3.266 for coef. of ln(e) (95% C.I. = ± 2.169)
t = 8.860 for coef. of $\ln(D_{50})$ (95% C.I. = ± 0.283)
n = 38

$Syx = \sqrt{\frac{\Sigma(Y_i - \hat{Y}_i)^2}{n-K-1}} = 1.248$ (s = 2.167)

(K = 2)

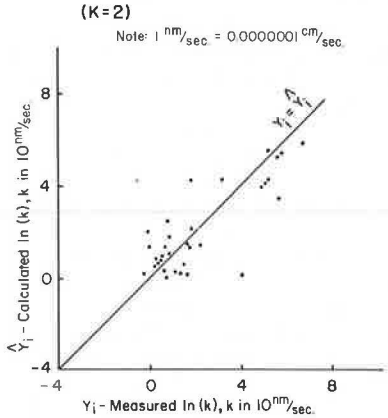

cause of this, the stochastic errors were smaller for the fine refuse than for the coarse refuse and thereby increased the coefficient of determination in the regression analysis.

Certain assumptions were made for the analyses in which inferences were made for the parent populations from which samples were drawn. These assumptions are mainly the independence and normality of data. Because of the methods and procedures used in developing and obtaining data, and the fact that each sample was obtained from an infinite population, the probabilistic sampling procedure was assured. Accordingly, the most important assumption, the independence of the random variables, is considered to be valid. The normality assumption is met because of the sample size, the use of t-distribution, and the transformation of variables. Visual inspection of the data distributions confirmed the normality assumptions.

CONCLUSIONS

The following conclusions can be drawn as a result of this study.

1. The laboratory permeability results obtained at almost full saturation and corrected to the constant temperature of 20°C show considerable scatter as can be seen from the following data:

Refuse	No.	Range (Nm)	Avg (Nm)	s (Nm)
Coarse	57	0.31 to 16 000	1837.0	3275.1
Fine	38	3 to 8860	634.1	1601.5

2. The approximate linear relationships between log k versus e and between k versus e^2, which are traditionally believed to be true for all soil types, cannot be reasonably established for coal refuse.

3. The best equations that can be used to describe the empirical relationships between the permeability and both void ratio and grain size are the multiple regression equations with both e and D_{50} as independent variables in accordance with the results of this study. This conclusion is true for both coarse and fine refuse.

4. Among all factors affecting permeability, void ratio is the most important. This suggests that the reduction in void ratio, particularly by compaction, can substantially reduce the permeability of the material in accordance with the statistical relations developed in this study.

5. Within the ranges of various material properties given below, the equations developed in this study can be used to describe and assess the permeability from various index properties.

Property	Coarse Refuse	Fine Refuse
Permeability, Nm	0.31 to 16 000	3 to 8860
Void ratio	0.202 to 1.14	0.495 to 1.256
Average size, mm	0.14 to 7.0	0.0022 to 0.4
Effective size, mm	—	0.000 23 to 0.088
Fine fraction	0.03 to 0.46	0.10 to 0.97

All refuse data used in this study came from Appalachian bituminous coal refuse, except coarse refuse data from the South Yorkshire Main Colliery of the Yorkshire bituminous coal refuse in England. This should also be considered as a limitation on the conclusions of this study.

ACKNOWLEDGMENTS

We wish to acknowledge Michael Baker, Jr., Inc., for the assistance of its staff and the use of its computer in many statistical analyses. This paper developed from the senior author's PhD dissertation, which was submitted to the University of Pittsburgh and prepared with financial assistance from the Continuing Education Program of Michael Baker, Jr., Inc.

REFERENCES

1. K. Bragg. Pollution Potentials and Interactions in Mine Waste Embankments in Canada: Their Costs and Prevention. Extraction Metallurgy Division, Canada Department of Energy, Mines and Resources, Ottawa, Rept. EMA 73-12, June 1973, pp. 1-23.
2. A. W. Bishop, J. N. Hutchinson, A. D. M. Penman, and H. E. Evans. Geotechnical Investigation into the Causes and Circumstances of the Disaster of 21st October 1966. In A Selection of Technical Reports Submitted to the Aberfan Tribunal, Her Majesty's Stationery Office, London, 1969, pp. 1-80.
3. Subcommittee on Labor, U.S. Senate Committee on Labor and Public Welfare. The Failure of Refuse Dams on Middle Fork, Buffalo. In An Engineering Survey of Representative Coal Mine Refuse Piles as Related to the Buffalo Creek, West Virginia, Disaster, Committee Print, 92nd Congress, 2nd Session, U.S. Government Printing Office, 1972, pp. 1-120.
4. C. Y. Chen, H. A. Elnaggar, and A. G. R. Bullen. Degradation and the Relationship Between Shear Strength and Various Index Properties of Coal Refuse. Proc., International Symposium on New Horizons in Construction Materials, Lehigh Univ., Bethlehem, Penn., Nov. 1-3, 1976, pp. 41-52.
5. H. A. Elnaggar, C. Y. Chen, and A. G. R. Bullen. Combustion Potential in the Utilization of Bituminous Coal Refuse in Geotechnical Construction. Proc., International Symposium on New Horizons in Construction Materials, Lehigh Univ., Bethlehem, Penn., Nov. 1-3, 1976, pp. 27-39.
6. R. K. Taylor and D. A. Spears. The Geotechnical Characteristics of a Spoil Heap at Yorkshire Main Colliery. Quarterly Journal of Engineering Geology, Vol. 5, No. 3, 1972, pp. 243-263.
7. F. J. Doyle, C. Y. Chen, R. D. Malone, and J. R. Rapp. Investigation of Mining Related Pollution Reduction Activities and Economic Incentives in the Monongahela River Basin. NTIS, Springfield, Va., PB 244-352/As, April 1975, pp. VIII 1-IX 101.
8. R. A. Busch, R. R. Backer, and L. A. Atkins. Physical Property Data on Coal Waste Embankment Materials. Bureau of Mines, U.S. Department of the Interior, R.I. 7964, 1974, 142 pp.
9. Analysis of Coal Refuse Dam Failure, Middle Fork, Buffalo Creek, Saunders, West Virginia. W. A. Wahler and Associates, Feb. 1973, Vol. 2; NTIS, Springfield, Va., PB 215-143/9.
10. R. A. Busch, R. R. Backer, L. A. Atkins, and C. D. Kealy. Physical Property Data on Fine Coal Refuse. Bureau of Mines, U.S. Department of the Interior, R.I. 8062, 1975, 40 pp.
11. J. J. Tuma and M. Abdel-Hady. Engineering Soil Mechanics. Prentice-Hall, Englewood Cliffs, N.J., 1973, pp. 96-101.
12. G. B. Sowers and G. F. Sowers. Introductory Soil Mechanics and Foundations. Macmillan, New York, 3rd Ed., 1970, p. 92.
13. T. W. Lambe and R. V. Whitman. Soil Mechanics. Wiley, New York, 1969, pp. 290-291.
14. E. S. Barber and C. L. Sawyer. Highway Sub-

drainage. Proc., HRB, Vol. 31, 1952, pp. 643-666.
15. R. C. Bates and W. R. Wayment. Laboratory Study of Factors Influencing Waterflow in Mine Backfill-Classified Mill Tailings. Bureau of Mines, U.S. Department of the Interior, R.I. 7034, Oct. 1967, pp. 1-27.
16. H. K. Mittal and N. R. Morgenstern. Parameters for the Design of Tailings Dams. Canadian Geotechnical Journal, Vol. 12, No. 2, May 1975, pp. 235-261.

Publication of this paper sponsored by Committee on Subsurface Drainage.

**Mr. Elnaggar was on the faculty of the University of Pittsburgh when this research was done.*

Soil Stresses and Displacements in a Concrete Pipe Trench Installation

Ross B. Corotis and Raymond J. Krizek, Technological Institute, Northwestern University
Thomas H. Wenzel,* Department of Civil Engineering, Marquette University

The field performance of a full-scale reinforced concrete pipe in a trench installation is described. Total normal stresses were measured by specially designed stress cells placed in the soil and at the soil-pipe interface. Relative displacements between the pipe wall and various discrete points in the soil immediately adjacent to the pipe were determined by means of settlement plates with stems extending through sleeves into the pipe. Stresses and relative displacements, as well as horizontal and vertical diameter changes, were monitored periodically as the height of cover above the pipe increased. In general, the experimental measurements are mutually consistent and compatible with previous experience and judgment; however, there are some differences between the experimental data and the results calculated from a plane strain, finite element model with appropriate soil parameters.

Described here is the field performance of a full-scale reinforced concrete pipe buried in a trench installation. Instrumentation was provided to measure the normal stresses at the soil-pipe interface and in the adjacent soil, the displacements in the soil above and below the pipe, and deformations of the pipe. Experimental measurements are shown to be mutually compatible and in qualitative agreement with intuitive expectations based on engineering judgment. Typical results at discrete points in the soil-pipe system are compared with values calculated by use of a plane strain, finite element model and soil parameters determined, insofar as possible, from uniaxial strain tests and triaxial compression tests on the actual disturbed and undisturbed soils from the field installation.

FIELD EXPERIMENT

The test site, which is shown in Figure 1, is located in East Liberty, Ohio, about 64 km (40 miles) northwest of Columbus, on the grounds of the Transportation Research Center of Ohio. A 1.5-m (60-in) inside diameter, 2300 D, B-wall concrete pipe (manufactured by the wet cast method) was installed in a trench with a cover of 7.6 m (25 ft). The required strength of the pipe was determined by means of the Marston-Spangler theory, and the pipe was installed in accordance with the specifications of the Ohio Department of Transportation. The pipe size selected is the result of a compromise between the smallest pipe that allowed reasonable access of personnel and instruments and the largest pipe that could be used with the available cover height, which was dictated by topography and economics. As shown in Figure 2, the installation consists of five 2.4-m (8-ft) lengths of instrumented pipe (the middle one of which is most heavily instrumented), several buffer sections at either end, and a vertical access shaft.

Prior to the manufacture of these pipe sections, an instrumented pipe was tested to ultimate load in a three-edge bearing test to ascertain (a) that the inclusion of internal instrumentation (with the associated holes and inserts) in the pipe cross section would not measurably reduce the strength of the section, (b) that the techniques for applying the instrumentation within the walls of the pipe were adequate to protect the instrumentation during casting, and (c) that measured results (when interpreted within the context of a theoretical model of the pipe only) realistically represent the actual values. Since the results of this test were favorable, the pipe sections for the field installation were manufactured in a similar manner.

The installation of the test pipe was undertaken in June 1971 and was completed within a period of 9 d. As indicated in the boring log shown in Figuro 3, two distinct soils were encountered during excavation. To a depth of approximately 3.7 m (12 ft) there was a coarse to very fine sand with stone fragments and some silt, and from 3.7 m (12 ft) to about 9.1 m (30 ft) there was a dark gray clayey silt; at a point about 9.1 to 10.7 m (30 to 35 ft) below the surface a very granular layer and considerable water were encountered. The soil increased in silt content with depth from 10.7 to 12.8 m (35 to 42 ft), at which point the boring was terminated. The pipe was bedded at a level about 9.4 m (31 ft) below the surface. As a consequence of the unstable nature of the top 4.5 to 6.0 m (15 to 20 ft), the trench was excavated with somewhat unsymmetrical, sloped sides with an approximate 1:1 ratio on one side and about 0.7:1 on the other as shown in Figure 2b; the width of the trench varied from about 3.0 to 3.7 m (10 to 12 ft); the greater width was near the vertical access shaft. Some photographs of the test installation are shown in Figure 4.

Although the laying of the pipe was done basically in accordance with practices recommended by the state of Ohio, a few points are worthy of note. First, the 15 cm (6 in) of compacted granular material at the bottom of the trench was not shaped to fit the contour of the pipe; hence, the pipe had essentially line support along the

bottom (Figure 4a). Second, the initial sidefill was placed in a 1-m (3-ft) layer to the springline of the pipe (Figures 4b and 4e), and only the surface of this layer was compacted by small manually operated vibratory tampers. Subsequently, the granular material was placed in approximately 30-cm (1-ft) layers to a height of 1.2 m (4 ft) above the crown of the pipe and compacted with these tampers (Figure 4f). Third, as the sidefill reached the top of the pipe, the groundwater infiltrating the trench virtually saturated the granular material, and several conditions of liquefaction were experienced when attempts were made to compact the sidefill with the tampers. However, as the fill progressed above the pipe, this condition was not encountered with as much severity. Fourth, the backfill from 1.2 to 7.6 m (4 to 25 ft) above the pipe consisted of random mixtures of the two excavated soils, making it virtually impossible to determine with any degree of reliability the point-to-point variations in the mechanical properties of this backfill. This material was compacted with a sheepsfoot roller (Figure 4h), but no specific standards were required or achieved. And fifth, very soon after installation, the groundwater saturated the granular material that enveloped the pipe, and some minor leaks in the pipe system developed. However, these leaks were sealed so that seepage into the pipe was maintained at tolerable levels, and no significantly adverse effects resulted.

Figure 1. Location of field site.

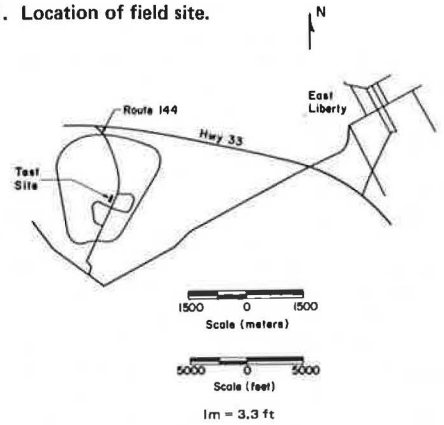

Figure 2. Longitudinal and cross sections of field installation.

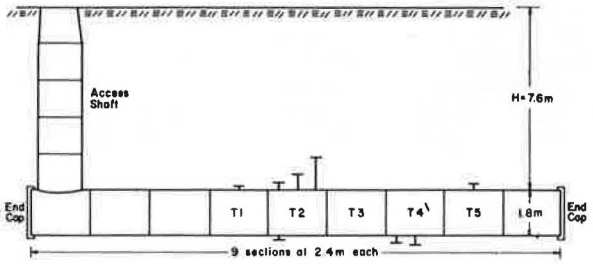

(a) Longitudinal Section Showing Locations of Settlement Plates

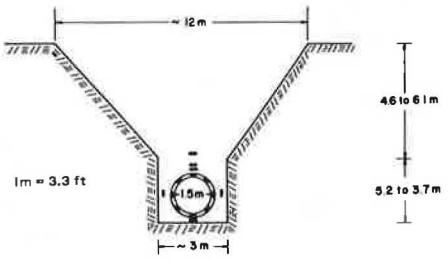

(b) Cross Section Showing Locations of Stress Cells

Stress Distributions

Ten 15-cm (6-in) diameter total stress cells were installed in the wall of the principal pipe (T3, Figure 2); single cells were placed every 45° [alternately in two planes spaced at ±75 cm (30 in) from the midplane] around the pipe with two cells at the top. These cells were placed in recesses made when the pipe was cast, and the surfaces of all cells were flush with the surface of the pipe. In addition, five 25-cm (10-in) diameter total stress cells were placed at discrete points in the soil surrounding the pipe [within 75 cm (2.5 ft) of the pipe]. Three cells were located above the pipe, one below, and one at the springline. The particular locations of these cells relative to the pipe are depicted in the cross-sectional view in Figure 2b. However, the cells were distributed in different transverse planes to avoid interaction among cells. The construction of these cells and an evaluation of their reliability have been reported by Krizek and others (2).

Stress and temperature measurements were obtained from a digital read-out voltmeter and converted to units of gauge pressure. Normal stress distributions around the pipe under various fill heights are shown in Figure 5. Those distributions were drawn by fitting curves to the symmetrized data, which were measured every 45°. The narrowness of the peak at the invert can be explained as an attempt to satisfy vertical equilibrium of normal stresses; furthermore, the fact that the pipe was laid on a flat bed provided for pipe contact with the compacted bedding over an approximately 10° or less arc. However, the following situation regarding vertical equilibrium of normal stresses on the pipe must be

Figure 3. Log of soil boring at field site.

Depth (m)	Standard Penetration Value N	Description	Physical Characteristics: Gravel (%)	Coarse Sand (%)	Fine Sand (%)	Silt (%)	Clay (%)	Liquid Limit (%)	Plasticity Index (%)	Water Content (%)	Class
1.5	10/7	Brown Stone Fragments with Sand	-	-	-	-	-	-	-	13	-
3.0	6/6	Gray Stone Fragments with Sand	-	-	-	-	-	-	-	3	-
4.6	6/7	Gray Sandy Clayey Silt with Stone Fragments	30	9	14	29	18	21	9	12	A-4a
6.1	3/5	Gray Sandy Clayey Silt	13	9	16	38	24	20	8	12	A-4a
7.6	8/8	Gray Sandy Clayey Silt	14	9	15	36	26	20	8	12	A-4a
9.1	6/20	Gray Sandy Clayey Silt with Stone Fragments	20	10	15	35	20	20	8	13	A-4a
10.7	18/24	Gray Gravel with Sand	49	24	13		14	NP	NP	14	A-1b
	16/20	Gray Stone Fragments with Sand and Silt	57	8	9	16	10	21	8	8	A-2-4
12.2	10/16	Gray Sandy Clayey Silt with Stone Fragments	31	12	13	27	17	20	8	10	A-4a

1m=3.3ft

Figure 4. Construction photographs of the test installation.

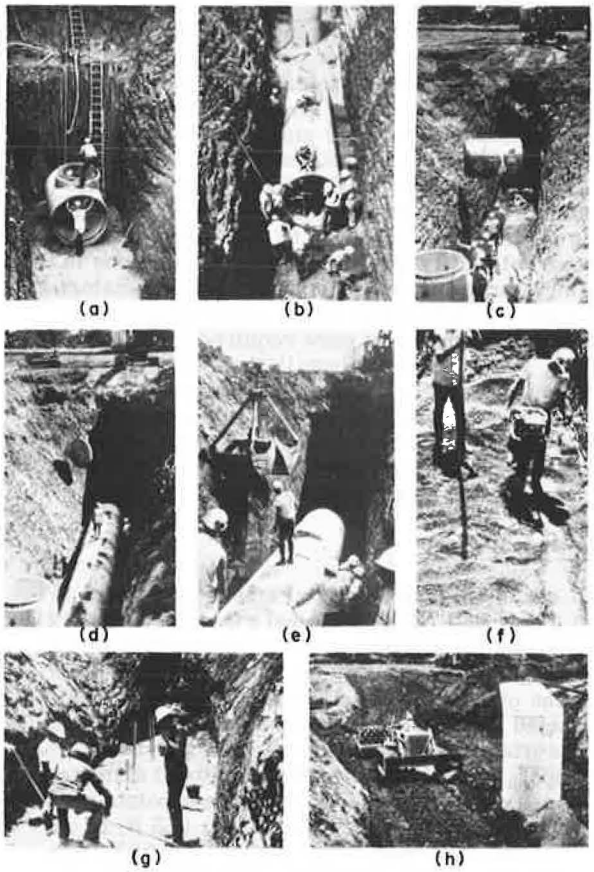

appreciated. The total stress cells measured only normal stresses, and no experimental data were obtained on shear stresses along the soil-pipe interface. Since shear stresses would, in general, not be zero, it follows that the complete stress distribution at the soil-pipe interface has not been obtained, although the satisfaction of equilibrium for an incomplete stress system is not actually necessary. Readings from symmetrically placed cells are reasonably similar, but the resulting stress distributions shown in Figure 5 are quite different from those suggested in the classical Marston-Spangler approach (Figure 6). In assessing the normal stress distribution depicted in Figure 6a, it is important to recall that the support at the bottom of the pipe has been assumed to be very narrow. This is a very substantial assumption and undoubtedly explains much of the difference between the Marston-Spangler analysis and the smoothed experimental curve. In general, the effect of time (stress measurements were taken for approximately 3 years) on the stresses at the soil-pipe interface caused increases of about 10 percent in some cells and no increases in others, with no apparent pattern.

Except for cell S11 at the crown of the pipe, all of the cells apparently functioned properly, although there is some discrepancy in the readings of replicate cells. The fact that cell S11 manifested virtually no increase in stress with an increase in fill height can probably be explained by improper performance of the cell itself (or the presence of an extremely soft spot in the immediate vicinity of the cell). The data from cell S18 have been used to develop the experimental stress distributions at the soil-pipe interface. The pairs of cells symmetrically placed on opposite sides of the pipe at the upper and lower quadrant points gave somewhat different readings, although they all followed consistent trends with increasing fill height. However, the measured differences be-

Figure 5. Normal stress distributions around pipe in field installation.

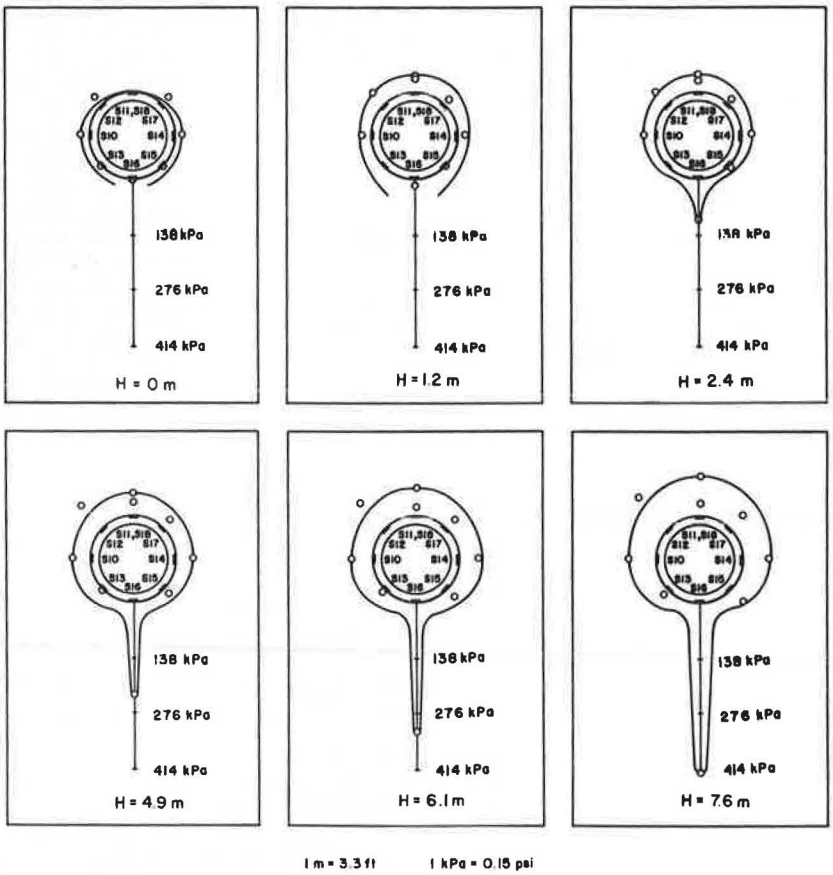

tween the readings on the two sides are not great and were probably caused by actual variations in the stresses from local nonhomogeneities in the soil. The cells located on opposite sides of the pipe at the springline gave excellent agreement. The three cells in the soil 15, 30, and 75 cm (6, 12, and 30 in) directly above the pipe yielded stresses that were mutually consistent [readings from the two cells closest to the pipe

Figure 6. Experimental and theoretical normal stresses on pipe at 7.6 m (25 ft) of fill height.

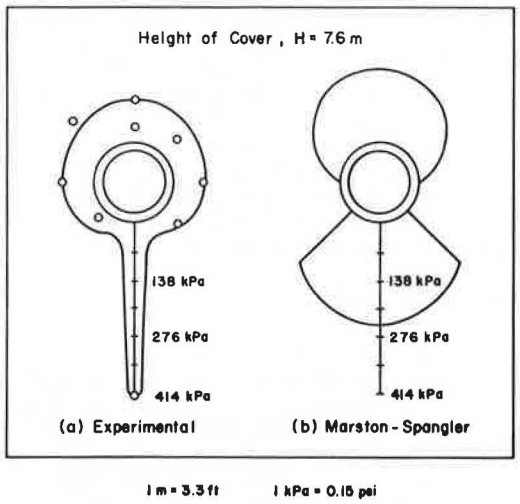

Figure 7. Experimental relative displacements between pipe and soil at 7.6 m (25 ft) of fill height.

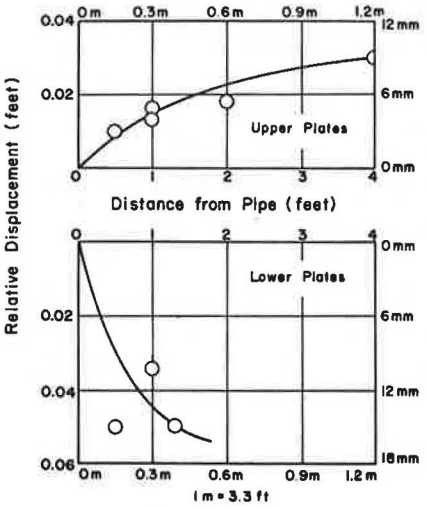

Figure 8. Finite element model of soil-pipe system.

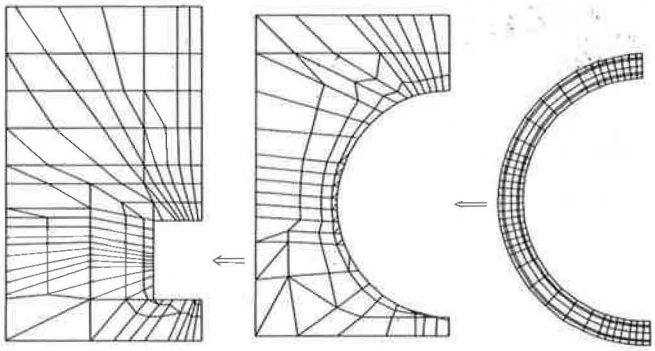

were essentially similar and slightly higher than that from the cell 75 cm (30 in) above the pipe], but about double the stress from cell S18 in the crown of the pipe. No obvious explanation can be advanced for this phenomenon. The cell 15 cm (6 in) directly below the pipe gave stresses that are somewhat higher (about 30 percent at greater fill heights) than those given by cell S16 embedded in the bottom of the pipe. This situation, as well as the fact that cell S16 yielded disproportionately low readings for low fill heights, suggests that the cell is resting on a low or a soft spot in the bedding. The horizontal stresses measured by the cell embedded in the soil at the springline 23 cm (9 in) from the pipe wall were about two-thirds of the interface stresses measured at the springline, which is entirely consistent with expectations.

Soil Displacements

The relative vertical displacements between the pipe wall and various discrete points in the surrounding soil were measured by settlement plates, whose vertical stems passed through sleeves in the crown and invert of the pipe, as illustrated in Figure 2a. Above the pipe, settlement plates were located every 30 cm (12 in) at points 15, 30, 60, and 120 cm (6, 12, 24, and 48 in) from the pipe wall. Settlement plates were also positioned at points 15, 30, and 40 cm (6, 12, and 16 in) below the pipe. The relative displacement between the pipe invert and some fixed benchmark was not measured, so the actual translation of the pipe itself is not known. In general, the relative displacements measured by these plates increased as the height of fill increased and as the distance of the plate from the pipe wall increased. The plots of relative displacement versus distance from the pipe wall are given in Figure 7, and the strain at any point in the soil may be visualized as the slope of the resulting curve at that point. Figure 7 shows that the strains in the soil attenuate rapidly with distance from the pipe wall. This attenuation has been suggested by virtually all continuum models of soil-pipe interaction, but there has been little substantiating experimental evidence.

COMPATIBILITY OF EXPERIMENTAL MEASUREMENTS

Some appreciation of the reliability of the foregoing experimental measurements can be obtained by examining the mutual compatibility of the data and their consistency with physical evidence. Perhaps the most obvious feature is the high stress intensity measured at the bottom of the pipe. As mentioned previously, this is a direct consequence of the flat bedding employed. Because of the difficulty of compacting the backfill under the haunches of the pipe, relatively low interface stresses would be expected to develop in this area, which was indeed the situation observed. The horizontal stresses developed at the springline indicate that the soil provides considerable lateral support to the pipe, which is consistent with judgment and the measured horizontal diameter changes. The measured interface stresses at the bottom of the pipe are about four times those measured at the top. Considerably greater strains would therefore be expected in the soil below the pipe. The strain in the soil at the soil-pipe interface may be approximated by taking the initial slope of the relative displacement-distance plots shown in Figure 7. Thus it is seen that the strain in the soil below the pipe is about five times that above the pipe. Since the same soil was used above and below the pipe, these comparative values lend considerable support to the argument that the data

are mutually compatible. A simple ratio of vertical stress to vertical strain at these points gives a value of 4000 or 5000 kPa (600 or 700 lbf/in^2), but it should be cautioned that such a value is useful primarily to identify a reasonable order of magnitude, because the actual stress and strain conditions in the lateral direction are not known. The situation probably cannot be modeled realistically by a uniaxial strain test. Despite some of these discrepancies in the data, the above comparisons and explanations indicate that most of the data reported here are probably within reasonable limits of reliability and accuracy.

STRESS-STRAIN BEHAVIOR OF SOILS

Piece-wise linear values for the modulus of elasticity and Poisson's ratio were determined from a series of uniaxial strain tests and triaxial compression tests on the granular backfill material used for this installation. Since density is known to exert significant influence on the stress-strain behavior of soils, specimens were tested at three densities: the maximum dry density determined from the standard Proctor compaction test, a density 10 percent above this value, and a density 10 percent below this value. The uniaxial strain tests, which constituted the basis for modulus value determinations in this work, were performed on disc-shaped specimens [about 6.3 cm (0.16 in) in diameter and 2.5 cm (0.06 in) thick] in accordance with the standard loading schedule for consolidation tests. All specimens were saturated prior to testing and allowed to drain freely during testing in order to approximate more closely the field conditions that prevailed at the site. The triaxial compression tests, which provided the basis for determining the value of Poisson's ratio, were conducted by subjecting cylindrical specimens [about 6.3 cm (0.16 in) in diameter and 12.5 cm (0.32 in) long] at approximately optimum water content (as determined from the standard Proctor compaction test) to a constant confining pressure and by increasing the axial load incrementally. Radial displacements were measured directly by means of electronic distance-measuring probes.

Constrained moduli (M) determined from the uniaxial tests were converted to the more conventional modulus of elasticity (E) by using 0.3 for Poisson's ratio (ν) in the relationship $E/M = (1 + \nu)(1 - 2\nu)/(1 - \nu)$. The uniaxial strain test was considered to be more representative of actual field conditions because the stress path in a uniaxial strain test (where the major and minor principal stresses increase proportionately) better approximates that followed by a soil element in the field installation than does the stress path in a triaxial test (in which the major principal stress increases while the minor principal stress is maintained constant, thereby causing unrealistic shear stresses that do not occur in the field). Because of the different stress paths and the resulting shear stresses, the modulus determined from a uniaxial strain test increases with an increase in the mean stress, whereas the opposite is true for the triaxial test. For the range of dry densities tested, initial tangent moduli of approximately 14 000, 7000, and 3500 kPa (2000, 1000, and 500 lbf/in^2) were obtained for specimens with the greatest, intermediate, and lowest density respectively. This compares favorably with the experimentally measured 4000 or 5000 kPa (600 or 700 lbf/in^2) determined simply by taking the ratio of measured vertical stresses and strains above or below the pipe.

Although the stress-strain properties of the granular backfill were studied rather extensively, the same thoroughness was not applied to the other soils comprising the installation. Two uniaxial strain tests were conducted on specimens trimmed from a block of undisturbed soil taken from the sidewall of the trench at approximately the springline of the pipe, and the results from these tests suggest the use of a constant modulus value of 5600 kPa (800 lbf/in^2) for this material. During the process of excavating and backfilling the trench with the natural soils, the materials from the upper and lower layers were mixed in an undetermined manner, and this situation, together with the assortment of rather large stone fragments in the soil and the fact that no specific compaction criteria were enforced, made a realistic determination of any modulus for this material virtually impossible. Hence, modulus values were selected on the basis of previous experience and ranged from about 2800 kPa (400 lbf/in^2) under low heights of fill to over 1200 kPa (8400 lbf/in^2) for high fill heights. Although no field or laboratory tests were performed on the undisturbed soils beneath the bedding of the pipe, its observed stiffness when the trench was open suggested the use of a high modulus, and a value of 52 000 kPa (7500 lbf/in^2) was selected.

ANALYTICAL COMPARISONS

Certain experimental data were compared with the results calculated from a mathematical model of the soil-pipe system. For this purpose, various supplementary mechanisms were incorporated into the general plane strain (justified on the basis of experimentally measured longitudinal strains in the pipe wall), finite element program (the elements of which are illustrated in Figure 8) developed by Wenzel (4). The program utilizes an empirical cracking mechanism and the mechanical properties of concrete and reinforcing steel to model the pipe (3). The pipe model consists of 320 quadrilateral elements; eight elements (including two overlay elements) are used to model a cross section of the pipe wall. The ability of the mathematical model to duplicate the response of concrete pipe was verified by means of an extensive series of more than 50 controlled load tests on pipes of different diameter, wall thickness, and reinforcement. The validated pipe model was then incorporated into a model of the soil-pipe system by the addition of 257 quadrilateral or triangular soil elements. For the trench installation described here, 97 elements form the in situ soil material, and the rest of the soil elements are added incrementally to simulate the backfill material. Idealized boundary conditions (complete fixity at the vertical and lower horizontal boundaries and complete freedom at the upper horizontal boundary) are assumed at the external boundaries (about one pipe diameter below the pipe and three diameters to each side of the pipe), and a no-slip condition is assumed to exist at the soil-pipe interface.

Since the granular backfill in the vicinity of the pipe was subjected to different degrees of compaction (for instance, the material in the haunch region was dumped in place with virtually no compaction, while the material above and below the pipe and at its springline was compacted rather well) and since the mechanical behavior of this soil is density-dependent (1), the properties assigned to each soil element of the mathematical model were selected to reflect the estimated initial density of that element. As the state of stress in a given element changed with an increase in the height of cover, the modulus of that element varied incrementally. In this way the nonlinear behavior of the soil and its effect on the pipe response were handled in the soil-pipe interaction model.

Typical comparisons between the experimentally

Figure 9. Comparison between experimental and theoretical results.

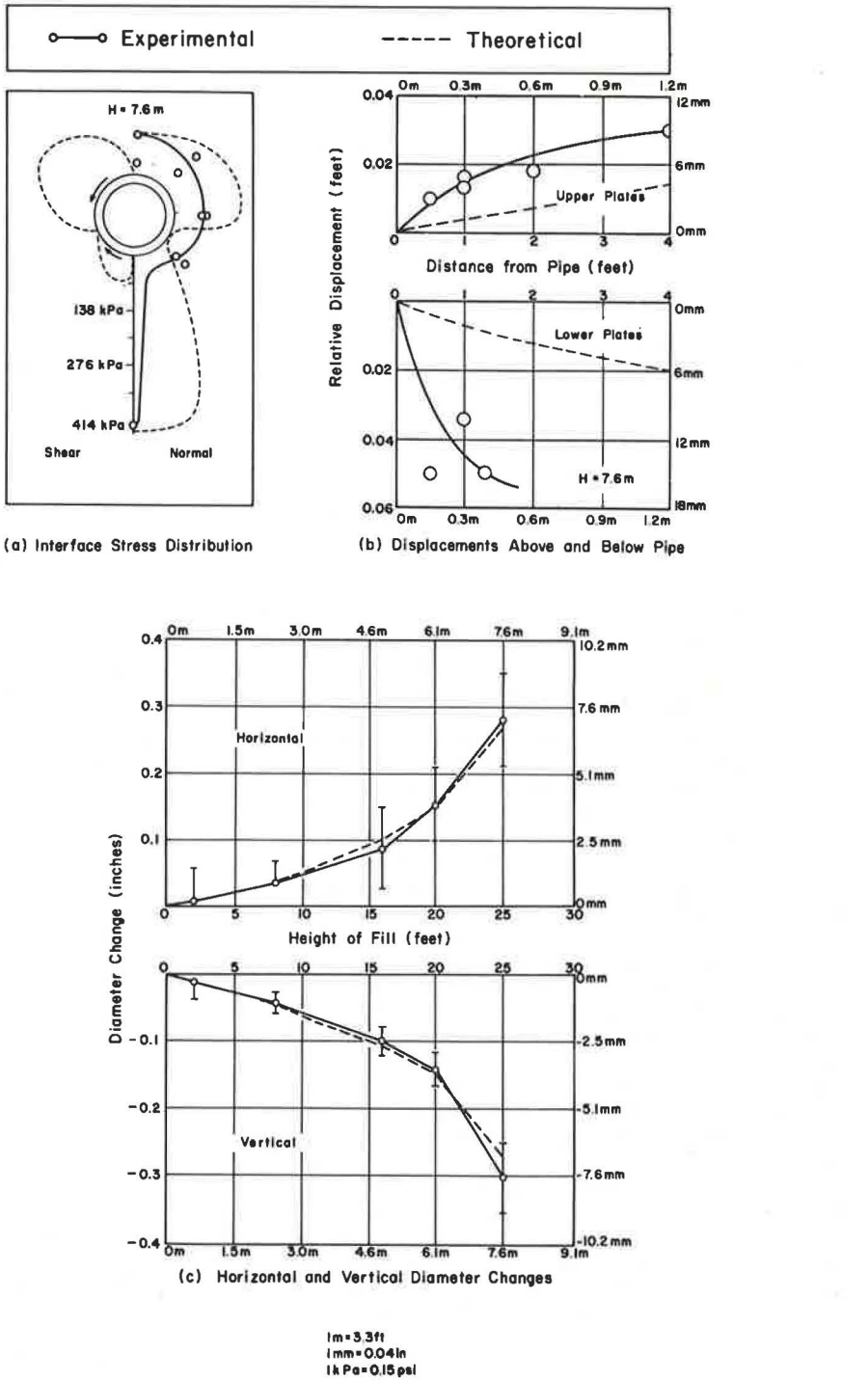

measured data and the results calculated from the mathematical model are given in Figure 9. Of significant importance in Figure 9a is the distribution of shear stresses along the soil-pipe interface. An integration of the vertical components of the computed shear stresses (based on a no-slip condition at the soil-pipe interface) shows that the net downward vertical shear force for the conditions described is essentially equal to the mass of the 1.8-m (6-ft) wide, 7.6-m (25-ft) deep mass of soil above the pipe, and this indicates that interface shear stresses cannot be neglected when establishing the vertical equilibrium of the pipe. Also, the condition of slip at the soil-pipe interface clearly plays a major role in determining the distribution of stresses acting on the pipe and consequently on its associated structural response. Furthermore, the shear stress distribution around the pipe serves to explain to a large degree the apparent concentration of normal stress at the bottom of the pipe. As mentioned previously, shear stresses were not taken into account when best-fit curves were passed through the experimental points shown in Figure 5. The experimental distributions of normal stresses were established on the basis of vertical equilibrium of normal stresses only, thus leading to the sharp peaks illustrated in Figures 5 and 9a. However, since a considerable upward vertical force is necessary

to balance the downward force caused by the shear stresses, the normal stresses along the bottom of the pipe must act over a much wider area than that suggested by vertical equilibrium of normal stresses only. Although there are no direct normal stress measurements to document the extent of this area (interface stresses were only measured at 45° intervals), the mathematical model does indicate that high normal stresses act over approximately the bottom 30° to 40° of the pipe, and the predicted intensity of the normal stress at the one point (bottom stress cell) where a measurement was obtained is in reasonable agreement with the measured value. The mathematical model indicates that lateral support by the soil in the haunch region is very low, as would be expected, but the lateral support at the springline of the pipe is substantial, predicted values being somewhat larger than measured values. The theoretical curves for both normal and shear stresses have been smoothed to even out the small discrete jumps between elements with differing mechanical properties. Except for very low heights of cover, the stress cells in the soil both above and below the pipe gave higher readings than the corresponding cells at the soil-pipe interface. Below the pipe the cell at the soil-pipe interface indicated about 420 kPa (60 lbf/in^2), and the cell in the soil gave a reading of 550 kPa (80 lbf/in^2) for a fill height of 7.6 m (25 ft). This observation might be explained by supposing that the interface cell rested on a soft or low spot in the bedding, although this is not known for certain. For the cells at 0, 15, 30, and 75 cm (0, 6, 12, and 30 in) above the pipe, the normal stresses under 7.6 m (25 ft) of fill were 97, 186, 242, and 152 kPa (14, 27, 35, and 22 lb/in^2) respectively, and the explanation is not so apparent. Although the mathematical model also indicates a slight increase in stress with distance above the pipe up to a few feet or a meter, this difference is not nearly as large as the measured difference. One explanation for the higher measured stresses is the possibility that the cells embedded in the soil might actually be "hard spots" that attract disproportionately high stresses, but this is not supported by the experience with these cells in other field locations and in laboratory calibration (2).

The calculated relative displacements between the pipe wall and discrete points in the adjacent soil, as shown in Figure 9b for 7.6 m (25 ft) of cover, are considerably lower than the measured values both above and below the pipe. Although no specific reason can be given for this discrepancy, the reliability of the field data is supported by the facts that (a) the ratio of the measured relative displacements below the pipe to those above the pipe is reasonably consistent with the corresponding ratio of the measured stresses at those two locations and (b) the approximate modulus values determined by simply taking the ratio of the measured vertical stresses to the measured vertical strains at these locations are in good agreement with moduli measured in laboratory stress-strain tests on specimens with comparable dry densities. These comparisons of stresses and displacements at discrete points constitute severe criteria by which to evaluate the ability of the mathematical model to predict experimental results, because they represent point values in a very heterogeneous system. Diameter changes, on the other hand, represent a more spatially integrated behavior. The horizontal and vertical diameter changes were measured at the center of each of the five test sections by a specially constructed portable extensometer. This instrument, which was fitted between stainless steel spheres epoxied to the inside pipe wall, was adjusted to have constant compressive force for all readings. Shown in Figure 9c are the mean and range of the five readings for each fill height. As this figure shows, the agreement between the measured and modeled changes in the vertical and horizontal diameters of the pipe is excellent.

CONCLUSIONS

Based on the limitations of the results reported here, certain conclusions can be drawn. First, with few exceptions the measured stresses and displacements at discrete points in the experimental installation are mutually consistent and compatible with judgment and previous experience. Second, although the stresses and displacements calculated at discrete points by a plane strain, finite element model are at variance with the corresponding experimental measurements, the excellent agreement between experimentally measured and theoretically calculated horizontal and vertical diameter changes of the pipe indicates that the ability of the mathematical model to predict the overall experimental behavior is very good. Third, both the experimental and theoretical distributions of interface stresses around the pipe are different from those suggested in the Marston-Spangler approach. Fourth, the soil at the springline of the pipe is capable of giving considerable lateral support to the pipe and, except for the higher stress levels at the bottom of the pipe and the lower stresses in the haunch region, the measured interface stresses around the pipe were nearly hydrostatic.

ACKNOWLEDGMENTS

This work was performed as part of an extensive research effort supported by the American Concrete Pipe Association to investigate the soil-structure interaction of buried concrete pipe. The soil tests and much of the original data reduction were performed by M. Hassan Farzin.

REFERENCES

1. R. J. Krizek and R. B. Corotis. Synthesis of Soil Moduli Determined From Different Types of Laboratory and Field Tests. Proc., Specialty Conference on in Situ Measurement of Soil Properties, ASCE, June 1975, pp. 225-240.
2. R. J. Krizek, M. H. Farzin, A. E. Z. Wissa, and R. T. Martin. Evaluation of Stress Cell Performance. Journal of Geotechnical Engineering Division, ASCE, Vol. 100, No. GT12, 1974, pp. 1275-1295.
3. R. A. Parmelee. Investigation of Soil-Structure Interaction of Buried Concrete Pipe. HRB, Highway Research Record 443, 1973, pp. 32-39.
4. T. H. Wenzel. The Design and Response of Circular Concrete Pipe. Department of Civil Engineering, Northwestern Univ., Evanston, Ill., PhD dissertation, 1975.

Publication of this paper sponsored by Soil Mechanics Section.

Mr. Wenzel was a research assistant in the Department of Civil Engineering, Northwestern University, when this research was done.